NAVAL POSTGRADUATE SCHOOL

MONTEREY, CALIFORNIA

THESIS

FORCE LIMITED VIBRATION TESTING AND SUBSEQUENT REDESIGN OF THE NAVAL POSTGRADUATE SCHOOL CUBESAT LAUNCHER

by

Vidur Kaushish

June 2014

Thesis Co-Advisors: James H. Newman
                                                                Young Kwon

Approved for public release; distribution is unlimited

THIS PAGE INTENTIONALLY LEFT BLANK

REPORT DOCUMENTATION PAGE		Form Approved OMB No. 0704–0188

Public reporting burden for this collection of information is estimated to average 1 hour per response, including the time for reviewing instruction, searching existing data sources, gathering and maintaining the data needed, and completing and reviewing the collection of information. Send comments regarding this burden estimate or any other aspect of this collection of information, including suggestions for reducing this burden, to Washington headquarters Services, Directorate for Information Operations and Reports, 1215 Jefferson Davis Highway, Suite 1204, Arlington, VA 22202–4302, and to the Office of Management and Budget, Paperwork Reduction Project (0704–0188) Washington, DC 20503.

1. AGENCY USE ONLY (Leave blank)	2. REPORT DATE June 2014	3. REPORT TYPE AND DATES COVERED Master's Thesis	
4. TITLE AND SUBTITLE FORCE LIMITED VIBRATION TESTING AND SUBSEQUENT REDESIGN OF THE NAVAL POSTGRADUATE SCHOOL CUBESAT LAUNCHER		**5. FUNDING NUMBERS**	
6. AUTHOR(S) Vidur Kaushish			
7. PERFORMING ORGANIZATION NAME(S) AND ADDRESS(ES) Naval Postgraduate School Monterey, CA 93943–5000		**8. PERFORMING ORGANIZATION REPORT NUMBER**	
9. SPONSORING /MONITORING AGENCY NAME(S) AND ADDRESS(ES) N/A		**10. SPONSORING/MONITORING AGENCY REPORT NUMBER**	

11. SUPPLEMENTARY NOTES The views expressed in this thesis are those of the author and do not reflect the official policy or position of the Department of Defense or the U.S. Government. IRB protocol number ____N/A____.

12a. DISTRIBUTION / AVAILABILITY STATEMENT Approved for public release; distribution is unlimited	12b. DISTRIBUTION CODE A

13. ABSTRACT (maximum 200 words)
The Naval Postgraduate School CubeSat Launcher (NPSCuL) is a five-sided structure capable of carrying up to 24 CubeSats to orbit. The vibration test environment for CubeSats flying on NPSCuL on the Atlas-V is extremely harsh, partly due to the input vibration environment from the launch vehicle itself, and partly due to amplification from the NPSCuL structure. This thesis documents the implementation of a relatively new technology, Force Limited Vibration Testing (FLVT), and the design of a stiffer structure to reduce the vibration environment for NPSCuL payloads.

Most acceleration-controlled vibration tests result in significant over-test. FLVT limits shaker forces, producing more realistic tests and potentially provides relief to payloads. Additionally, increasing the stiffness of NPSCuL using an isogrid design, aimed to increase its first-fundamental frequency, could result in less displacement at higher frequencies for a given amount of input energy, possibly improving the payload vibration environment.

It was found that FLVT was very successful in reducing vibration environments for NPSCuL payloads. Although redesigning NPSCuL using an isogrid design achieved the goal of increasing system stiffness, it did not reduce the vibration environment. None the less, lessons learned from the redesign process will be valuable for continuing vibration environment reduction efforts.

14. SUBJECT TERMS Force Limited Vibration Testing, Isogrid, Increasing stiffness, Finite Element Analysis, Random Vibration, Sine Sweeps, Dynamic Analysis, Stress Analysis	**15. NUMBER OF PAGES** 127
	16. PRICE CODE

17. SECURITY CLASSIFICATION OF REPORT Unclassified	18. SECURITY CLASSIFICATION OF THIS PAGE Unclassified	19. SECURITY CLASSIFICATION OF ABSTRACT Unclassified	20. LIMITATION OF ABSTRACT UU

THIS PAGE INTENTIONALLY LEFT BLANK

FORCE LIMITED VIBRATION TESTING AND SUBSEQUENT REDESIGN OF THE NAVAL POSTGRADUATE SCHOOL CUBESAT LAUNCHER

Vidur Kaushish
Civilian, Department of Defense
B.S., University of Michigan, 2009

Submitted in partial fulfillment of the
requirements for the degree of

MASTER OF SCIENCE IN ASTRONAUTICAL ENGINEERING

from the

NAVAL POSTGRADUATE SCHOOL
June 2014

Author: Vidur Kaushish

Approved by: James H. Newman
                 Thesis Co-Advisor

                 Young W. Kwon
                 Thesis Co-Advisor

                 Knox T. Millsaps
                 Chair, Department of Mechanical and Aerospace Engineering

iii

THIS PAGE INTENTIONALLY LEFT BLANK

ABSTRACT

The Naval Postgraduate School CubeSat Launcher (NPSCuL) is a five-sided structure capable of carrying up to 24 CubeSats to orbit. The vibration test environment for CubeSats flying on NPSCuL on the Atlas-V is extremely harsh, partly due to the input vibration environment from the launch vehicle itself, and partly due to amplification from the NPSCuL structure. This thesis documents the implementation of a relatively new technology, Force Limited Vibration Testing (FLVT), and the design of a stiffer structure to reduce the vibration environment for NPSCuL payloads.

Most acceleration-controlled vibration tests result in significant over-test. FLVT limits shaker forces, producing more realistic tests and potentially provides relief to payloads. Additionally, increasing the stiffness of NPSCuL using an isogrid design, aimed to increase its first-fundamental frequency, could result in less displacement at higher frequencies for a given amount of input energy, possibly improving the payload vibration environment.

It was found that FLVT was very successful in reducing vibration environments for NPSCuL payloads. Although redesigning NPSCuL using an isogrid design achieved the goal of increasing system stiffness, it did not reduce the vibration environment. None the less, lessons learned from the redesign process will be valuable for continuing vibration environment reduction efforts.

THIS PAGE INTENTIONALLY LEFT BLANK

TABLE OF CONTENTS

THIS PAGE INTENTIONALLY LEFT BLANK

LIST OF FIGURES

xi

THIS PAGE INTENTIONALLY LEFT BLANK

LIST OF TABLES

THIS PAGE INTENTIONALLY LEFT BLANK

LIST OF ACRONYMS AND ABBREVIATIONS

ABC	Aft Bulkhead Carrier
ADaMSat	AS&T Development and Maturation Satellite
AFSPC	Air Force Space Command
AP	auxiliary payload
ASD	acceleration spectral density
AS&T	Advanced Systems and Technology
CAD	Computer Aided Design
Cal Poly	California Polytechnic State University
CG	center of gravity
CLA	coupled loads analysis
CSEWI	California Space Education and Workforce Institute
DOF	degree of freedom
DSD	displacement spectral density
DRMS	displacement root-mean-square
EDU	engineering development unit
EELV	Evolved Expendable Launch Vehicle
ESPA	EELV Secondary Payload Adapter
FEM	finite element model
FEMCI	Finite Element Modeling Continuous Improvement
FLVT	force limited vibration testing
FRF	frequency response function
GEMSat	Government Experimental Multi-Satellite
GRACE	Government Rideshare Advanced Concepts Experiments
GRMS	root-mean-square acceleration measured in G's
GSE	ground support equipment
ICD	interface control document
ICP	integrated circuit piezoelectric
JPL	Jet Propulsion Laboratory
LV	launch vehicle
MPE	maximum predicted environment

NASA	National Aeronautics and Space Administration
NASTRAN	NASA Structure Analysis
NEA	non-explosive actuator
NPS	Naval Postgraduate School
NPSCuL	Naval Postgraduate School CubeSat Launcher
NRO	National Reconnaissance Office
OSL	Office of Space Launch
OUTSat	Operationally Unique Technologies Satellite
P2M2	P-POD mass model
P-POD	Poly-Picosatellite Orbital Deployer
PSC	Planetary Systems Corporation
PSI	pounds per square-inch
RBE	rigid body element
RMS	root-mean-square
SAD	Splitter Auxiliary Device
SDOF	single-degree-of-freedom
SHC	socket head cap
SVF	Shuttle Vibration Forces
TDFS	two-degree-of-freedom system
ULA	United Launch Alliance
ULTRASat	Unique Lightweight Technology and Research Auxiliary Satellite

ACKNOWLEDGMENTS

This thesis was a collaborative team effort and could not have been completed without the support and guidance of my advisors, colleagues, family and friends.

I owe special thanks to Dr. Newman, my thesis advisor. He has constantly provided encouragement while allowing me to work at my own pace. His support and mentorship have been crucial to the development and completion of this thesis. He gave me the opportunity to work at Naval Postgraduate School at an important juncture in my life; for that, I will be forever grateful. I want to thank Dr. Young Kwon, who agreed to be my co-advisor and provided invaluable support and direction for the finite element models developed in this thesis. I also owe thanks to Dr. Rudy Panholzer for supporting my work and checking on my progress every week without fail.

I also want to make a special mention of Dave Callen and Dave Williamson from the National Reconnaissance Office. They have long been supporters of NPSCuL, and their faith in this project has allowed it to become the success it is today.

This thesis would not have been possible without my colleagues, Dan Sakoda and Wenschel Lan. They have an extraordinary amount of experience with structural analysis, and much of the practical analysis knowledge that I have today, I owe to them. Levi Owen, our machinist, also deserves special mention for bringing to life the complex and sometimes challenging designs that I have asked him to machine.

To Joe Maly, CSA Engineering, David Hinkley, Aerospace Corporation, and Fran Gulick, United Launch Alliance, I owe thanks for taking time out of their busy schedules to discuss my NPSCuL-v2 design and encouraging me to look at the silver lining.

I owe special thanks to my family, including my mother, Amita Kaushish; brother, Manu Kaushish; sister, Jaya Kaushish; sister-in-law, Devika Chawla; and brother-in-law, Akhil Dhawan; for always encouraging me to do what I believe is right and supporting me through my life as a graduate student.

And last but not least, I owe thanks to my girlfriend, Jessica, and my friends Saurabh and Mrinalini for reminding me of my goals whenever I get complacent.

THIS PAGE INTENTIONALLY LEFT BLANK

I.   INTRODUCTION: THE NPS CUBESAT LAUNCHER

The Naval Postgraduate School CubeSat Launcher (NPSCuL, pronounced NPS "cool") is a five-sided box comprising a base-plate, four walls, four brackets and an Evolved Expendable Launch Vehicle (EELV) Separating Payload Adapter (ESPA) compatible, non-separating adapter ring. Additionally, a box known as the Splitter Auxiliary Device (SAD) mounts to one of the walls of the NPSCuL structure. The function of the SAD is to provide a pass-through from the launch vehicle (LV) primary and secondary power harnesses and instrumentation harnesses, to eight Poly-Picosatellite Orbital Deployer (P-POD) harnesses. A picture of NPSCuL with the SAD mounted to the structure is shown in Figure 1.
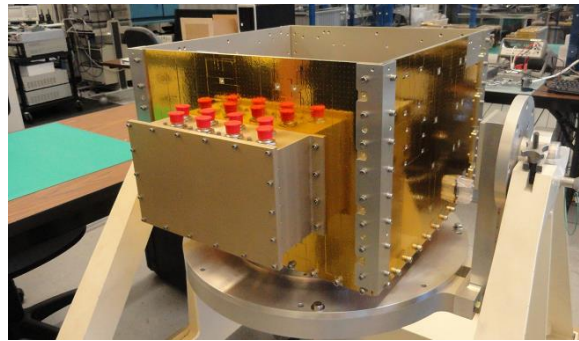
Figure 1.   NPSCuL with SAD Attached

NPSCuL was designed to carry eight P-PODs. The P-POD, shown in Figure 2, is a standardized CubeSat deployment system developed by the California Polytechnic State University (Cal Poly) in San Luis Obispo [1]. Each P-POD can carry anywhere from one to three CubeSats, depending on the CubeSat size, giving NPSCuL the capability of carrying anywhere from eight to 24 CubeSats with a full complement of P-PODs.

The P-POD is an aluminum box with a door and spring mechanism. The door release is controlled by a non-explosive actuator (NEA). Once the NEA is actuated, it releases the P-POD door, which springs open due to torsion springs at the door hinge. The CubeSats inside the P-POD are deployed by the main P-POD spring, shown in Figure 2 [1].

Figure 2.   Cal Poly Mk-IIIR P-POD and Cross Section, from [2]

CubeSats are a sub-type of a class of satellites called nano-satellites, adhering to the CubeSat standard. They were originally developed to provide a real space-hardware building experience to university students. Now they have matured to a point where they are also deemed suitable to meet commercial and national objectives, such as Earth observation and space situational awareness. The CubeSat standard was developed by Cal Poly and Stanford University's Space Systems Development Laboratory in 1999 [2]. Standardization of the form factor of a satellite is advantageous as some development, test and integration processes can be standardized, resulting in more cost effective and responsive satellite development programs. The standard basic CubeSat, known as a "1U', is defined by the CubeSat standard to have 10 cm cubed of volume, and a nominal mass of 1.33 kg. Other common sizes include 1.5U (10 cm x 10 cm x 15 cm), 2U (10 cm x 10 cm x 20 cm) and 3U (10 cm x 10 cm x 30 cm), shown in Figure 3 [2].
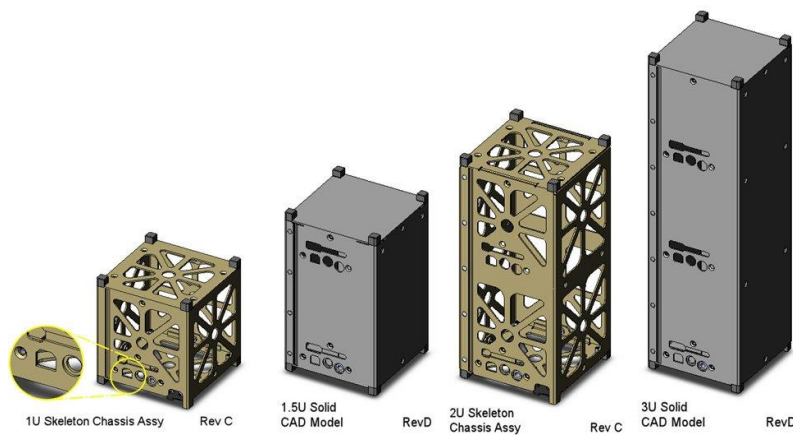
Figure 3.   Common CubeSat Configurations, from [3]

It is worth noting that although the CubeSat standard calls out mass and dimension limits on CubeSats, developers are constantly pushing the envelope, which has led to innovation, updates to the CubeSat standard and upgrades to the P-POD. A larger form factor, known as a "6U," is slowly gaining acceptance and popularity within the CubeSat community. NPSCuL is compatible with the P-POD and 6U dispensers designed by the National Aeronautics and Space Administration (NASA) Ames Research Center and the Planetary Systems Corporation (PSC).

A. CONCEPT

The concept of clustering P-PODs in an NPSCuL was developed during the 2006 Small Satellite Conference hosted by the University of Utah and published the following year at the same conference [4]. With the advent of CubeSats, the need for rapidly responding to U.S.-based launch opportunities had become increasingly evident. Launch opportunities could arise from primary or secondary payloads failing to meet a given launch schedule, or from launch providers wanting to maximize payload capability for a given LV.

NPSCuL was developed to provide CubeSat launch opportunities on U.S. EELVs for government, commercial, research and educational institutions. NPSCuL was envisioned as a standardized bus for interfacing multiple P-PODs to a launch vehicle. The intent was to develop a satellite that could be either a primary or secondary payload, and could enter the launch vehicle integration flow at a late stage, in the event that a primary or secondary payload backed out at the last minute [5]. Though late-stage manifesting has not been achieved yet, NPSCuL has been manifested on four missions as an auxiliary payload, and was launched successfully as part of the Operationally Unique Technologies Satellite (OUTSat) on National Reconnaissance Office (NRO) L-36 in September 2012, and as part of the Government Experimental Multi-Satellite (GEMSat) on NRO L-39 in December 2013. NPSCuL is currently manifested on the Unique Lightweight Technology and Research Auxiliary Satellite (ULTRASat) on Air Force Space Command-5 (AFSPC-5) scheduled to launch in May 2015, and the Government Rideshare Advanced Concepts Experiments (GRACE) mission on NRO L-55 in August 2015.

The original NPSCuL was designed to take full advantage of the 400 lbs mass and large volume allocation of an ESPA payload, as documented by Roßberg [6]. The design was presented at the 2007 Small Satellite Conference, where the NRO Office of Space Launch (OSL) showed interest in further developing the NPSCuL concept due to the project's potential to benefit the space community [7]. Early funding for NPSCuL was received through a grant from the California Space Education and Workforce Institute (CSEWI).

The NRO worked with the United Launch Alliance (ULA) to utilize NPSCuL on ULA's newly developed Aft Bulkhead Carrier (ABC) plate. The mass, weight and center of gravity (CG) requirements for the ABC are more constrained than the ESPA requirements that NPSCuL was originally designed to [6]. This led to the evolution of NPSCuL into a design briefly known as the NPSCuL-Lite.

B. EVOLUTION OF DESIGNS

The original NPSCuL, also known as the D-advanced structure, was designed to carry up to fifty 1U CubeSats in ten 5U P-PODs, as shown in Figure 4 [6]. Neither the 5U P-POD nor the D-advanced structures were ever built.
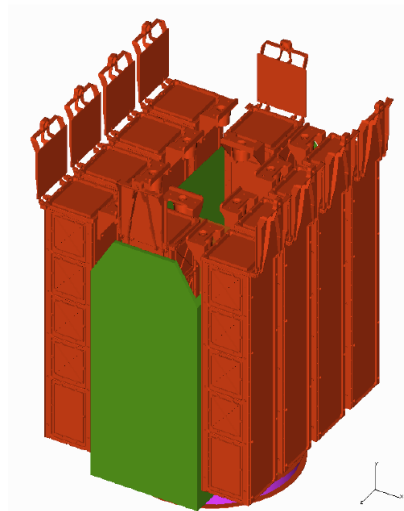
Figure 4.   NPSCuL D-advanced Design, from [6, p. 26]

During this time, ULA was developing its ABC plate concept, which used a 15 inch bolt-hole circle for mounting, compatible with the ESPA bolt-hole circle. However, the ABC required a lower mass and smaller volume envelope than an ESPA payload. The NPSCuL design was updated to be more lightweight and compact, in response to a launch opportunity on an ABC plate on NRO L-41, as part of the Advanced Systems and Technology (AS&T) Development and Maturation Satellite (ADaMSat) mission [8]. The design was called the NPSCuL-Lite, however, the "Lite" was later dropped as this design became the baseline NPSCuL design.

The ABC plate is mounted at a unique location; on the aft end of the Centaur stage of the Atlas-V launch vehicle, shown in Figure 5. Three helium bottles were mounted on the Centaur aft bulkhead; however, an engineering decision was made to remove one of the three bottles. The removal of one Helium bottle opened up room for a secondary payload on the Centaur aft bulkhead.
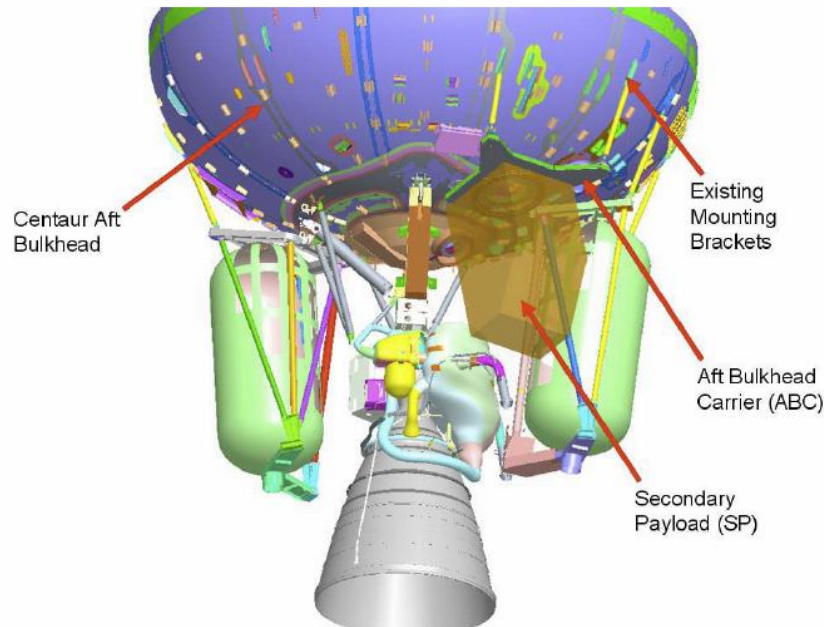
Figure 5.   Atlas V Centaur Stage with ABC and Secondary Payload, from [9]

The ESPA ring allows a maximum mass of 400 lbm for a secondary payload [6, p. 5], whereas the ABC program allowed a maximum mass of 170 lbm, later updated to

189 lbm. The volume constraints on the ABC plate are also more stringent. The redesigned NPSCuL, shown in Figure 6, is capable of carrying eight P-PODs to orbit, giving it a maximum payload capacity of 24 1U CubeSats.
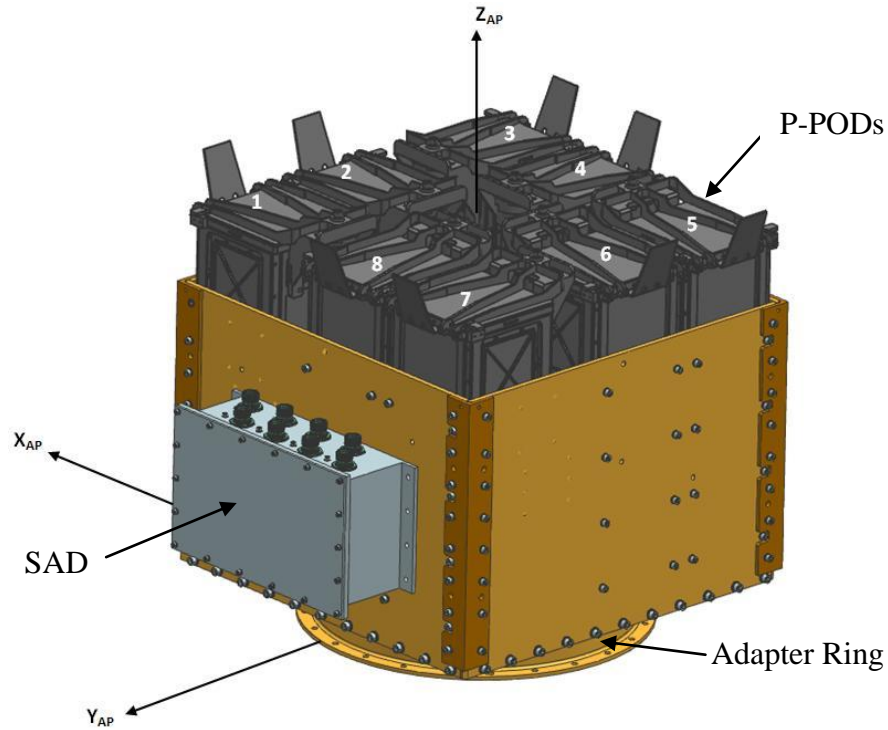
Figure 6.   NPSCuL Design for ADaMSat and Subsequent Missions

NPSCuL, made of Aluminum 7075 T7351, comprises four ¼ inch thick walls, one ½ inch thick baseplate and four L-shaped brackets; one at each wall-to-wall interface and an adapter ring to interface the NPSCuL structure to the LV. The standard 15" ESPA-compatible bolt-hole circle interfaces NPSCuL to the ABC plate. Additionally, the SAD avionics box is mounted to one of the four walls on the structure. The SAD routes the LV-provided power and sequencing to each P-POD.

The origin of the NPSCuL coordinate system lies at the geometric center of the aft-plane of the adapter ring. The positive Z-axis is along the vertical axis, the Y-axis is in

the direction of the SAD, and the positive X-axis is perpendicular to the Y and Z-axes and completes the orthogonal coordinate system. The P-PODs are labeled from one through eight as shown in Figure 6.

The *ABC User's Guide* specifies that the auxiliary payload (AP) shall be capable of withstanding acceleration load factors, not including factors of safety, of 7g's axially, and 5g's in each of the lateral directions, applied simultaneously [9, pp. 3–16]. A finite element model (FEM) for NPSCuL showed positive margins; however, during a qualification test that occurred in the summer of 2009, a test failure was observed [5]. The qualification test utilized a flight-like, full-scale NPSCuL model, with relatively high fidelity mass models for the loaded P-PODs and avionics box. During the test, the fasteners securing one of the P-POD mass models (P2M2s) to the NPSCuL structure backed out one by one until the P2M2 came loose entirely, at which point the test was aborted. This test failure motivated an extensive effort to understand the cause of the failure and remedy the problem. This test failure paved the way for the future successes of the testing program.

It was determined that the causes of the failure were threefold [5, pp. 52–56]:

1. The mating surfaces on the P2M2's and NPSCuL walls were not sufficiently flat, which resulted in gapping during the vibration test, which then caused the fasteners to lose pre-load. The mating interface on the P2M2's was a flat panel, as opposed to the flight-like rails that are present on P-PODs.

2. The use of countersunk fasteners requires tight machining tolerances to get an even load distribution along the fastener head, which has a large surface area due to the countersink angle.

3. A fastener analysis had not been conducted for each bolted interface on the structure.

To remedy the problems listed above, the following corrective actions were taken:

1. The P2M2 design was updated to incorporate rails, similar to those present on P-PODs. A flatness tolerance of +/-0.005 inches was called out on all mating surfaces throughout the NPSCuL structure.

2. The updated design moved away from countersunk fasteners wherever possible. The countersunk fasteners were replaced with socket head cap

fasteners, particularly at the NPSCuL to P-POD interface. Six countersunk fasteners are still used on the NPSCuL structure, on the SAD wall, due to integration constraints.

3. A thorough fastener analysis was conducted, with loads derived from the NPSCuL FEM. Updated torque values which ensured positive margins of safety on yield, ultimate, gapping, shear and tensile strength were calculated. Additionally, the number of fasteners securing the P2M2s to the NPSCuL structure was increased from six to eight.

Additionally, the original P2M2s were composed of several parts to simulate the mass and CG of a loaded P-POD. After the test failure, it was noticed that the fasteners bolting the P2M2s together were beginning to lose torque, and the objective of the vibration test was not to test the P2M2 design, but the design of the NPSCuL structure. As a result, in addition to modifying the rails on the P2M2s, the design was simplified to a monolithic piece of aluminum, while maintaining the mass and CG of a loaded P-POD. A second qualification test, performed using Force Limited Vibration Testing (FLVT) on an updated NPSCuL engineering development unit (EDU), was conducted in June 2011. The test was successful and NPSCuL was qualified to fly on the ABC plate.

C. OUTSAT MISSION

NPSCuL was slated to fly on the ABC plate, as part of the ADaMSat mission manifested on NRO L-41, in 2010. The schedule was aggressive and highly success-oriented for both NPSCuL and its CubeSat payloads; however, the payloads were not able to support the required delivery date six months prior to launch and as a result, ADaMSat was de-manifested from the launch. Even though ADaMSat was de-manifested, the NRO still showed interest in launching CubeSats from the ABC on future flights.

Toward the end of 2010, NPSCuL was manifested on NRO L-36 as part of OUTSat, pictured in Figure 7. Prior to conducting a full scale qualification test to the levels specified in the ABC-to-OUTSat interface control document (ICD) [10], i.e., 7.6 root-mean-square acceleration or GRMS, a few low level random vibration tests were run. Scaling up the responses measured at the NPSCuL wall to P-POD interface yielded

high vibration levels, in excess of 30 GRMS. Though the NPSCuL structure would be able to survive the extrapolated vibration levels, they were felt to be too challenging for most CubeSats.

The reasons for the high levels at the NPSCuL to P-POD interface are twofold:

1. The input vibration levels specified in the ABC to OUTSat ICD are harsh to begin with and conventional vibration testing methods are known to result in over-test of the item being tested.

2. The NPSCuL structure amplifies the vibration levels input at its base, like most structures do.
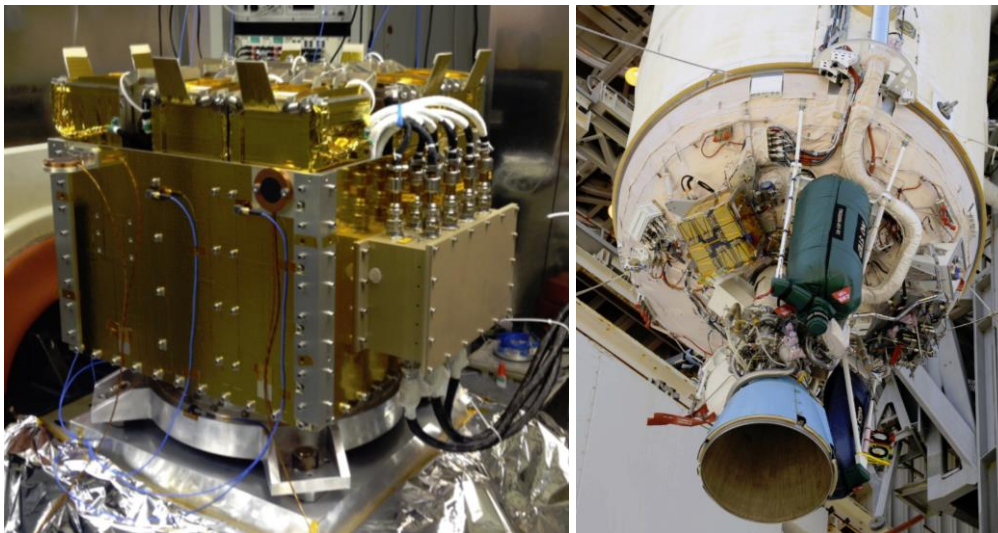
Figure 7. OUTSat Acceptance Test (Left), OUTSat Mated to Centaur Stage (Right), from [11]

D. THESIS OBJECTIVES

The purpose of this thesis is to investigate, describe, and develop methods to reduce over-test of NPSCuL and its payloads and to reduce amplification that occurs in the "structural range" of vibration testing, generally defined as 100 Hz or lower. Reducing over-test can be achieved by implementing a method known as force limited vibration testing, or FLVT, and the second goal can be achieved by increasing the frequencies of the primary modes of the integrated NPSCuL structure, so that they move closer to or above 100 Hz. Chapters II and III outline the methods for achieving the goals described above.

9

FLVT was successfully implemented for the OUTSat flight, which launched as a secondary payload on NROL-36 on September 14, 2012. NPSCuL was subsequently manifested on NROL-39 as part of GEMSat, launched on December 5, 2013. No structural design changes were implemented on NPSCuL for the GEMSat mission, and although, as of this writing, the updated structure has not been manifested on the ULTRASat and GRACE missions, a variant of the updated structure may fly on future NPSCuL missions.

II. REDUCING THE VIBRATION ENVIRONMENT

Spacecraft are generally required to undergo vibration testing to show that they are capable of surviving launch vibration environments. Through the process of vibration testing on the ground, problems that could potentially result in flight failures are identified and remedied, if possible. The vibration test requirements vary from program to program.

A. VIBRATION TEST REQUIREMENTS

OUTSat was manifested to fly as an auxiliary payload on the Centaur upper stage of an Atlas V LV. The OUTSat to Atlas V/ABC ICD specifies a maximum predicted environment (MPE), which is essentially the maximum predicted random vibration environment that the spacecraft would experience. This is based on a statistical significance of 95% probability and 50% confidence [10]. For OUTSat to be compatible with the MPE, each component of OUTSat had to adhere to requirements specified by the program.

In flight hardware vibration testing, the following terminology is important [12, p. 18]:

1. **Acceptance Tests:** Acceptance tests are vehicle, subsystem, and unit tests conducted to demonstrate that flight hardware is free of workmanship defects, meets specified performance requirements, and is acceptable for delivery. Acceptance tests are conducted at MPE levels, generally for a duration of 1 minute per axis.

2. **Proto-qualification Tests**: Proto-qualification tests are conducted to demonstrate satisfaction of design requirements using reduced amplitude and duration margins. This type of test is generally selected for designs that are one of a kind, and where the test unit will be used for flight. Proto-qualification tests are generally conducted at 3dB above MPE, i.e., the square root of 2 times the MPE GRMS, for a duration of 2 minutes.

3. **Qualification Tests:** Qualification tests are conducted to demonstrate satisfaction of design requirements, including margin, for designs that have no demonstrated flight history. Tests are generally conducted on a non-flight qualification unit. This test approach is valuable for designs that will have multiple launch opportunities, as designs that have been through a qualification test do not need to go through subsequent proto-

qualification tests. Additionally, all flight units of a qualified design only need to go through acceptance testing. Qualification tests are generally conducted at 6dB above MPE for a duration of 3 minutes.

The test strategy for the OUTSat mission required the NPSCuL Engineering Development Unit (EDU) to undergo a qualification test. Qualifying the NPSCuL design itself would require subsequent NPSCuL flight units to only undergo a system level acceptance test. The test suite agreed upon by the OUTSat community included low-level sine sweeps and random vibration tests, described in detail in sections 3 and 4. The OUTSat test strategy for NPSCuL, P-PODs and CubeSats is summarized in Figure 8.
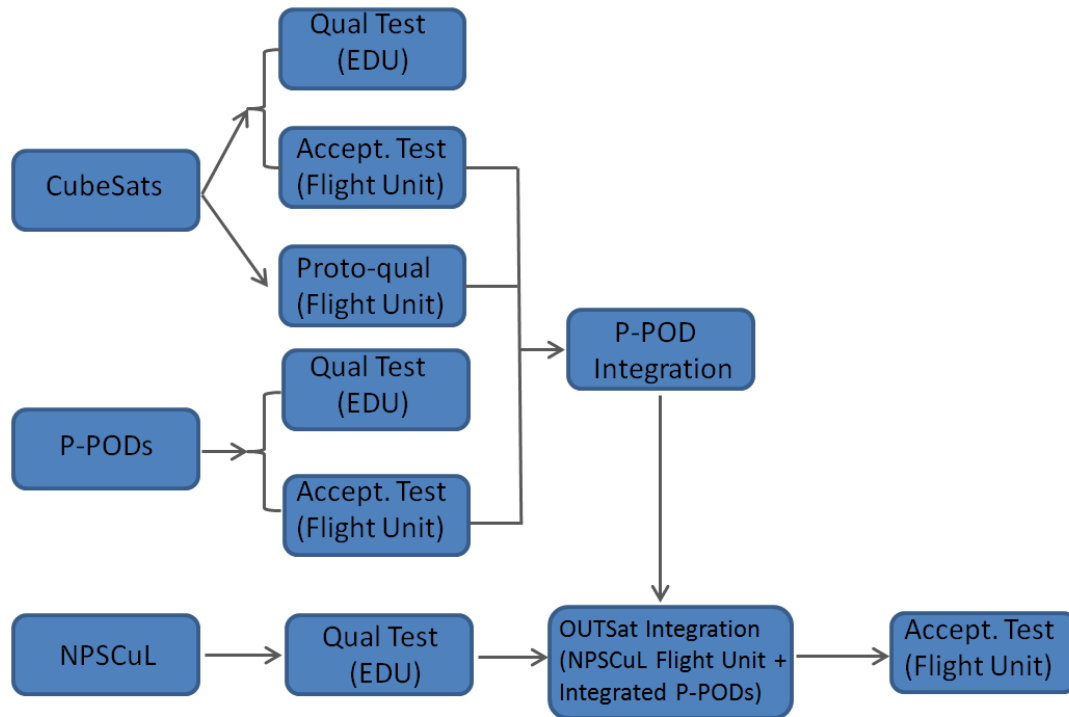
Figure 8.   OUTSat Test Strategy, after [13]

1.   Test Article Description

The test article for the OUTSat qualification test, shown in Figure 9, consisted of a flight-identical NPSCuL EDU, the SAD EDU, one flight-like P-POD with an NEA and door switches, one flight-like P-POD with an NEA mass simulator and door switches and six P2M2s. All items except for the SAD were coated with Class Three gold chemical

conversion coating, also known as Alodine to satisfy the grounding requirement levied by the LV provider. A test harness was built to monitor the P-POD door switches during the vibration test. The total weight of the test article was 170 lbs.
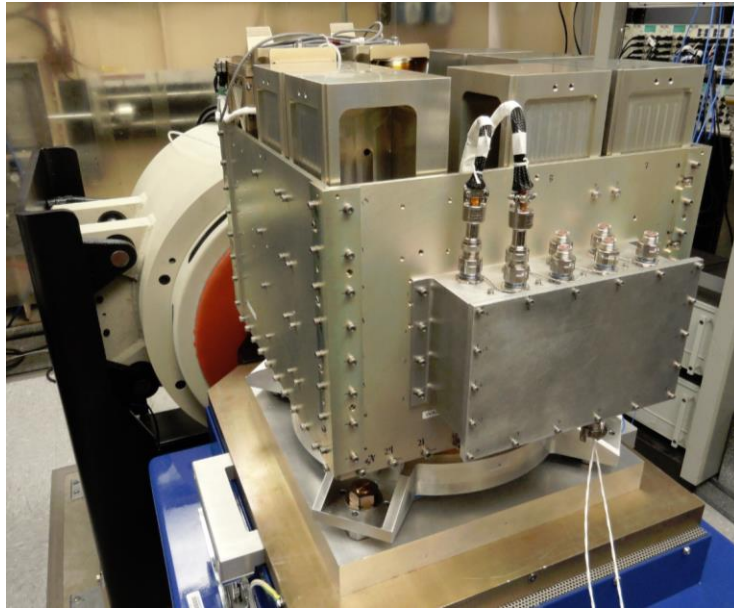
Figure 9.   OUTSat Qualification Test Article

All the fasteners on the structure were torqued to values determined from the NPSCuL fastener analysis. Locking helicoils were utilized as a method of secondary back-out prevention on the bracket-to-wall, wall-to-baseplate, adapter ring to baseplate, and SAD to wall joints. Since Cal Poly prefers to use free-running helicoils on the P-POD to NPSCuL interface, AE-10, manufactured by the Vishay Corporation, was utilized as thread-lock to provide secondary back-out prevention. Though AE-10 provided adequate secondary back-out prevention, it was hard to remove without creating debris. To simplify integration and de-integration procedures for subsequent NPSCuL missions, AE-10 was replaced by Scotch Weld 2216 staking compound.

The OUTSat test article was mounted to the shaker table using an adapter plate. The shaker utilized was a Ling 6000VH, which is rated to output a root-mean-square (RMS) force of 6000 lbf. The Ling 6000VH is an electromagnetic shaker which can be oriented vertically or horizontally. In the horizontal orientation, the shaker interfaces with

a slip table. By utilizing both the vertical and horizontal orientations of the shaker, and rotating the test-article appropriately, testing can be conducted in all three Cartesian axes. The slip table utilized for all OUTSat testing is oil-lubricated by a continuous oil pressure system.

2.   NPSCuL FEM

A widely used method for simulating loading conditions and conducting a modal analysis is through a finite element model (FEM). While conducting analysis on an FEM, the structure is idealized by representing it using simplified small elements: "The shapes of these elements are defined by nodes. Each element has its own mass and stiffness matrices, with as many rows and columns as there are degrees of freedom (DOFs). Depending on its type, an element has mass and stiffness terms for between one and six DOFs at each node" [14, p. 575].

An FEM for the existing NPSCuL structure was previously created and validated against the OUTSat EDU. Usually, FEMs are only able to accurately predict the first two or three modes in each axis for a given structure. A test structure undergoes either a sine sweep or tap test to measure the modal frequencies of the actual structure. The FEM is then adjusted until the first two or three modes in each axis are in agreement with the results from the sine sweep or tap tests.

The NPSCuL FEM was modeled using thin shell elements for the walls, brackets, baseplate and ring, and lumped mass elements for the loaded P-PODs and SAD. The mass of the FEM was ~170 lbm, with the system CG at 0.04 inches in the X-axis, 0.45 inches in the Y-axis and 9.94 inches in the Z-axis. Visualizations of the FEM modal results are shown in Figure 10, and summaries of the frequencies and effective mass fractions are shown in Table 1.
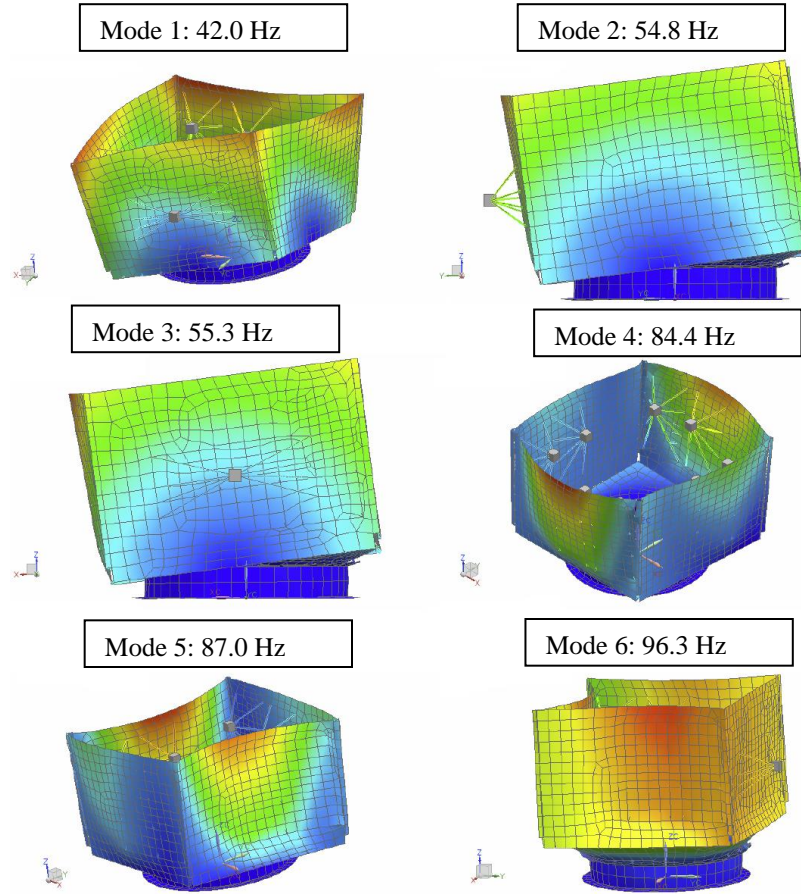
Figure 10.   NPSCuL FEM Modal Results Visualization

Mode	Frequency	Normalized Effective Mass		
		X	Y	Z
1	42.0	0.000	0.002	0.000
2	54.8	0.651	0.023	0.005
3	55.3	0.023	0.673	0.000
4	84.4	0.001	0.000	0.181
5	87.0	0.001	0.000	0.039
6	96.3	0.003	0.000	0.690

Table 1.   FEM Normal Modes and Normalized Effective Mass, after [15]

Effective mass provides information about the dominance of each mode. The concept of effective mass is discussed in detail in Chapter II, Section C.2. The first mode occurs at 42.0 Hz. This mode has extremely low mass participation, and involves bending of the corners of the NPSCuL structure. The second mode occurs at 54.8 Hz and is a

15

rocking mode about the Y-axis. The third mode occurs at 55.3 Hz and is a rocking mode about the X-axis. Both the X and Y-axis primary modes have high mass participation fractions, and from OUTSat and GEMSat vibration testing, it is evident that these modes contribute significantly to the overall GRMS seen by P-PODs mounted to NPSCuL. Two localized panel bending modes occur at 84.4 Hz and 87.0 Hz. They have low effective mass fractions and deformation is localized to the NPSCuL walls. The Z-axis mode is a "pogo" mode, with the NPSCuL structure moving up and down vertically along the Z-axis, while the walls bow inward and outward. The FEM predicts that this mode occurs at 96.3 Hz.

By analyzing the mode shapes and effective masses, it was determined that the first mode at 42.0 Hz is not a concern as it has a very low effective mass fraction. The two rocking modes at 54.8 Hz and 55.3 Hz have high effective mass fraction and significantly contribute to the GRMS seen by NPSCuL payloads. Similarly, the pogo mode at 96.3 Hz also contributes to the GRMS seen by the NPSCuL payloads.

3.   Sine Sweeps

Sine sweeps are low-level vibration tests conducted at a constant acceleration across the frequency range of interest for a particular test article. They are utilized to characterize system dynamics prior to and post any high level vibration tests. A constant, low-level acceleration is input at the base of the article to be tested and responses are measured at areas of interest. The response accelerometers provide frequency and acceleration amplitude information for system resonances. Shifts in resonant frequencies or acceleration magnitudes by up to ~10% between the pre- and post-test sine sweeps are acceptable. As a practice, if the shifts in frequency and acceleration amplitude exceed the 10% threshold, testing should be halted until a reasonable cause for the shifts can be determined. Shifts greater than 10% can indicate structural damage or change in boundary conditions, which could imply loss of pre-load on fasteners.

For the OUTSat mission, sine sweeps were run from 20–2000 Hz at 0.25 Gs, whereas for the GEMSat mission, sine sweeps were run through the same frequency

range at 0.5 Gs to establish better control due to the increased mass of the structure. A sweep rate of four octaves per minute was selected as it provided adequate resolution for the purposes of characterizing the test article.

4. Random Vibration Testing

A random dynamic environment is one where the average properties of the time history signal characterizing the environment might be the same each time the environment occurs, but the exact time history signal is not the same and, hence, the exact value of the signal at a specific time cannot be predicted in advance, based upon a previous measurement of the environment [16].

A random dynamic environment can be either time-invariant or time-varying, depending on whether the average properties of the time history signals vary with time. Most dynamic environments experienced by a space vehicle during the launch phase are time-varying.

Every LV provider specifies a random vibration spectrum for its payload mounting locations. For the NPSCuL mounting location, on the aft-end of the Centaur stage, the LV provides a maximum expected random vibration environment. The AP to LV ICD states that the AP shall be compatible with the MPE levels shown in Figure 11 [10, pp. 3–18]. This implies that either the integrated flight unit needs to undergo random vibration testing at proto-qualification levels, if it has not been previously qualified, or it has to be tested to acceptance levels if it has been previously qualified.
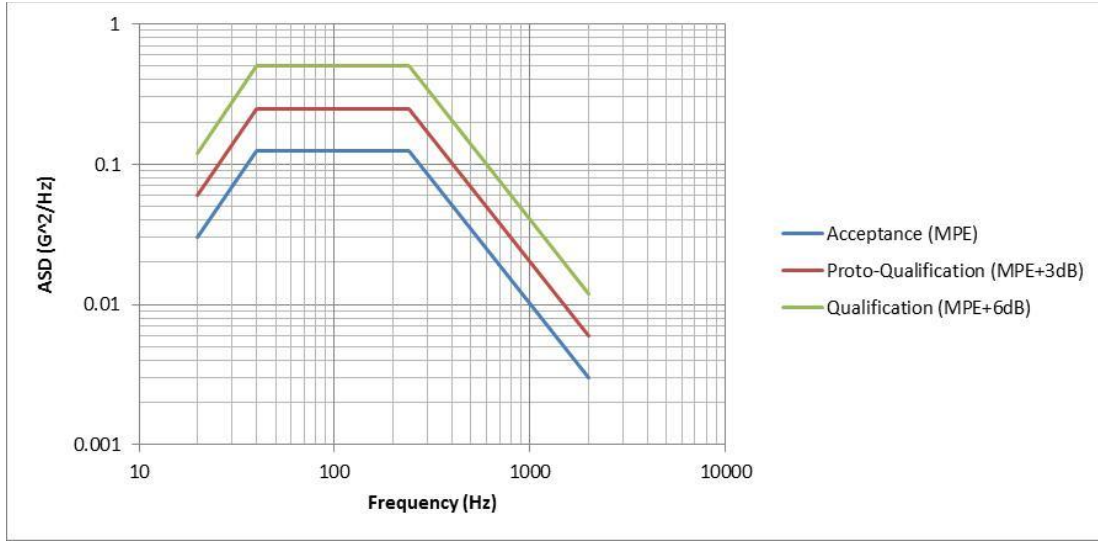
Figure 11.   Maximum Random Vibration Environment at AP to ABC Interface

In Figure 11, the abscissa represents frequency, and the ordinate represents acceleration spectral density (ASD), having units of g^2/Hz. ASD is commonly used to report data for random vibration analyses. An ASD curve provides the distribution of energy as a function of frequency. The GRMS is the square root of the area under an ASD curve in the frequency domain. The GRMS value is often used to determine overall energy of a particular random vibration event. It is important to note that though two ASD curves may have the same GRMS value, they may differ significantly in terms of energy distribution over the frequency range. When analyzing an ASD plot, it is important to note the distribution of energy over the frequency range. Frequencies below ~100Hz are commonly referred to as 'structural' as displacements for a given input at frequencies below 100Hz cause relatively large displacements, and hence result in higher stresses.

The effect of frequency on displacement can be seen from the example of a simple, single-degree-of-freedom (SDOF) oscillator. The equation of motion for an SDOF oscillator is shown in Equation 1.1.

$$m \bullet \ddot{x}(t) + k \bullet x(t) = 0 \qquad\qquad 1.1$$

where 'm' is the system mass and 'k' is the spring stiffness.

18

The natural frequency, ω, of the oscillator defined by Equation 1.1 is shown in Equation 1.2.

$$\omega = \sqrt{\frac{k}{m}}$$

1.2

The displacement, which is the solution to the SDOF equation of motion, is shown in Equation 1.3.

$$x(t) = A\sin(\omega t)$$

1.3

where A is the amplitude of oscillation, ω is the frequency in radians per second and t is the time variable.

The second derivative of Equation 1.3 yields the equation for acceleration in an SDOF oscillator, as shown in Equation 1.4.

$$\ddot{x}(t) = -A\omega^2 \sin(\omega t)$$

1.4

Taking the ratio of Equations 1.3 and 1.4, yields a relationship between displacement and frequency for a given acceleration, as summarized in Equation 1.5.

$$x(t) = \frac{-(\ddot{x}(t))}{\omega^2}$$

1.5

From Equation 1.5, it is evident that the displacement and frequency for a SDOF oscillator are inversely related. Thus, displacement decreases with increasing frequency.

B.   WHITE-SPACE AND OVER-TEST

The American aerospace industry has evolved over time to be somewhat risk-averse, and has chosen a path of conservatism to increase the chances for mission success. This practice of increased conservatism especially impacts secondary/auxiliary payloads, which are required to "Do No Harm" to the primary spacecraft. This inclusion of conservatism can be seen in the derivation of random vibration environments and testing criteria for satellites.

The LV provider, in this case ULA, envelopes all peaks seen from all instrumented historical flight data for a given launch vehicle, to come up with the MPE. In the process of enveloping peaks, the GRMS value of the resulting envelope exceeds the GRMS value that would be experienced during flight. Since the MPE derivation plot

is ULA proprietary, it is not shown herein. Further, the LV-providers require payloads to test to levels that are 3dB above MPE for proto-qualification, or 6dB above MPE for qualification [12, p. 89].

The Finite Element Modeling Continuous Improvement (FEMCI) group has developed guidelines for deriving a test specification from random vibration data. The guidelines are summarized below [17, p. 10]

1. Start with the random vibration data as measured from test or derived from a random vibration analysis.

2. Plot the Minimum Workmanship level for the component or satellite. For all NPSCuL mission, minimum workmanship is defined in MIL-STD-1540E.

3. Enclose the response curve inside the test specification curve using the following rules:

    a. Slopes should be less than + 25 dB/octave or greater than -25 dB/octave. These values are constrained by shaker limitations.

    b. Frequency bands should be greater than 10 Hz to ensure good control is achieved during a vibration test.

    c. Ensure that the test specification is greater than or equal to Minimum Workmanship throughout the test frequency range.

    d. Drop the test specification curve into large valleys.

    e. Sharp peaks can be cut off at about half their height (-3dB).

    f. The overall GRMS level should be kept within 1.25 times the GRMS of the response curve. This is not applicable for plots where cross-axis responses are being taken into consideration. If cross axis responses are included in the test specification, the test specification GRMS may exceed 1.25 times the response GRMS.

Figure 12 shows an example of test specification derivation from generic random vibration data. As can be seen from Figure 12, the envelope includes "white-space" between the envelope curve and the actual flight data curve, which increases the GRMS input during ground testing. Additionally, when launch vehicles instrument the payload attachment areas, the measurements provide data for a hard mount. In reality, satellites are mounted to a plate or bracket, which is in turn mounted to the launch vehicle. Due to the difference in mounting conditions and compliance in a mounting plate or bracket, the measured environments can be higher than those that would actually be seen in flight.
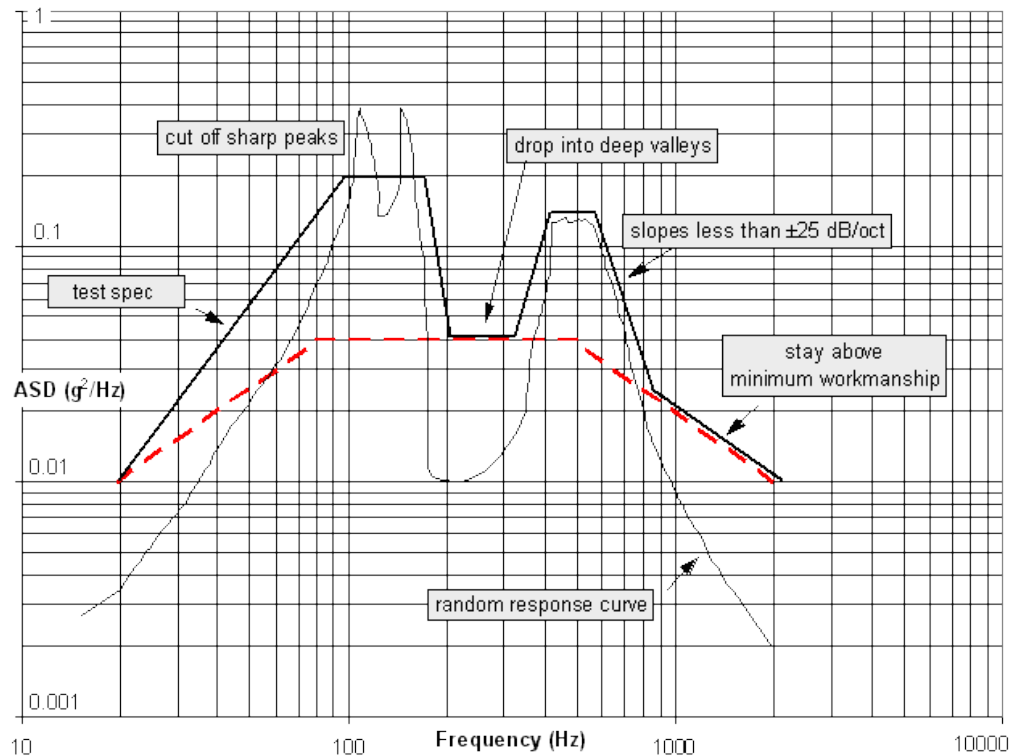
Figure 12.   Random Vibration Test Specification Derivation, from [17]

It should also be noted that NPSCuL is a launcher for CubeSats. The MPE vibration environment provided by ULA, i.e., 7.6 GRMS, is input at the base of NPSCuL. The responses are then measured at the NPSCuL-to-P-POD interface. Since CubeSats complete testing before delivery for final integration into NPSCuL, NPS is required to envelop the responses measured at the NPSCuL-to-P-POD interface, adding additional conservatism into the equation. These responses are defined as the MPE for CubeSats. Individual CubeSat programs, may decide to test to either proto-qualification or qualification levels. Thus, payloads on NPSCuL have conservatism added many times over to the vibration levels. Due to the stringent test requirements levied on NPSCuL and its payloads, CubeSats have no choice but to test-to and design-to these conservative vibration levels.

In an effort to provide relief to CubeSats from a random vibration perspective during the OUTSat launch campaign, NPS evaluated a few options which included testing CubeSats flight units to proto-qualification levels while they were mounted to an

NPSCuL EDU. In theory, this would expose the CubeSats to less conservative random vibration environments, since they would no longer be testing to a derived test specification, but to actual levels seen on NPSCuL for a given input spectrum. Due to unavailability of P-PODs for such ground testing, the CubeSats were integrated into TestPODs (see Figure 13) made by Cal Poly. The TestPODs were integrated into NPSCuL in the location that the CubeSat being tested was expected to fly. Also, since all CubeSats were not available to test at the same time, certain slots on NPSCuL were occupied by P2M2s (see Figure 14).
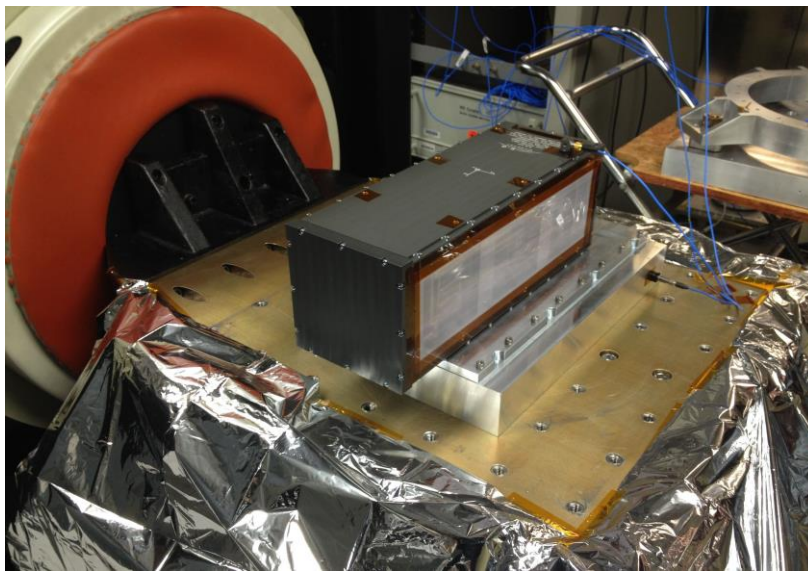
Figure 13.   Cal Poly TestPOD on Slip Table
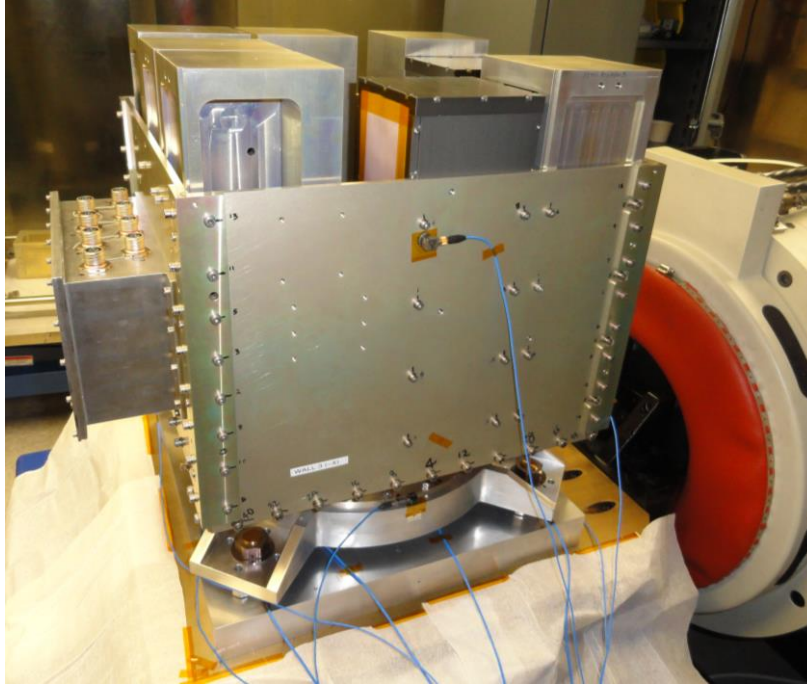
Figure 14.   OUTSat Proto-Qual Testing with 2 TestPODs and 6 P2M2s

While testing CubeSats on NPSCuL did eliminate the conservatism introduced by enveloping vibration response data, it also changed the system dynamics. It was found that the TestPOD had somewhat different dynamic characteristics than the P-POD and CubeSats being tested using this approach were exposed to high vibration environments in the structural range (below 100Hz). It was also found that the combined system response was dependent on the mass distribution and ratio of P2M2s to TestPODs.

Testing CubeSats on NPSCuL also had drawbacks from a programmatic standpoint. Due to the unique nature of the NPSCuL structure, CubeSats mounted in each of the eight locations shown in Figure 6, experience different vibration environments. As expected, the P-PODs located toward the four corners of the structure, i.e., P-PODs 1, 3, 5 and 7, see lower responses than P-PODs located toward the middle of the walls, i.e., P-PODs 2, 4, 6 and 8. Thus, CubeSats that underwent proto-qualification testing while mounted to NPSCuL, were tied to a specific position on the structure. This was deemed to be undesirable to OSL as it limited flexibility in final CubeSat position choices on NPSCuL.

23

Building on the lessons learned from the OUTSat mission that included maintaining flexibility of CubeSat positions on NPSCuL, it was decided that the option to proto-qualify a CubeSat on the NPSCuL structure would be eliminated for the GEMSat mission. Instead, an envelope of all in-axis and cross-axis data, for each of the three axes of vibration, would be provided to the CubeSat developers, that would allow CubeSats to be integrated into NPSCuL in any position. This method was perceived to be more advantageous to the OUTSat testing methodology, as it added the ability to make changes to the final CubeSat positions without any re-testing.

C. FORCE LIMITED VIBRATION TESTING

1. Background and Motivation

All satellites are required to undergo some amount of vibration testing to prove that they are flight worthy and to remedy problems that could result in flight failures. Launch providers require potential payloads to implement random vibration tests to a given derived acceleration specification, with some specified positive margin as described in Chapter II, Section B.

Most satellite providers fulfill this requirement by utilizing established acceleration-controlled vibration tests. However, sometimes acceleration-controlled vibration tests can result in significant over-test and cause failures that would not occur in flight. These test-induced failures can prove to be costly as they can cause scheduling issues and high costs to fix a problem that probably wouldn't occur during flight.

The over-test resulting from traditional, acceleration-controlled vibration tests is associated with the infinite mechanical impedance of shakers and the standard practice of controlling the input acceleration to the frequency envelope of the flight data. This approach results in artificially high shaker forces at the test article resonant frequencies [18, p. iii]. Mechanical impedance, as referenced to herein, refers to apparent mass, or the ratio of force and acceleration.

To successfully pass the ground-based vibration-test, satellite providers have resorted to three techniques in the past [19, pp. 16–17]:

1. Over-designing the satellite structure and components to ensure that they can withstand the high ground-based test environments. This often adds cost to a program and is not a preferred long-term solution.

2. Simulate the mechanical impedance of the flight mounting structure. This approach requires fabrication of flight-like mounting structures for ground-based tests. Since most mounting structures for flight are complex (e.g., Honeycomb), this approach can significantly increase the cost of a satellite program.

3. Limit the responses of the satellite to match predicted flight environments. This approach utilizes the satellite FEM to predict in-flight responses. The FEM is used to conduct all pre-test analyses of the structure, and utilizing that same FEM to predict flight environments compromises the role of testing as an independent method of verification of the satellite design and analysis. Additionally, response limiting at a particular location requires the FEM to be complex, and even with complex FEMs, the accuracy of the results, particularly in the higher frequencies, is not adequate.

The availability of piezoelectric tri-axial force gauges has made possible a vibration testing approach of measuring and limiting the reaction force between the shaker and the test article [18, p. iii]. Force limiting simulates impedance characteristics of the flight mounting structure, thereby enabling a more realistic vibration test. There are many methods for deriving the force limit, however, the method evaluated herein is known as the semi-empirical method due to its simplicity and ease of implementation. The semi empirical method requires only the acceleration specification and the test item mass. Other, more complex methods include the simple two-degree-of-freedom System (TDFS) and complex TDFS methods.

FLVT was developed at the Jet Propulsion Laboratory (JPL) and has previously been used only on a handful of missions, which include the CASSINI spacecraft that is currently orbiting Saturn. For the CASSINI mission, FLVT resulted in notches of -8 dB and -14 dB below 100Hz. The implementation of FLVT on the CASSINI spacecraft is outlined in the Monograph for Force Limited Vibration Testing, written by Scharton [20]. Force limits for the CASSINI test were derived using the semi-empirical method. Additional validation of the semi-empirical approach for force limit derivation was conducted on the Shuttle Vibration Forces payloads 1 and 2 (SVF -1 and SVF-2), which flew on two space shuttle missions. The results from the SVF 1 and 2 missions showed

that the flight environment measurements for the SVF mounting configuration were less than half of the random vibration loads specified in the shuttle payload designer's guide [21]. These results were the motivation for implementing FLVT on all NPSCuL missions.

2.   The Central Cause of Over-Test

As mentioned in Chapter II, Section 1, the primary cause of over-test on all acceleration-controlled, ground-based, random vibration testing, is the difference in boundary conditions between the ground test and the flight configuration.

During all ground-based testing, the test article is mounted to a rigid adapter plate on a shaker, and is excited in a single axis at a time. The adapter plates are designed to be rigid, so as to keep the primary mode of the adapter plate outside the frequency range of the test. The motivation of keeping the primary mode of the adapter plate outside of the test frequency range is to minimize the influence of the adapter plate on the test response measurements.

In flight configuration, the flight article is attached to a mounting structure that has more compliance than the rigid mount of the test structure. The compliance exists in all six DOFs, whereas on a rigid shaker mount, there is minimal compliance in five of the six DOFs.

This leads to a concept known as the dynamic absorber effect [18]. For the TDFS shown in Figure 15, the primary oscillator is directly excited by the source, and the secondary oscillator is excited due to its connection to the primary oscillator. The dynamic absorber effect, as postulated by Scharton, states that the motion of the primary oscillator will be zero, or very near zero at the natural frequency of the secondary oscillator. This effect occurs even if the natural frequencies of the two oscillators are different [20, p. 3–3].
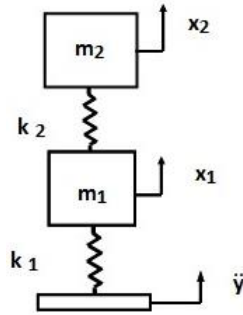
Figure 15.　　　Two Degree of Freedom System

For the purposes of aerospace vibration testing, one can compare the launch vehicle to the source, the mounting structure to the primary oscillator and the satellite to the secondary oscillator. The dynamic absorber effect implies that the acceleration at the interface between the mounting structure and flight article drops at certain system frequencies, and these frequencies correspond to the resonant frequencies of the test item when mounted to a rigid base [20, p. 3–3].

During ground-based vibration testing, it is desirable to adequately model the vibration absorber effect into the testing strategy and test procedures. Over the past few decades, various methods have been developed to implement more realistic ground-based vibration tests. These include the following [19, pp. 16–20]:

1. **Impedance Simulation:** This process involves simulating the mechanical impedance of the spacecraft mounting hardware for the purposes of vibration testing. This method requires a portion of the spacecraft mounting structure to be incorporated into the vibration test. While this approach may be feasible for testing small components such as printed circuit boards, where the mounting structure may be as simple as an electronics box, it is generally not considered feasible for entire spacecraft structures since the mounting structure is usually a more complex composite structure or shelf.

2. **Response Limiting:** Response limiting has been widely utilized to implement more flight-like, ground-based vibration tests. The process for response limiting requires an analytical prediction of responses at pre-determined locations on the spacecraft. These responses are determined from a coupled loads analysis of the combined spacecraft and mounting structure FEMs. During the actual vibration tests, the responses are measured at the same locations where the analytical predictions are made and a response limit corresponding to the analytically derived limit is implemented. The input acceleration spectrum is notched if the measured

27

response exceeds the derived response at any of these locations. While this method can be effective, it is not preferred, as the FEM is utilized to predict test responses, and testing is usually conducted with the aim of independently verifying the FEM. Further, the FEM predicted frequencies don't predict the exact test article frequencies. The measured and predicted frequencies are usually within 10% of each other. This adds to uncertainty in the response predictions from the FEM.

3. **Force Limited Vibration Testing:** The recent development and availability of high range force sensors has made it possible to conduct force limited vibration tests. The process of force limiting involves the derivation of a force limit spectrum for a spacecraft in a given configuration. Conventional acceleration controlled tests are not flight-like, for reasons mentioned above. It has been found that running a dual control test, with control of both force and acceleration input from the shaker, results in more flight-like tests, while reducing over-test of the spacecraft. Various methods for deriving the force limit exist. These include the simple TDFS method, the complex TDFS method and the semi-empirical method. While the first two methods require impedance and apparent mass information about the mounting structure, the semi-empirical method does not, making it the preferred approach for deriving force limits. All force limiting is done in real-time, and is not dependent on results of the finite element analysis, making it preferable to response limiting.

Since force limiting is the preferred approach of the three methods mentioned above, it was decided, with ULA consensus, to implement it during the NPSCuL vibration tests. The validity of FLVT has been thoroughly investigated by Scharton and JPL, and the approach has flight heritage on various missions, the most high-profile of which is the CASSINI mission. FLVT, though first implemented over 20 years ago, has not been widely implemented on aerospace hardware testing. The reasons for the lack of widespread implementation include the high initial investment to upgrade vibration facilities with equipment necessary for force limiting, and the slow evolution of established practices in the aerospace industry, which involve over-designing and over-testing satellites to rule out any chance of flight structural failures. The following section details the semi-empirical approach for determining force limits.

3. Semi-Empirical Force Limits

The semi-empirical approach aims to envelop the force input at the fundamental frequency of a test item for a given mounting configuration. For a sine test, the equations for the semi-empirical approach can be summarized as [18, p. 8]:

$$F_s = CM_0 A_s \quad \text{for} \quad f < f_0 \tag{1.6}$$

$$F_s = CM_0 A_s \left(\frac{f_0}{f} \right) \quad \text{for} \quad f \geq f_0 \tag{1.7}$$

where F_s is the amplitude of the force limit, C is a dimensionless constant which depends on the configuration, M_0 is the total mass of the test item, A_s is the input acceleration amplitude and, f is the frequency and f_0 is the frequency of the mode with greatest effective mass, also known as the primary mode. It is important to note that f_0 is determined by conducting a sine sweep on the actual device under test. It is a measured value from the sine sweeps, and is not the derived value from the test article FEM. For all NPSCuL vibration testing, sine sweeps were conducted both in the upward direction, i.e., from 20 Hz - 2000 Hz, and in the downward direction, i.e., 2000 Hz – 20 Hz. The fundamental mode was determined to be at the frequency where the force in the direction of vibration peaked, and for consistency, the sweep in the downward direction was utilized for making that measurement. For the purposes of determining the force limits, the measured fundamental frequency was rounded down to the nearest whole number, so as to ensure that force limiting was initiated prior to approaching the first fundamental frequency of the test article.

The form of the equation relevant to random vibration tests is [18, p. 8]:

$$S_{FF} = C^2 M_0^2 S_{AA} \quad \text{for} \quad f < f_0 \tag{1.8}$$

$$S_{FF} = C^2 M_0^2 S_{AA} \left(\frac{f_0}{f} \right)^n \quad \text{for} \quad f \geq f_0 \tag{1.9}$$

where S_{FF} is the force spectral density and S_{AA} is the acceleration spectral density. The exponent 'n' is included to reflect the decrease in payload residual mass with increasing

frequency. To understand residual mass, it is necessary to understand the concept of effective mass. A simple way of looking at effective mass is to model each mode of a system as a SDOF mass spring damper. The effective mass concept is directly related to the modal reaction force measurement to unit base-driven acceleration. The sum of the effective masses of all the modes is equal to the total mass of the structure [22]. Generally speaking, the effective mass reduces as the mode number increases, with the primary mode having the highest effective mass. It is practically impossible to capture all the normal modes of a structure. That is where the concept of residual mass comes into play. Residual mass is defined as the total mass of the structure minus the effective mass of the modes which have natural frequencies below the excitation frequency. The residual mass also drops off with increasing frequency.

To account for this roll-off in residual mass, the exponent, n, is factored into Equation 1.9. For most structures, including NPSCuL, this value of the exponent is taken to be 2. The value of the exponent, n, can be adjusted to fit the experimental measurements of apparent mass of the test structure [18, p.8].

In equations 1.8 and 1.9, the test item mass, M_0, the acceleration spectral density, S_{AA}, the frequency, f, and the fundamental frequency are known. The value of C for large strut mounted hardware, such as NPSCuL is generally accepted as $\sqrt{2}$. To arrive at this value of C, which is "semi-empirically" determined, experts from the Aerospace Corporation were consulted. Based on their experience with similar sized hardware in a similar mounting configuration as NPSCuL, the value of C as $\sqrt{2}$ was determined appropriate. Further guidance for the value of C comes from the Force Limited Vibration Testing NASA technical handbook. The handbook states that the normalized force specification plot for a simple TDFS, shown in Figure 16, can be utilized to arrive at a reasonable C value. The handbook states that the ordinate on the plot can be substituted for the value of C^2 for a given payload to source mass ratio. The maximum mass of NPSCuL is 189 lbs, and the mass of the ABC plate with all its struts and attachment hardware is ~24 lbs. The load mass to source mass ratio for this configuration is 7.88, which yields a C^2 value of ~1.25. In the normalized force specification plot shown in Figure 16, all three curves representing different quality factors and hence damping ratios

converge for load to source mass ratios greater than 1. The C^2 value selected for NPSCuL was 2, which is higher than the value derived from Figure 16, since there is a lack of test data to support the usage of a value below 2. Additionally, it was agreed upon by all parties involved, i.e., NPS, ULA, OSL and the Aerospace Corporation, that $C^2 = 2$ would add enough conservatism to account for additional mass participation from the upper stage mounting location, while not causing any under-test.
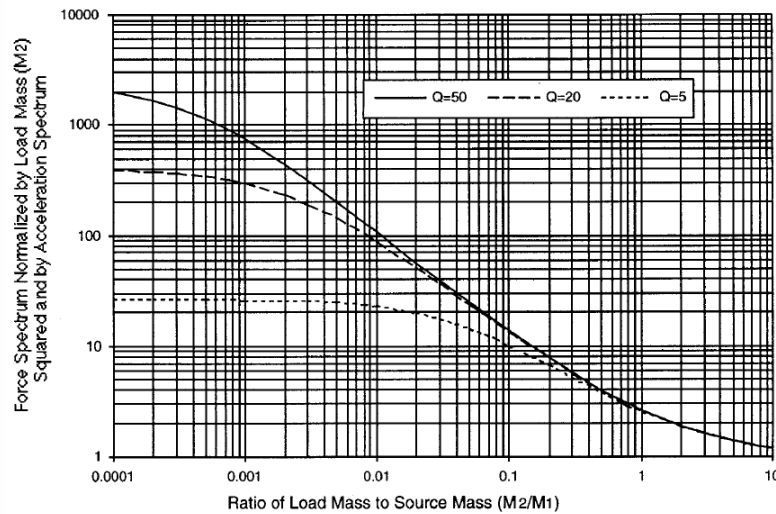
Figure 16.   Normalized Force Specification from simple TDFS, from [18, p. 11]

For all NPSCuL vibration tests, the force limit was implemented from 20–500 Hz. The 20–500Hz range enveloped the first seven modes of NPSCuL in the X and Y axes, and the first four modes of NPSCuL in the Z axis. Though the NASA handbook on force limiting recommends that force limiting should only be carried out for approximately the first three modes in each axis of the system under test, all parties involved in the vibration testing of NPSCuL agreed that force limiting up to 500 Hz, which includes more than the first three modes in each axis of test, would be acceptable, since the force value of C selected for NPSCuL testing was conservative to begin with. It is worth noting that the 500 Hz cutoff was arbitrarily selected for the ABC program. FLVT cutoffs for other programs should be evaluated on a case by case basis, in consultation with the LV provider.

The force limits for testing a 189 lbm integrated NPSCuL structure, at qualification levels, were derived using the acceleration specification shown in Figure 11, and equations 1.8 and 1.9. Though OUTSat had a mass of 167 lbm, data presented henceforth is for an NPSCuL EDU with a mass of 189 lbm, to encompass the maximum allowable NPSCuL mass and to provide a direct comparison with results presented in Chapter III. A graphical representation of the force limit at qualification levels in the Z direction is shown in Figure 17. It is important to note that the plot shown in Figure 17 is valid for a specific NPSCuL configuration, as the inputs to equations 1.8 and 1.9 are measured from the sine sweeps for a given configuration. The force limits need to be re-evaluated each time the test configuration is changed.
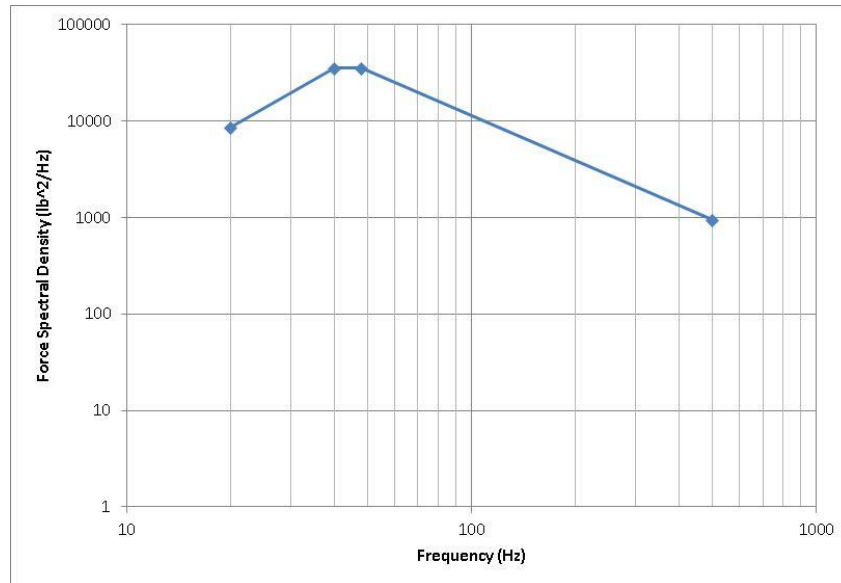
Figure 17.   Z-Axis Force Limits at Qualification Levels for Integrated NPSCuL

4.   FLVT Setup

Setting up a force limited vibration test can be expensive, and force limiting equipment is not readily available at many vibration testing facilities. The main expense lies in procuring adequately-sized piezoelectric force sensors and associated hardware.

Force sensors are inserted in series with the test item and the shaker, and they need to be preloaded so as to always operate in compression. Several force sensors may

be required, depending on the force and moment ranges expected during testing. Special fixtures need to be developed to mount the test article to the shaker, with the force sensors in series. Generally, a shaker adapter plate that interfaces directly with the bolt-hole pattern on the shaker is manufactured. A second plate, referred to herein as the FLVT plate, interfaces with the test article and shaker adapter plate. It is recommended that the weight of the plate above the force sensors be limited to 10% of the weight of the test item. This is necessary as the force sensors measure the sum of forces required to accelerate both the FLVT plate and the test item [18, p. 7]. Maintaining the weight of the FLVT plate to within 10% of the test item can be challenging, and exotic materials with high strength to weight ratios like magnesium can be utilized to overcome that challenge. Though magnesium has a high strength to weight ratio, it is highly flammable and difficult to machine due to the risk of fire. Special fire extinguishers need to be procured to extinguish a magnesium fire, so the benefits gained by using magnesium may be outweighed by the cost of machining it. For NPSCuL, the FLVT plate was manufactured from Aluminum 7075-T7351, and its weight marginally exceeded the 10% of test item weight limit, i.e., the plate weight came in at 10.3% of the test item weight. This was deemed acceptable after consulting with Scharton.

Force sensors are placed at each attachment point between the two plates. The attachment between the two plates, at each sensor location, is made using special threaded studs and bushings provided by the sensor manufacturer. The studs pass through the FLVT plate and through the inside diameter of the force sensors, and thread into the shaker adapter plate. A plastic bushing around the stud ensures that the force sensor is secure against the stud. A nut on the FLVT side of the stud completes the mechanical connection between the two plates and force sensors.

For NPSCuL testing, the maximum expected force input from the shaker, and hence reaction force at the shaker to NPSCuL interface, is approximately 9600 lbf at qualification levels for an un-notched test, using three sigma loads. Calculating the maximum expected loads is critical in determining the force sensor range for FLVT. The sensors should be sized such that there is adequate margin between the maximum predicted reaction force per sensor and maximum allowable sensor force for each of the

33

test axes. In the case of NPSCuL, it was decided to utilize four force sensors for vibration testing, making the maximum force seen per sensor approximately 2400 lbf. Accordingly, a force sensor manufactured by PCB Piezotronics, model 260A03, with appropriate ranges in all three axes was selected. The sensor is an integrated circuit piezoelectric (ICP) force sensor, which means it incorporates a charge amplifier within the sensor. A constant current power source is required to operate the sensor. An image of the sensor is shown in Figure 18 and its characteristics are summarized in Table 2.

Figure 18.   Tri-Axial Piezoelectric Force Sensor, Model# 260A03, from [23]

Manufacturer	PCB Piezotronics
Model	260A03
Sensitivity (Z Axis)	0.25 mV/lb
Measurement Range (Z Axis)	10,000 lb
Measurement Range (X or Axis)	4,000 lb
Full Scale Output (Z Axis)	±2.5 VDC
Full Scale Output (X or Y Axis)	±5.0 VDC
Preload	40,000 lbf

Table 2.   Force Sensor (Model# 260A03) Characteristics, after [23]

While torqueing the nuts on the FLVT plate, it is important not to exceed the full scale output in the Z axis, i.e., 2.5 VDC or 10,000 lbf per incremental increase in preload. Exceeding the value specified in Table 2 can cause damage to the sensor. Care must also be taken to utilize a balanced torque sequence and to ensure that the final pre-load values on all sensors do not deviate significantly from each other. For NPSCuL, the preload values on

all sensors were maintained within 5% of each other. Additionally, while the manufacturer recommends a preload of 40,000 lbf, it may not be practical to achieve. The NASA handbook on FLVT specifies three requirements for selecting the preload [18, p. 5]:

1. The preload must be sufficient to prevent unloading due to dynamic forces and moments

2. The maximum stress on the transducers does not exceed the stress induced by the maximum load set specified by the manufacturer

3. The preload is sufficient to carry shear loads without slip

For NPSCuL, preload was maintained between 30,000 lbf and 35,000 lbf. This was determined to be adequate to ensure that the sensors always operate in compression, that the maximum stress does not exceed the manufacturer's specifications, and that there is adequate friction to prevent any slipping. It was also found that the force sensor sensitivity remains valid for the aforementioned preload range. Figure 19 shows the FLVT setup.
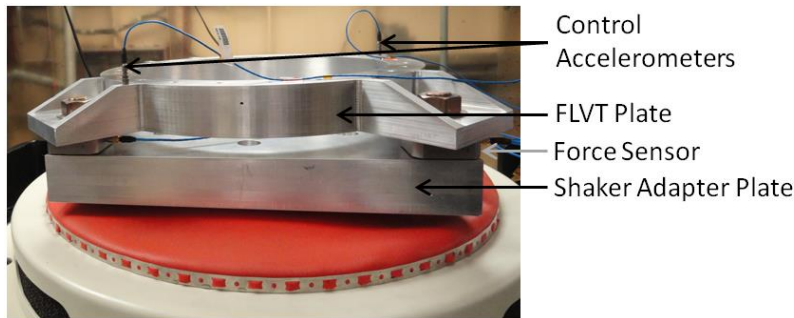
Figure 19.   Force Limited Vibration Testing Setup

To simplify connections in the FLVT setup, it is desirable to ensure that the Cartesian axes are aligned on all force sensors utilized. Each force sensor is connected to a summation module using microdot to BNC connectors. The summation module sums the forces in the X, Y and Z axes in the force sensor coordinate system. The summed forces are measured, and force limits are implemented to limit shaker forces into the test article.

To test the FLVT setup, a baseline sine sweep and random vibration test were conducted on the setup alone. Two accelerometers were used for control. The random vibration test verified that good control could be established at the FLVT to spacecraft interface. The test tolerances for random vibration are outline in Table 3. In some cases, i.e., if the input vibration levels exceed the test requirements, it is acceptable to exceed the tolerances outlined in Table 3; as it ensures that the test article is not under-tested.

Frequency Range	Maximum Control Bandwidth	Test Tolerance
20 – 100 Hz	10 Hz	± 1.5 dB
100 – 1000 Hz	10 percent of midband frequency	± 1.5 dB
1000 – 2000 Hz	100 Hz	± 3.0 dB

Table 3.   Random Vibration Test Tolerances, after [12, p. 27]

Since the sine sweep is only used as a baseline comparison point, no tolerance requirements are levied on the test. Further, a transfer function between the force measured and input acceleration should yield a mass that is approximately equal to the mass of the hardware above the force transducers.

5.   FLVT on NPSCuL

Once verification of the FLVT setup is complete, the test article, in this case the NPSCuL EDU, is attached to the FLVT plate using hardware and torque values similar to the flight configuration. The NPSCuL EDU, as setup for testing herein, consisted of the NPSCuL structure, eight P2M2s, and the SAD and weighed 189.6 lbm. The test article was then instrumented using accelerometers, as required. For NPSCuL FLVT, two control accelerometers were installed on opposite sides of the FLVT plate, at the plate to NPSCuL interface. This serves to ensure that both sides of the interface see similar acceleration. Additionally, P-POD positions 1, 2, 3 and 4 (see Figure 6) were instrumented using tri-axial accelerometers at the NPSCuL to P-POD interface. Readings from these accelerometers were utilized to derive vibration environments for CubeSats flying on NPSCuL.

Due to instrumentation limitations, all eight P2M2s could not be instrumented with accelerometers. It was postulated, and later verified during the GEMSat qualification test, that P2M2s on opposite walls would see similar vibration environments, depending on whether they are located at the corner or center position on each wall. The FLVT setup with NPSCuL attached is shown in Figure 20.

NPSCuL to P-POD Interface

NPSCuL Input Environment
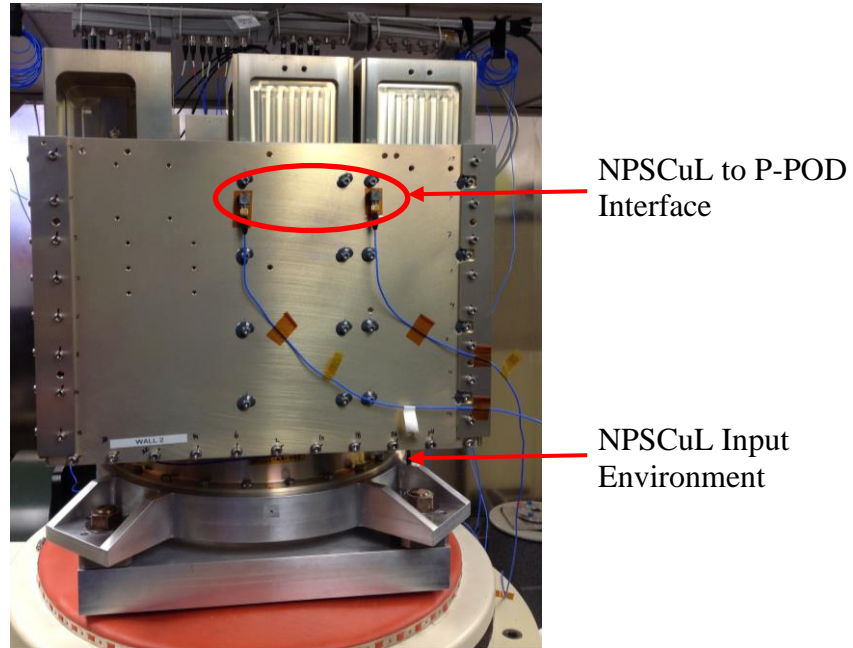
Figure 20.   NPSCuL EDU FLVT Setup

To verify that the setup was correctly calibrated for the NPSCuL EDU, and to determine the first fundamental frequency of the test structure, a baseline sine sweep at 0.25 G from 20 Hz - 2,000 Hz was conducted both in the upward and downward directions. A plot of the measured "Z" axis forces measured during the Z axis sine sweep is shown in Figure 21. From the figure, it is evident that the first Z-axis mode for the integrated NPSCuL EDU lies at approximately 111 Hz. This value is used as an input for the force limiting equations outlined in Chapter II, Section C.3. Similarly, for the X and Y axes, the first fundamental mode was at 46 Hz and 45 Hz, respectively. For X and Y axis force sensor data plots, see Appendix A.
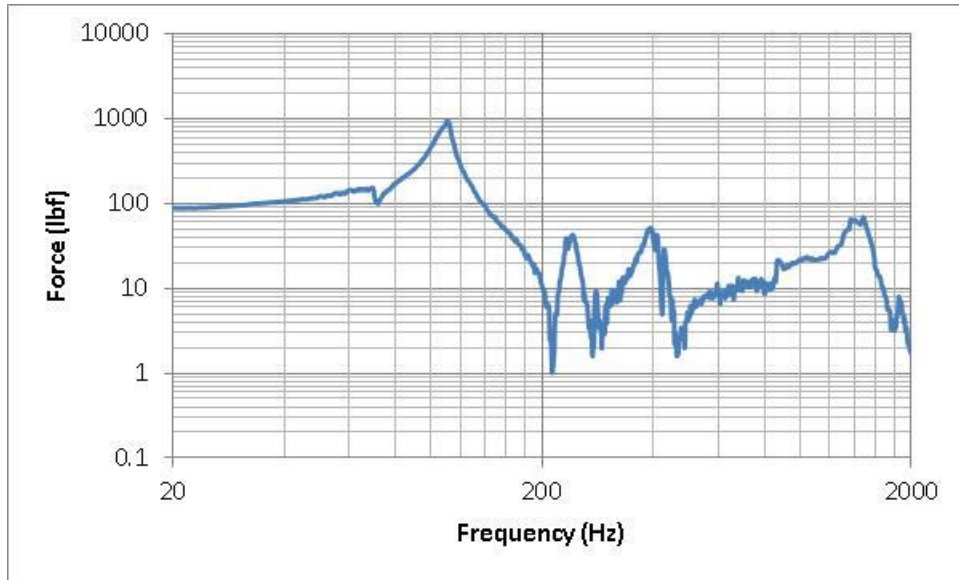
Figure 21.   Z-axis Force, NPSCuL EDU Z-Axis Sine Sweep

Before proceeding with any random vibration testing, it is important to ensure that the force sensors are correctly calibrated for the combined FLVT setup. This is accomplished by plotting a transfer function between the measured force in the direction of vibration and the measured acceleration in the same direction. The ratio of those two values yields the apparent mass. The transfer function between the measured force and measured acceleration from the Z-axis sine sweep during the NPSCuL EDU FLVT is shown in Figure 22. From basic structural dynamics, it is known that rigid body motion occurs at frequencies much lower than the first fundamental frequency of a structure. At frequencies much smaller than the first fundamental frequency, the apparent mass must be approximately equal to the mass of the test item and any fixtures above the force transducers. The actual mass of the items above the force transducer for the NPSCuL EDU test was 211 lbm, whereas the measured mass was 215 lbm at 20.1 Hz. The two values are within 1.9 % of each other, showing that the force transducers were correctly calibrated for the given setup. For all NPSCuL testing, the measured apparent mass at frequencies significantly below the test item fundamental frequency was always within 5% of the measured mass, as a result of which no further calibration of the force sensors was required.

38
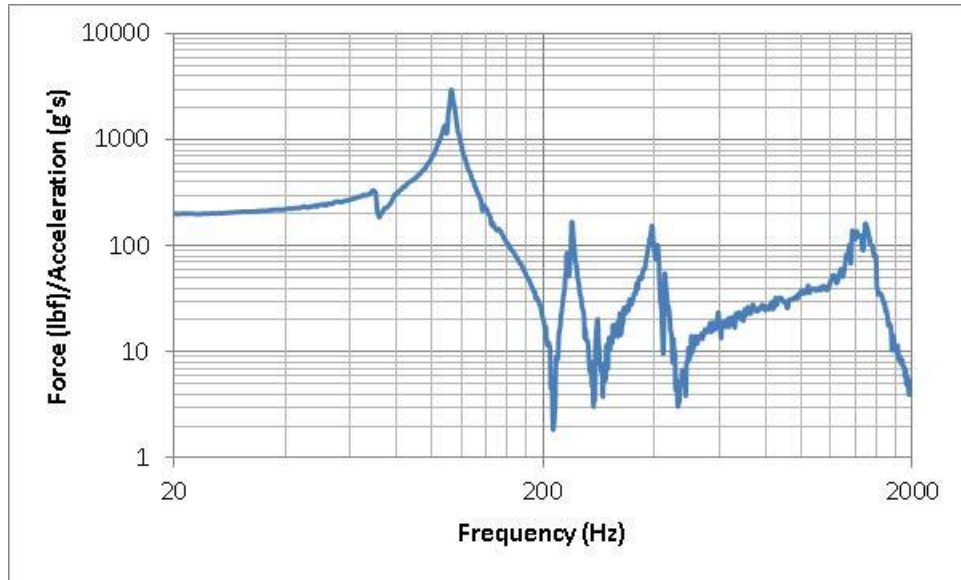
Figure 22.   Transfer Function of Force and Acceleration, NPSCuL EDU FLVT Test, Z-Axis Sine Sweep

Once calibration is verified and the fundamental frequency of the test article is known, equations 1.8 and 1.9 are utilized to derive the force limits for the test setup. For NPSCuL testing, a dual control approach was utilized, i.e., both acceleration and force measurements were used to control the test. Two control accelerometers at the NPSCuL to FLVT plate interface were used to measure the acceleration input, and the force sensors were used to measure force input by the shaker. The random vibration test was controlled to the acceleration spectrum provided by the LV; however, if the input force exceeded the derived force limits, the acceleration input was notched at the frequencies where the exceedance occurred.

To establish good control, testing was commenced at 12 dB below MPE, stepping up in 3 dB increments to the target level, while dwelling at each level below qualification for 20 seconds. Additionally, the test operator could increase the dwell time at any level below 6 dB below MPE, in case additional time was required to achieve good control. While MIL-STD-1540E states the durations for acceptance, proto-qualification and qualification tests as one, two and three minutes respectively, the additional time spent at levels below the target level should also be factored in to every test plan to account for any fatigue effects that may affect sensitive structures or instruments.

The effectiveness of FLVT was determined by running both a force limited random vibration test and a traditional acceleration controlled random vibration test. To rule out any variations from differences in setup, the exact setup was tested for both cases, i.e., no fixture, configuration, mass or instrumentation changes were made to the test setup. Both tests were run in each of the three Cartesian axes, to 3dB below MPE at the NPSCuL to FLVT plate interface, i.e., 5.4 GRMS. Figures 23–25 show comparisons of the force plots, control plots and response plots for both cases, for the Z-axis test. See Appendix B for plots from the X and Y axis tests.
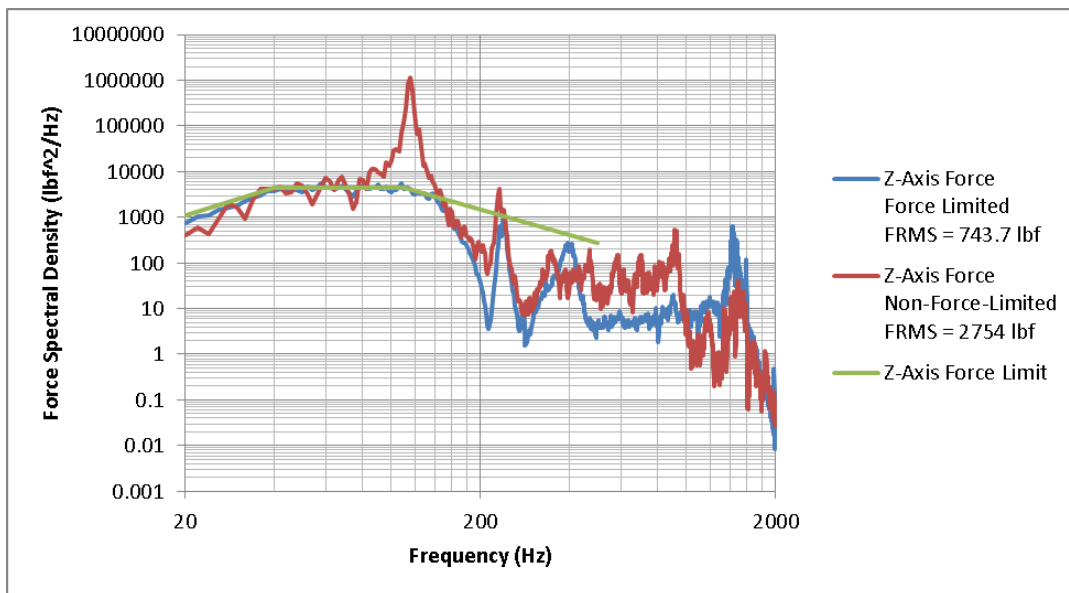
Figure 23.   Force Measurement, Z-Axis Test, MPE – 3dB
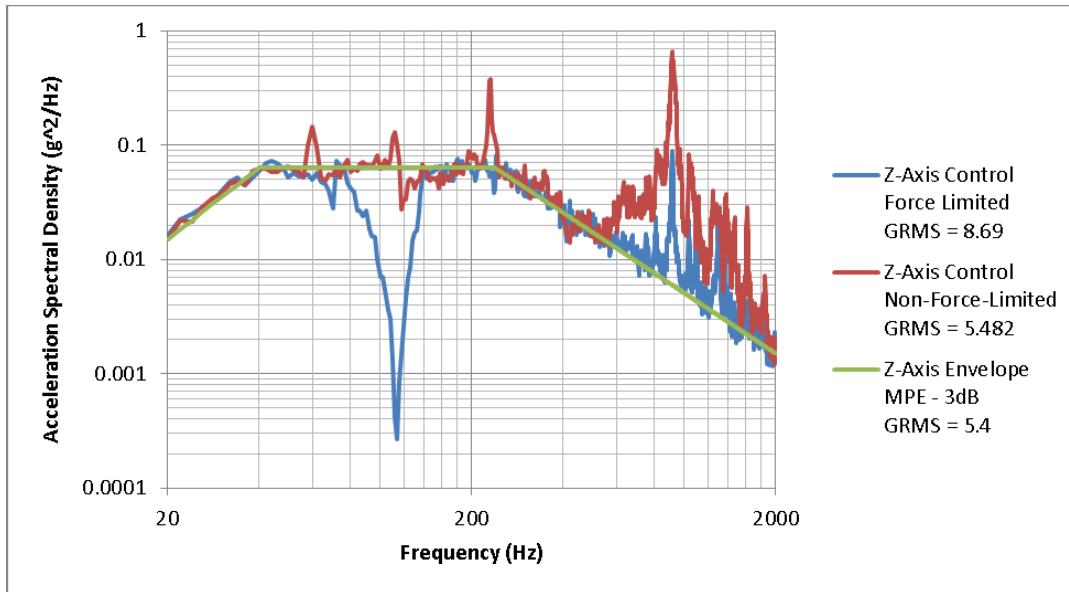
Figure 24.   Control Acceleration, Z-Axis Test, MPE – 3dB
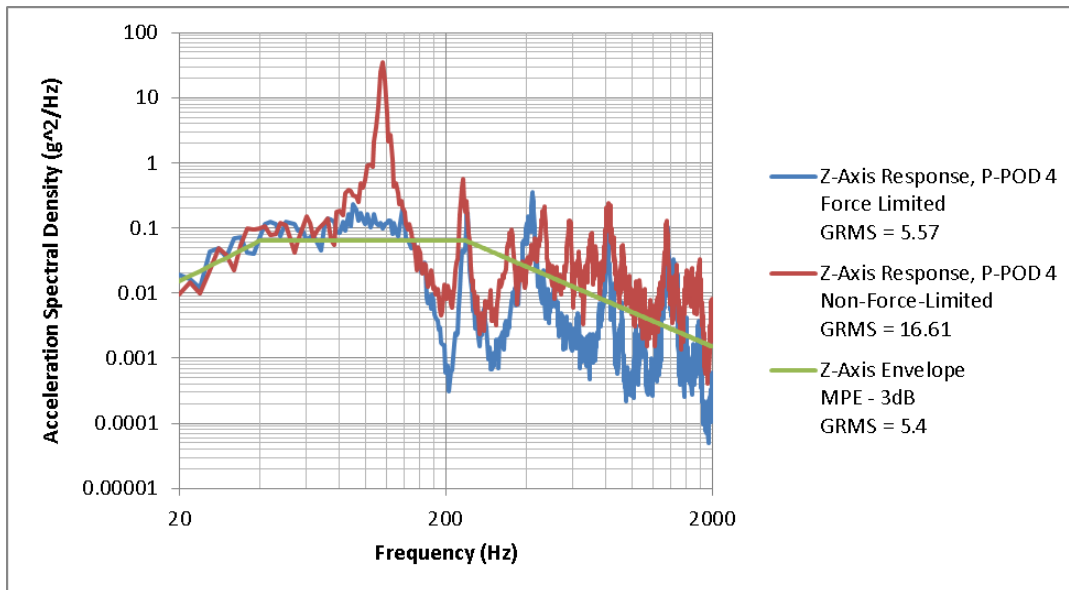
Figure 25.   Response Measurement, P-POD 4, Z-Axis Test, MPE – 3dB

From Figure 23, it is evident that force limiting causes a significant reduction in input force for the NPSCuL structure in the Z-axis. Similarly, a comparison of the control plots for a force limited and non-force limited test, seen in Figure 24, shows a notch in the control acceleration plot for the force limited test. FLVT provides significant relief at the test item fundamental frequency; on the order of 23 dB. NPSCuL amplifies the input

GRMS by a factor of ~3 in the Z axis in the un-notched configuration. It is also worth noting that the controller is unable to establish good control above 600 Hz for the non-force limited test and above 800 Hz for the force limited test, as a result of which the full benefit of force limiting is not seen on the overall GRMS value for the force limited test, due to a higher-than-required GRMS input in those frequency ranges. Since the measured input random vibration profile is above the input random vibration envelope requirement levied by the LV provider, and the structure is over-tested in these frequency ranges, the test is still considered valid. The lack of good control in the high frequency range was determined to be due to combined test item and FLVT plate resonances that cannot be reduced even by reducing the drive signal from the shaker. A stiffer FLVT plate can result in improved control, however, that would result in the plate exceeding the 10% of test item weight guideline outlined in NASA-HDBK-7004B.

Finally, a comparison of the responses measured at the NPSCuL to P-POD interface at P-POD position 4, shows the effectiveness of force limiting for NPSCuL payloads. Without force limiting, a large peak is seen at the NPSCuL resonant frequency at approximately 111 Hz. The area under this curve, which is effectively the energy input into the payload at the given frequency, is very large and would not be seen during flight. Implementation of FLVT reduces the ASD value of the peak, thereby reducing the energy input into P-POD 4. The value by which the magnitude of the peak is reduced is approximately equal to the depth of the notch seen in the control plot shown in Figure 24, i.e., ~ 23 dB, thereby significantly improving the vibration environment for NPSCuL payloads. A summary of the response acceleration for all three axes is shown in Table 4.

	X Axis P-POD 2	Y Axis P-POD 4	Z Axis P-POD 4
Un-notched GRMS	11.9	10.9	16.6
Notched GRMS	10.8	8.83	5.57
Relief Percentage	9.29 %	18.8 %	66.4 %

Table 4.   Response GRMS Comparison for Un-notched and Notched Random Vibration Tests at MPE – 3dB

From Table 4, it is evident that force limiting does help reduce vibration environments seen by NPSCuL payloads during vibration testing, and it is most effective in the Z axis. However, proto-qualification testing is conducted at input levels that are 6 dB higher than the input levels used to arrive at the values in Table 4, and all CubeSats on ABC missions need to be tested to proto-qualification levels at a minimum.

For the OUTSat mission, proto-qualification levels were derived by enveloping position-specific data from the OUTSat qualification test, during which FLVT was implemented. CubeSat positions within NPSCuL were decided prior to CubeSat proto-qualification testing, and CubeSats were given position specific proto-qualification levels. The OUTSat qualification test configuration consisted of the NPSCuL structure, six P2M2s, two P-PODs with CubeSat mass models and a SAD EDU.

During the OUTSat acceptance test, which consisted of eight P-PODs instead of 2 P-PODs and 6 P2M2s, higher than expected damping was observed, resulting in lower than predicted acceptance levels. The increased damping was due to the inclusion of harnessing and P-PODs containing more joints than P2M2s. The additional joints help dissipate some of the energy input into the OUTSat system. For the GEMSat mission, the OUTSat acceptance test levels were enveloped using methods outlined in Chapter II Section B, and scaled up by 3 dB to arrive at proto-qualification levels. Additionally, since OSL desired generic levels that would be compatible with any position on NPSCuL to maintain payload location flexibility, cross-axis responses from the acceptance test were also included in the enveloping process. See Appendix C for GEMSat random vibration level details.

The resulting proto-qualification levels, though reduced due to the implementation of FLVT and the additional damping seen in flight configuration, are still considered severe by potential NPSCuL CubeSat payloads. The proto-qualification random vibration levels for the GEMSat mission were 21.4 GRMS in the X-axis, 22.5 GRMS in the Y-Axis and 14.8 GRMS in the Z-Axis. While these levels are definitely an improvement over the levels that would have been seen during an un-notched test, further

43

reduction in levels was deemed desirable by the CubeSat community. In an attempt to improve the dynamic characteristics of the NPSCuL structure, an isogrid redesign, outlined in Chapter III, was attempted.

III.   REDESIGNING THE STRUCTURE: THE NEXT GENERATION

A.   PROPOSED DESIGN CHANGES

NPSCuL is the primary structure for its CubeSat payloads, in that it is the primary load path between the LV and the CubeSats. The load is transferred from the LV, to NPSCuL, to the P-PODs, which in turn transfer it to the CubeSats. The function of the primary structure is to withstand the loads experienced during launch. It is desirable to make the structure strong enough to withstand the launch loads, but also to keep the weight low, so as to maximize payload capacity.

The existing NPSCuL design, weighs 39.7 lbs, not including the SAD, P-POD, CubeSats, harnesses or fasteners. The structure also has an allowable volume envelope as defined in Figure 26, which includes the P-POD doorstops.
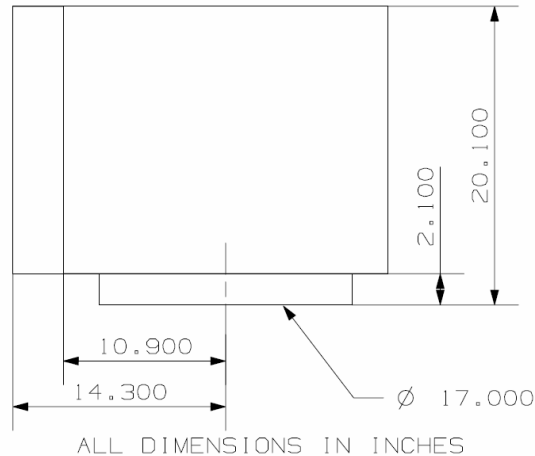
Figure 26.   NPSCuL Maximum Allowable Volume Envelope

P-PODs mount to the NPSCuL walls via eight #10–32 fasteners, using a bolt-hole pattern shown in Figure 27. Two P-PODs are mounted to each NPSCuL wall. These hole locations cannot be easily changed as any changes would require changing the P-POD bolt hole pattern, which is now an industry standard.
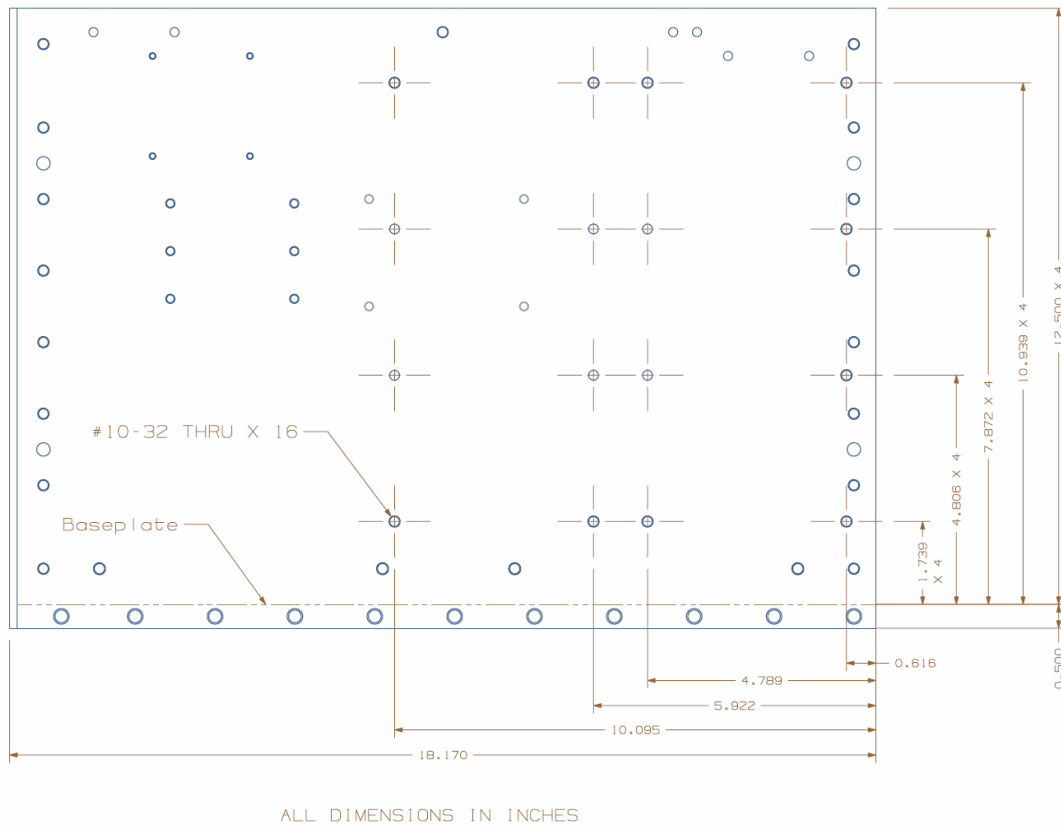
Figure 27.   NPSCuL Wall Showing P-POD Mounting Holes

To improve the environment seen by NPSCuL payloads, an attempt was made to reduce the effect of the three primary modes, discussed in Chapter II, Section 2. The base assumption while making design modifications was based on the results of Equation 1.4, which implies that as frequency increases, displacement for a given vibration input decreases. One method of achieving an increase in the natural frequency of a structure is by increasing the system stiffness while keeping the system mass constant, as is evident from Equation 1.2. Increasing the natural frequency of the walls by increasing their stiffness, would theoretically reduce the effect of localized panel bending.

To increase the stiffness of the NPSCuL walls, a decision was made to double the existing wall thickness. No trade studies on varying wall thicknesses were conducted due to schedule constraints. To maintain the mass of the existing ¼ inch thick NPSCuL walls, it would be necessary to reduce the ½ inch wall mass by 50%. To achieve this, an isogrid

design approach, outlined in Chapter III, Section B, was utilized. Additionally, since much of the modal strain energy was present in the adapter ring to baseplate joint, an approach that involved eliminating the joint between the adapter ring and baseplate by combining the two parts into a single part was attempted. The thickness of the baseplate was also increased from ½ inch to ¾ inch. To ensure that the redesigned NPSCuL structure was not any heavier than the original NPSCuL, the mass of the rectangular baseplate section was reduced by drilling a simple pocketed pattern, shown in Figure 30. Finally, the corner brackets from the original NPSCuL structure were eliminated, as the thicker walls could accommodate a direct wall-to-wall joint. The elimination of the four corner brackets added 2.42 lbm to the redesigned NPSCuL mass budget. The redesigned NPSCuL is henceforth referred to as the NPSCuL-v2, whereas the original NPSCuL design is referred to as NPSCuL-v1.

B.   ISOGRID: THEORETICAL CONCEPTS

An isogrid panel is a plate or face sheet with triangular integral stiffening ribs, commonly referred to as stringers [23]. The concept for isogrid structures was developed in 1964 by Dr. R. Meyer, who was tasked by NASA to find the optimum stiffening pattern for compressively loaded domes. The goal was to find a structural arrangement that negated the shortcomings of the known 0 to 90-degree and 45-degree patterns without increasing panel weight. The most promising concept was found to be the triangulation of stiffening members that took advantage of the fact that trusses are very efficient structures. It consisted of a lattice of intersecting ribs forming an array of equilateral triangles. The new structure was referred to as "Isogrid," since it behaves like an isotopic material [24].

A visual representation of a section of an isogrid panel is shown in Figure 28, where 'a' is the length of the equilateral triangle side, 'b' is the rib width, 'd' is the rib depth, 'h' is the equilateral triangle height and 't' is the thickness of the faceplate or skin.

47
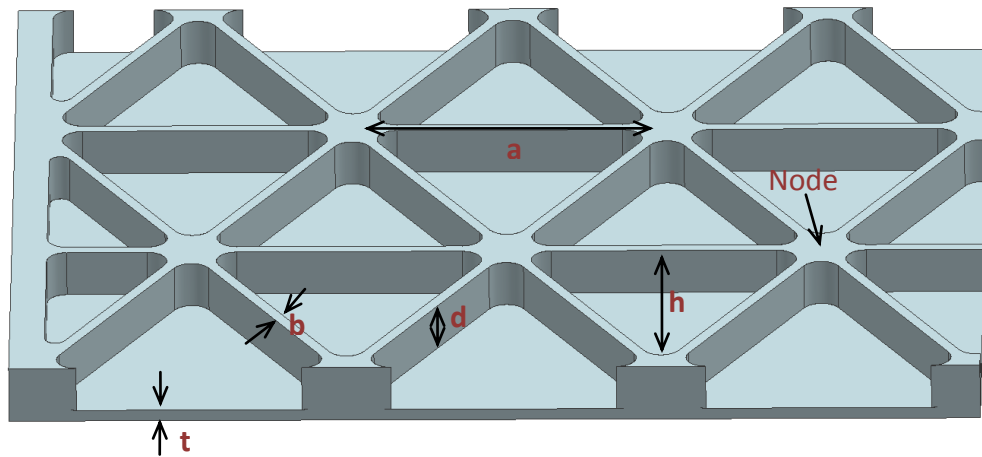
Figure 28.   Isogrid Parameter Definitions

The main resource for quick, back-of-the-envelope, isogrid design calculations is the *Isogrid Design Handbook* [25] prepared by the McDonnell Douglas Astronautics Company. The handbook outlines equations that can be utilized to estimate maximum rib and skin stresses for an isogrid structure.

Due to the hole-pattern constraints outlined in Section 3.A, it was necessary to divide the NPSCuL wall into sections with varying equilateral triangle heights. Additionally, it was necessary to maintain certain thick sections on the NPSCuL walls to allow for wall-to-wall mounting holes and to accommodate the P-POD bolt-hole pattern. This was necessitated as it was desirable to have the P-POD mounting holes located at the isogrid nodes. Isogrid structures are most efficient if the main load paths pass through the nodes. Having off-node load paths requires re-enforcement of the ribs and skin around the off-node load path, which can lead to increase in overall panel mass.

Since the Isogrid Design Handbook does not outline equations for analyzing a non-uniform isogrid panel, the equations outlined in the handbook were not utilized for analyzing the NPSCuL-v2 wall panels. Instead, all analysis relied on the FEM developed and is described in Chapter 3, Section 4.D. For completeness, however, useful equations from the handbook are summarized in Equations 1.10 - 1.15.

$$h = \frac{\sqrt{3}}{2}a \ ,$$ 1.10

48

where h is the triangle height and a is the length of the equilateral triangle side.

$$t* = \left(\frac{\beta}{1 + \alpha} \right)$$ 1.11

$$E* = E\left(\frac{(1 + \alpha)^2}{\beta} \right)$$ 1.12

$$\alpha = \frac{bd}{th}$$ 1.13

$$\beta = \sqrt{3\alpha(1 + \delta)^2 + (1 + \alpha)(1 + \alpha\delta^2)}$$ 1.14

$$\delta = \frac{d}{t} \ ,$$ 1.15

where $t*$ is the equivalent thickness and $E*$ is the equivalent modulus of elasticity that can be used in traditional structural monocoque equations, b is rib width, d is the rib depth, t is the face-sheet thickness, and $\alpha, \beta,$ and δ are non-dimensional parameters defined above. Additional equations for calculating panel buckling loads, pressure strength and shear strength are outlined in the NASA *Isogrid Design Handbook*.

C.   NPSCUL-V2

The NPSCuL-v2 design process included stiffening the sidewalls by doubling the wall thickness and reducing the panel weight by implementing an isogrid design. The baseplate and adapter ring were fused into a single part, as shown in Figure 30. This part is called the unibase.

OSL and NPS desired to have the NPSCuL-v2 structure ready in time for the ULTRASat and GRACE launches that were then scheduled for December 2014. The launches have since slipped to May 2015 for ULTRASat and August 2015 for GRACE. Due to schedule constraints and delivery dates that arose in response to the ULTRSat and GRACE launch schedules at the time, it became necessary to design, build and test NPSCuL-v2 within a period of four months. Given the short development cycle, it

became necessary to select a design direction and proceed with the analysis and manufacturing without conducting detailed trade studies. A decision was made to not exceed the NPSCuL-v1 structural weight while increasing the stiffness of the new structure.

Using that constraint, along with the volume and interface constraints levied by the LV provider, a decision was made to design a ½ inch thick isogrid wall. A ½ inch thick wall also allowed the four walls to be fastened to each other without using any brackets, which allowed more weight to be allocated to the unibase. The web depth was limited to no greater than four times the skin thickness, due to machining constraints. Exceeding the limit mentioned above can cause chatter while machining, which is not desirable as it becomes difficult to maintain a smooth surface finish. Maximizing the web depth on a ½ inch thick wall resulted in a 0.4 inch deep web, with 0.1 inch thick skin. The rib thickness was maintained at 0.1 inch, similar to the skin thickness.

The wall was sectioned into four pieces as shown in Figure 29. The isogrid equilateral triangles were sized to ensure that the P-POD mounting holes were located at the isogrid nodes. All fasteners used on NPSCuL-v2 are socket head caps (SHCs), and to make their heads flush with the wall exterior surface, all fastener holes are counter-bored. To allow adequate material between the counter bore and the triangle corners, a distance of 1/16 inches was maintained between the triangle corners and the counter-bored holes.

For sections B and D, shown in Figure 29, the triangle height required to maintain the nodes at the P-POD bolt holes was 1.937 inches. Using Equation 1.10, the length of the triangle side required to maintain that height was found to be 2.236 inches. In both sections B, C and D, shown in Figure 29, it can be seen that a few thick sections remain and the isogrid pattern is not continuous. This is due to the fact that the mounting points for the P-POD are fixed, but not uniformly spaced, and the isogrid has to be designed around these mounting points. For future revisions of NPSCuL, optimizing these thicker sections for mass may be evaluated.

While designing section A, the aim was to fit three complete triangles between the left edge of the wall and section B. This prevents the triangle size from getting too large,

50

and also provides mounting locations for ground support equipment (GSE) required during integration and test activities. The triangle height required to fit three triangles in the given area was 2.179 inches. The equilateral triangle side length associated with a height of 2.179 inches is 2.516 inches. The resulting wall panel had a mass of 6.2 lbm.
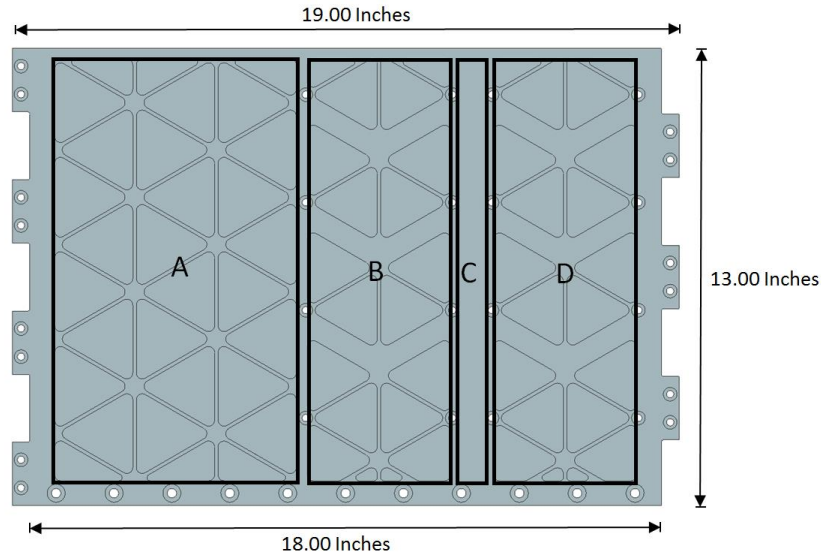
Figure 29.   NPSCuL-v2 Wall with Isogrid Pattern

To ensure that the effective thickness of the re-designed wall was at least equal to the thickness of the NPSCuL-v1 ¼ inch thick wall, equations 1.10 - 1.15 were utilized to derive the effective thickness of the re-designed walls. Since the re-designed isogrid wall does not have a continuous isogrid pattern, assumptions were made to arrive at the worst case effective thickness. It was assumed that the wall consisted of a continuous isogrid pattern with the larger of the two triangle sizes. The resulting equivalent thickness of the wall was found to be 0.36 inches, which is greater than the NPSCuL-v1 wall thickness of 0.25 inches. With the greater effective thickness, the re-designed wall is expected to be stiffer than the NPSCuL-v1 wall.

The unibase design was developed in consultation with The Aerospace Corporation, in El Segundo, California. Since the rocking modes on the NPSCuL-v1 design contributed significantly to the harsh vibration environment seen by the NPSCuL payloads, the base of the original structure was modified to increase stiffness. Increased

stiffness was achieved by removing the joint between the NPSCuL ring and baseplate and fusing the two parts together. The joint between the two parts was filleted to allow for a favorable stress distribution. Since the joint between the adapter ring and baseplate was removed, and since the corner brackets were not utilized on NPSCuL-v2, the number of joints reduced from 204 to 172. Joints between two interfaces often lead to a reduction in the vibration environment as energy is dissipated at structural joints. While the reduction in joints on NPSCuL-v2 would lead to an expectation of lower damping, the benefit gained from increasing stiffness was expected to outweigh the benefit gained from increased damping.

The flanged section of the unibase was modified for ease of access, to allow for easily available ratcheting tools to be utilized while fastening the 24 bolts that secure NPSCuL to the shaker during testing and the ABC plate during flight. The ability to use ratcheting tools significantly reduces processing time during integration and test activities.

In addition to the changes mentioned above, the thickness of the rectangular plate section of the unibase, shown in Figure 30, was increased to 0.75 inches from 0.5 inches. The skin of the baseplate was maintained at 0.2 inches in the pocketed sections, since the baseplate carries a large part of the total load during vibration. The rib thicknesses were also maintained at 0.2 inches. A minimum of 1.0 inch of material was maintained along the outer edge of the baseplate to allow adequate room for the NPSCuL wall to baseplate fasteners.
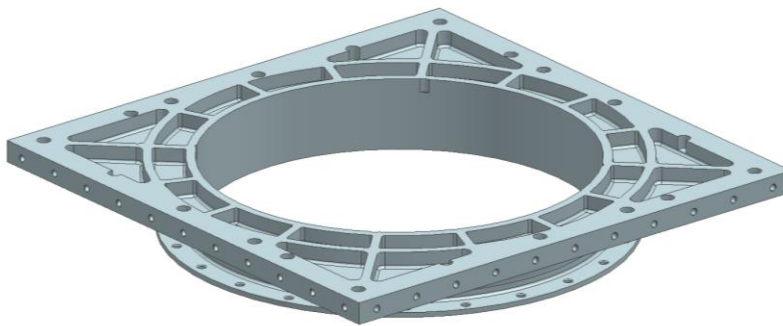
Figure 30.   NPSCuL-v2 Unibase

The overall height of the unibase was 2.45 inches, whereas the overall height of the NPSCuL-v1 adapter ring and baseplate was 2.6 inches, as shown in Figure 31. By lowering the height of the unibase by 0.15 inches, as compared to the NPSCuL-v1, the overall Z-direction CG of the integrated re-designed NPSCuL-v2 would also be lowered by 0.15 inches. This was also expected to be beneficial for reducing the vibration environment, as a lower CG results in lower amplification.
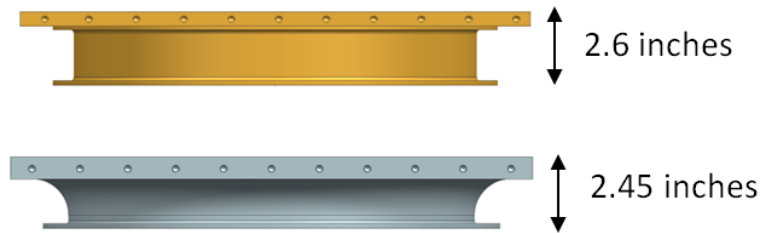
Figure 31.   Comparison of NPSCuL-v1 Baseplate/Adapter Ring (Top) and NPSCuL-v2 Unibase (Bottom) Heights

A comparison of the NPSCuL-v1 Computer Aided Design (CAD) model and the NPSCuL-v2 CAD model is shown in Figure 32. Table 5 summarizes the mass properties of the NPSCuL-v1 and NPSCuL-v2. From Table 5, it is evident that the goal of keeping the mass of NPSCuL-v2 at or below the mass of the NPSCuL-v1 structure was achieved.
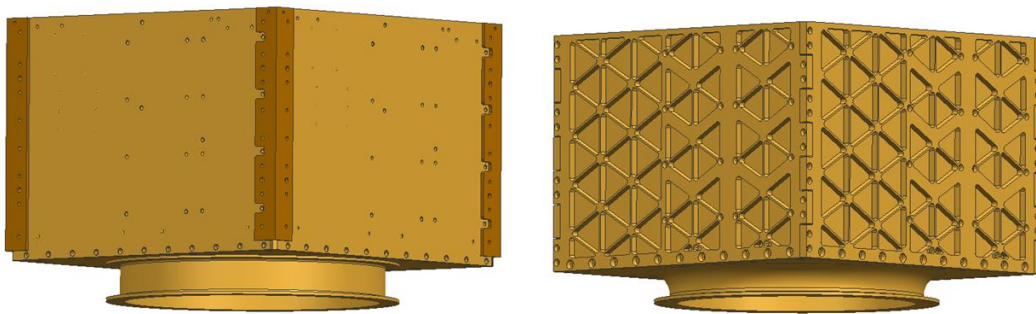
Figure 32.   NPSCuL-v1 Design (Left) and NPSCul-v2 Design (Right)

Components	NPSCuL-v2	NPSCuL-v2
Wall Mass x 4 (lbm)	23.54	24.80
Bracket Mass x 4 (lbm)	2.40	N/A
Adapter Ring Mass (lbm)	3.40	N/A
Baseplate Mass (lbm)	10.29	N/A
Unibase Mass (lbm)	N/A	14.60
Total Mass (lbm)	39.63	39.40

Table 5.   NPSCuL-v1 and NPSCuL-v2 Mass Summary

D.   FINITE ELEMENT ANALYSIS

After completing the NPSCuL-v2 CAD design, it was necessary to show, via a finite element stress analysis, that the design would be able to survive the LV provider-specified loads. It was also necessary to determine the primary modes of the NPSCuL-v2 structure in each of the three Cartesian axes. The NPSCuL-v2 FEM was developed using a software package called NX, Version 8.5, and the FEM solver used was NASA Structure Analysis (NASTRAN).

> The analysis software assembles the mass and stiffness matrices for the elements into global matrices for the overall structure. Each node has six DOFs—three translations and three rotations—so the total number of DOFs in the model equals six times the number of nodes minus any constrained DOFs. [14, p. 575]

While creating an FEM from CAD geometry, it becomes necessary to idealize the CAD geometry to make the analysis efficient. For instance, small holes are often not modeled, and fillets are removed.

Before developing a finite element model, it is important to understand the purpose that they will be used for. For the NPSCul-v2 model, the uses are twofold:

- Internally by NPS to ensure that stress margins are positive
- Externally by ULA for dynamic analysis

A stress model needs to be detailed enough to model localized stress concentrations, and a dynamic model needs to be simple and predict global behaviors of the structure. The dynamic model is used by ULA for their coupled loads analysis (CLA) to determine the impact of NPSCuL on the primary spacecraft.

Once the model type has been selected, the element type and level of detail needs to be determined. This process can be time consuming and is often based on engineering judgment. A summary of some of the commonly used finite element types is shown in Table 6.

Element Type	Features and Applications
Rod	- Carries only axial loads - Good for truss members with pinned ends
Beam	- Carries all axial loads, shears, and moments - The user can specify offsets for centroid and shear center - Good for modeling beams, frame members, and stringers
Shell	- Five DOFs per grid (no out-of-plane rotation) - Good for modeling shells and detailed modeling of thin walled structures - Triangular and quadrilateral shapes; quads don't have to be rectangular
Shear	- Carries in-plane shear loads - Good for representing buckled skin that carries shear by diagonal tension
Solid	- No rotational degrees of freedom; relies on force couples to carry moments - Good for detailed modeling of thick-walled structures to predict how stress varies through the thickness

Table 6.   Common Types of Finite Elements [14, p. 577]

1.   Wall FEMs

Prior to creating an FEM of the integrated NPSCuL structure, FEMs of the individual components were first created. The initial aim was to create an FEM complex enough to accurately model stress distributions, but simple enough to have a manageable model size and run-time. This FEM is referred to as the Wall-FEM-1.

For the Wall-FEM-1, the NPSCuL wall was idealized and partitioned along the isogrid triangle ribs and at boundaries between the thin face sheet and the thicker outer sections. The partitioned wall is shown in Figure 33.
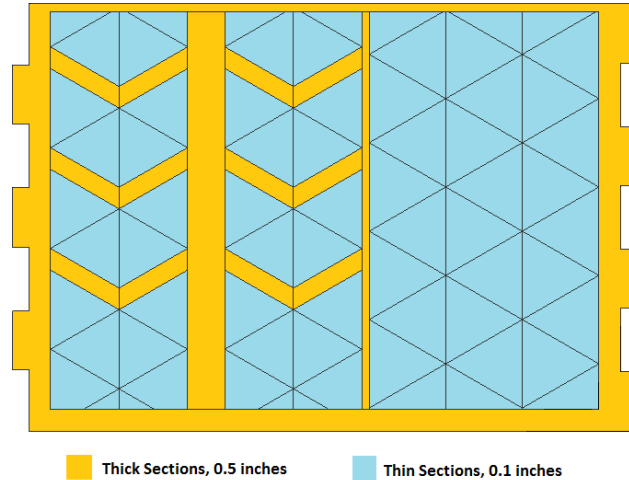
Figure 33.　　Wall-FEM-1 Idealized and Partitioned Model, Bottom View

Since the aim of the Wall-FEM-1 model was to create a simplified finite element model, the isogrid face sheet was meshed using shell elements, known as CQUAD4, with a thickness of 0.1 inches. The thicker sections around the edges and in-between the various isogrid patterns were meshed using shell elements with a thickness of 0.5 inches. When using shell elements with varying thicknesses, it becomes necessary to ensure that the plane of origin of the elements of differing thickness line up with each other. To ensure that all the shell elements line up, it becomes necessary to offset the mid-plane of the thicker shell sections. The auto-mesh tool was utilized to define the mesh size, which varied between 0.15 and 0.25 inches. During the auto-mesh process, triangular shell elements were also allowed to be inserted into the mesh. After the shell meshing process was completed, an element quality check was conducted on all elements, and all elements that failed the default element quality check determined by the software package, were manually fixed by re-orienting element nodes.

The isogrid ribs were modeled using beam elements with rectangular cross-sections. The width of the element was 0.1 inches, with a height of 0.4 inches. Beam elements were manually inserted onto the shell mesh at the boundaries of the isogrid triangles. As was the case with the shell elements, it is necessary to apply an offset to the beam elements to ensure that they are appropriately aligned with the shell elements. It is

also necessary to ensure correct orientation of the beam elements. This can be easily visualized by altering the display of the FEM to view the beams as solids. The Wall-FEM-1 is shown in Figure 34.
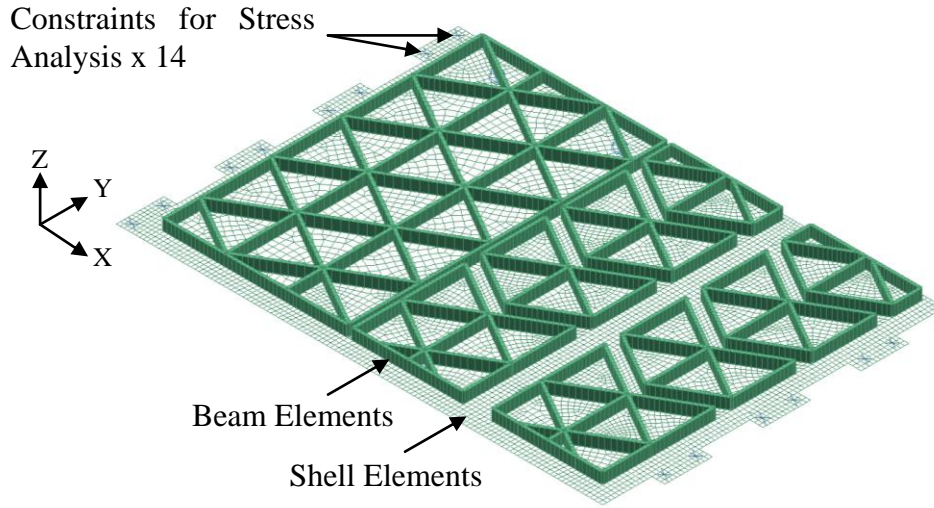
Figure 34.   Wall-FEM-1 Consisting of Thin Shell and Beam Elements (Beam Elements Shown as Solids for Visual Clarity)

The material properties utilized for the wall, i.e., material properties for Aluminum 7075-T7351 are summarized in Table 7.

Material Property	Value
Mass Density (ρ)	0.101 lbm/in^3
Young's Modulus (E)	1.03E7 lbf/in^2
Poisson's Ratio (v)	0.33
Shear Modulus (G)	3.9E6 lbf/in^2

Table 7.   Material Properties for Aluminum 7075-T7351 [26]

With the FEM complete, a real Eigenvalue solution, also known as a modal solution was conducted on the wall, with free-free boundary conditions. The term free-free implies that no boundary conditions are applied to the wall FEM. Such a solution should yield six rigid body modes, i.e., modes that cause an infinite deflection along all the unconstrained DOFs. These modes generally occur at very low frequencies (small positive

values close to zero Hz), and are not utilized for any analysis. The first four mode shapes that have physical meaning and their modal frequencies are shown in Figure 35.

Mode 1: 170.6 Hz   Mode 2: 208.2 Hz

Mode 3: 431.2 Hz   Mode 4: 464.1 Hz

Figure 35.   Wall-FEM-1 Mode Shapes and Frequencies

A stress analysis was also conducted on the Wall-FEM-1. The wall was fixed along two opposite edges, shown in Figure 34. Gravity loads with values of 5 G's in the X and Y axes and 7G's in the Z axis, all in the local wall coordinate system, were applied. These loads are the same as the design loads outlined in the OUTSat to AtlasV/ABC ICD. This loading condition does not have any significance, and was only utilized to create a common loading condition by which various wall FEM's could be evaluated.

Elemental Von-Mises stresses for the FEM were recovered and plotted. In a body that is acted upon by stresses in all three directions, Von-Mises stress gives the equivalent stress at a point in the body. This property of Von-Mises stress makes it one of the most widely used criteria for predicting failure when designing a structure. The maximum section stress results are shown in Figure 36. As expected on a wall with opposite edges fixed, the maximum stress occurs at the locations where the fixed boundary conditions are applied.

58

914.24
838.38
762.53
686.68
610.82
534.97
459.12
383.26
307.41
231.56
155.70
79.85
4.00

Units = lbf/in^2(psi)
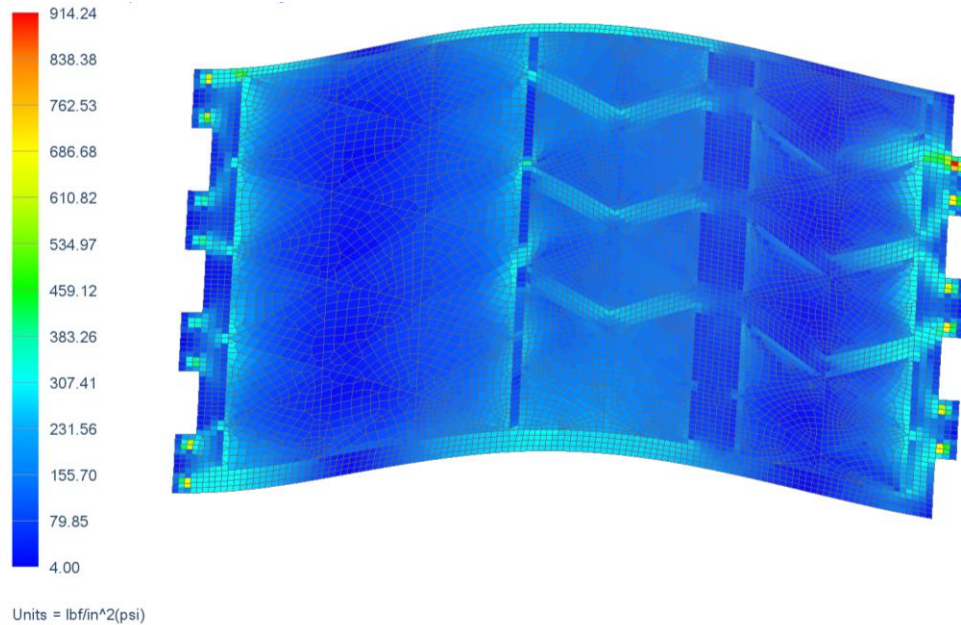
Figure 36.   Wall-FEM-1 Stress Analysis Results

A second modelling approach was attempted where the face sheet of the isogrid wall was modeled using CQUAD4 shell elements, the thicker sections were modeled using 10-noded tetrahedral elements and the isogrid ribs were modeled using vertically oriented CQUAD4 shell elements. This FEM is referred to as Wall-FEM-2 and is shown in Figure 37. The advantage of using 10-noded tetrahedral elements over the simpler 4-noded elements is the added ability of modeling complex shape functions of the FEM. It is important to note that solid elements and shell elements have differing degrees of freedom. Solid elements have three translational DOFs, whereas shell elements have five DOFs. While combining shell and solid elements together, it becomes necessary to resolve this discrepancy by joining the two elements together using the rigid body element -3 (RBE3). RBE3s are most commonly used to transmit forces from a reference point to several non-collinear points, and they can also be used to transition between different element types.
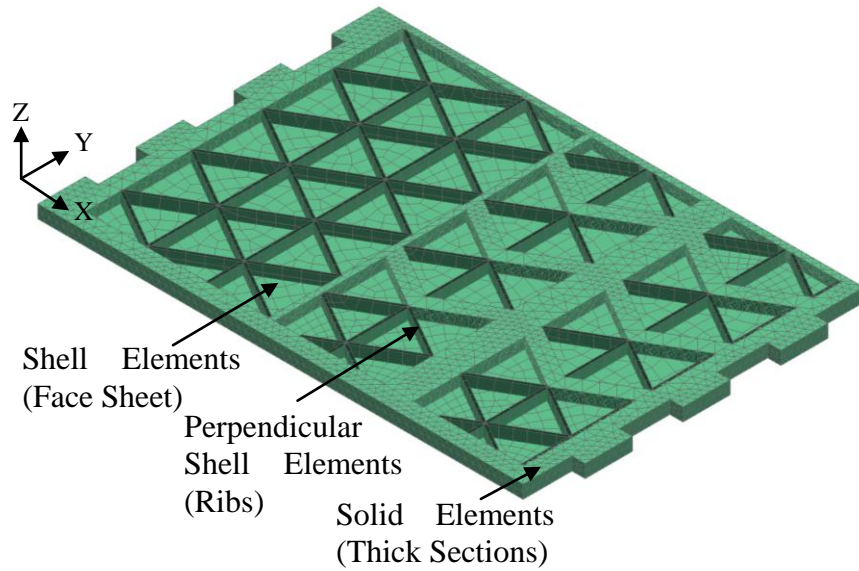
Figure 37.   Wall-FEM-2 Consisting of Thin Shell and Solid Elements

With the FEM complete, a modal solution was conducted on the wall, with free-free boundary conditions. The first four mode shapes that have physical meaning and their modal frequencies are shown in Figure 38.
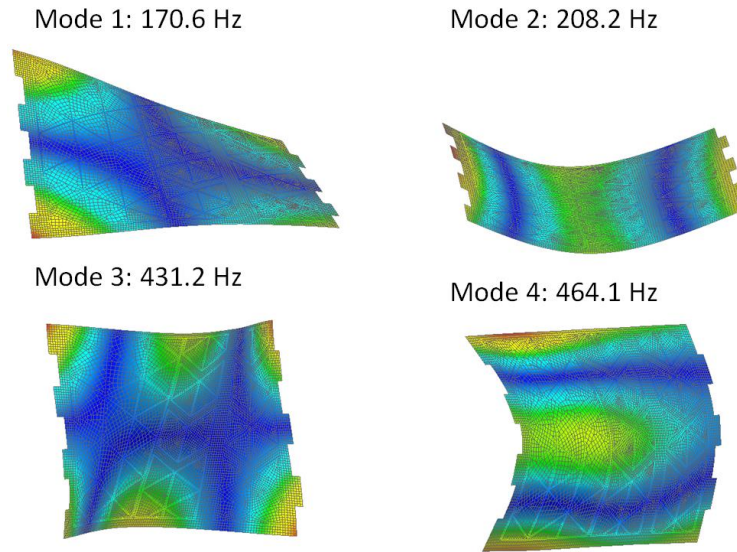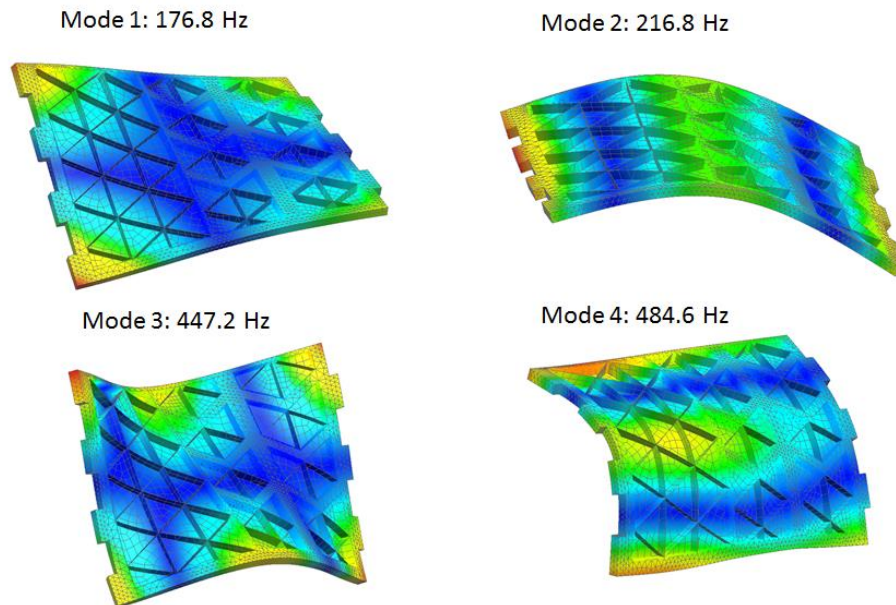

Figure 38.   Wall-FEM-2 Mode Shapes and Frequencies

A stress analysis was also conducted on the Wall-FEM-2. The wall was fixed along two opposite edges, similar to the Wall-FEM-1 model. Gravity loads with values of 5 G's in the X and Y axes and 7G's in the Z axis, all in the local wall coordinate system, were applied.

Elemental Von-Mises stresses for the FEM were recovered and plotted. The stress results are shown in Figure 39. The stress results in this case are counter-intuitive, with the maximum stresses occurring on the top and bottom flanges of the wall, instead of at the locations where the wall is constrained. A possible reason for this is localized effects occurring at locations where shell and solid elements are joined together. Due to the nature of the stress results, this model was ruled out as a possible stress model.
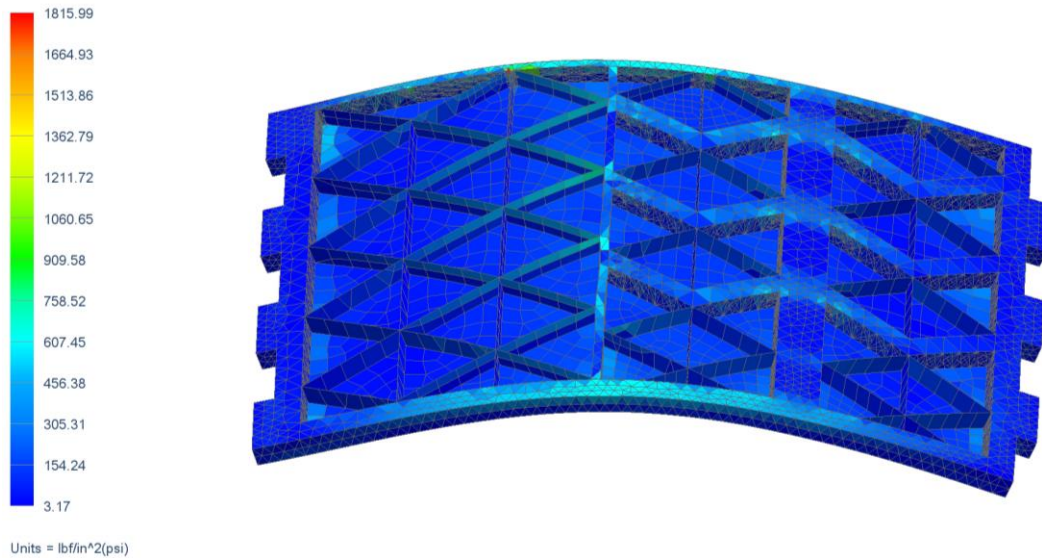
Figure 39.   Wall-FEM-2 Stress Analysis Results

A third model, known as Wall-FEM-3, composed of only 10-noded tetrahedral elements, was created to rule out any issues arising from utilizing a mix of elements with varying degrees of freedom. An FEM consisting of only higher-order solid elements is desirable for detailed modeling of stress distributions within a structure. Solid element models are complex and generally have large file sizes and long run-times. It becomes necessary to use an appropriate element size so as to warrant the increase in complexity and run-time.

To arrive at an appropriate element size for the Wall-FEM-3, five wall FEMs were created, having element sized of 0.35 inches, 0.3 inches, 0.25 inches, 0.2 inches and 0.15 inches respectively. A minimum of two elements were maintained through the smallest thickness in the wall. All five wall models were constrained along two opposite edges, similar to Wall-FEM-1. An FEM for the model having element sizes of 0.2 inches is shown in Figure 40.
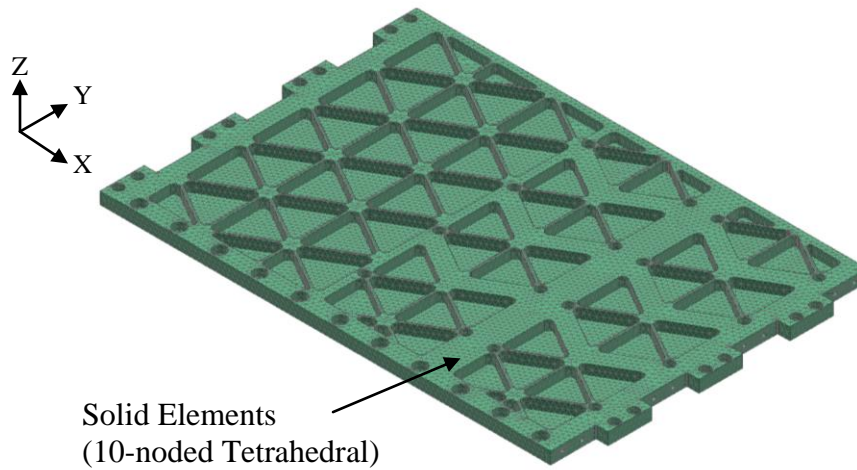
Figure 40.   Wall-FEM-3 Consisting of 10-noded Tetrahedral Elements

A stress analysis was conducted on all five FEMs, to arrive at an adequate element size for Wall-FEM-3. Gravity loads with values of 5 G's in the X and Y axes and 7G's in the Z axis, all in the local wall coordinate system, were applied.

Elemental Von-Mises stresses for the FEMs were recovered and plotted. The stress results for a 0.2 inch element size are shown in Figure 41.
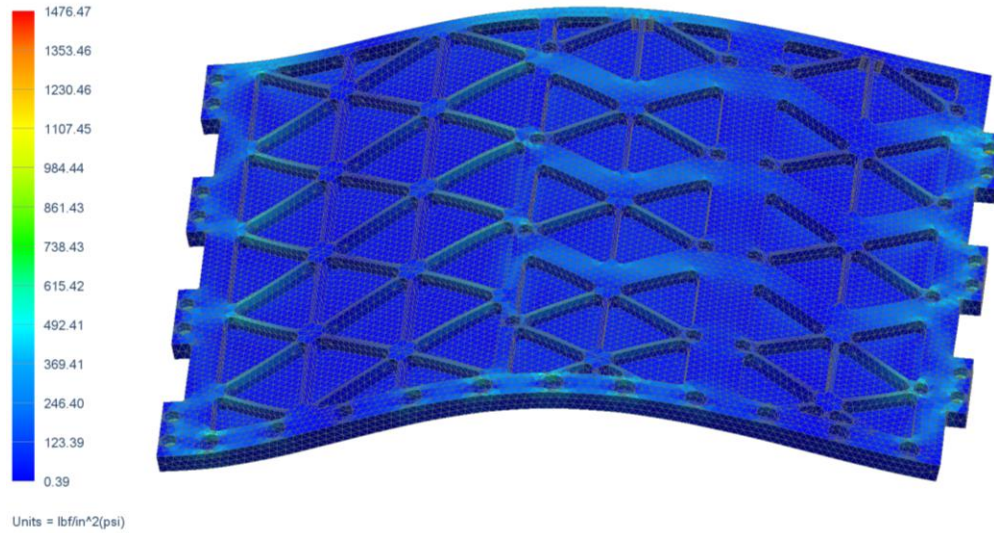
Figure 41.   Wall-FEM-3 Stress Analysis Results

The stress results from all five FEMs are summarized in Table 8. Stress is measured in pounds per square-inch or psi.

Model Element Size	Number of Nodes	Maximum Stress (psi)
0.35 inches	268,207	1771
0.30 inches	303,243	1797
0.25 inches	356,094	1858
0.20 inches	490,835	1476
0.15 inches	792,250	1587

Table 8.   Summary of Solid Element Wall FEM Stress Results

From Table 8 it is evident that the stress results converge with decreasing element size. It is also seen that the number of nodes, and hence model complexity, increase significantly with decreasing element size. Ideally, an element size of 0.15 inches or smaller would be selected for the wall FEM. However, since the model complexity, and hence FEM runtime nearly doubles by going from an element size of 0.20 inches to 0.15 inches, and since the stress results of both those FEMs are within 111 psi or 6.9% of each other, an element size of 0.2 inches was deemed acceptable for Wall-FEM-3.

A modal analysis was conducted on Wall-FEM-3, with free-free boundary conditions. The first four mode shapes that have physical meaning and their modal frequencies are shown in Figure 42.

Mode 1: 177.4 Hz   Mode 2: 210.2 Hz

Mode 3: 440.0 Hz   Mode 4: 472.3 Hz
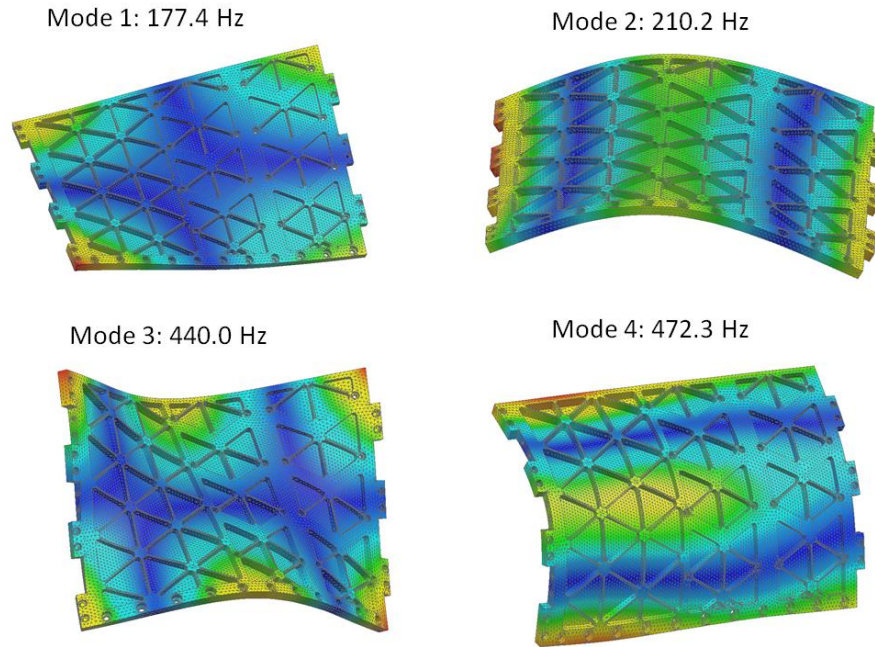
Figure 42.   Wall-FEM-3 Mode Shapes and Frequencies

An impact hammer modal test or tap test was conducted on a manufactured NPSCuL-v2 wall to confirm that the predicted modal frequencies were within the generally accepted range of 10% of the measured modal frequencies. A full scale wall was suspended from a rigid bar using nylon wire to simulate a free-free boundary condition. The wall was then instrumented with a tri-axial accelerometer as shown in Figure 43.
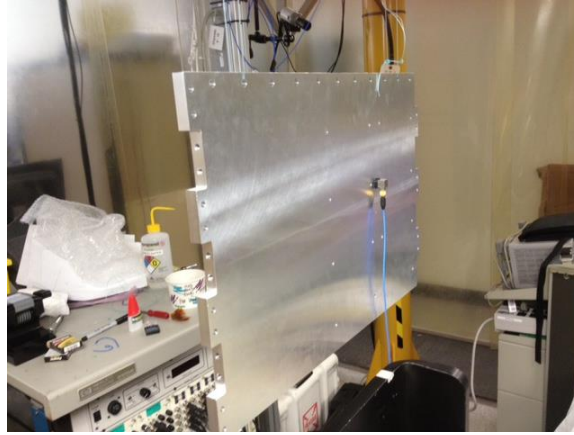
Figure 43.   NPSCuL-v2 Wall Tap Test

The accelerometer was attached to the wall using wax and was connected to a signal analyzer. An impact hammer, also connected to the signal analyzer, was utilized to "tap" the wall, providing an input broad spectrum impulse forcing function. The signal analyzer was setup to display a frequency response function (FRF). The accelerometer was moved to five locations on the wall and five averaged readings were taken at each location. A comparison of the modal frequencies measured from the tap test and the modal frequencies derived from the Wall-FEM-1, Wall-FEM-2 and Wall-FEM-3 are summarized in Table 9.

From Table 9, it can be seen that all three wall FEMs predict the wall modal frequencies to within 3.8% of the frequencies measured from the tap test. All three FEMs are suitable for a dynamic model; however, due to added accuracy and reduced complexity, Wall-FEM-1 is the obvious choice for the assembled NPSCuL-v2 dynamic model.

Mode	Tap Test Frequency (Hz)	FEM-1 Frequency (Hz)	% Diff. Tap Test	FEM-2 Frequency (Hz)	% Diff. Tap Test	FEM-3 Frequency (Hz)	% Diff. Tap-Test
1	174	171	1.7	177	1.7	177	1.7
2	209	208	0.5	217	3.8	210	0.5
3	432	431	0.2	447	3.5	440	1.9
4	472	464	1.7	485	2.8	472	0

Table 9.   Comparison of Tap Test Modal Frequencies and FEM Derived
Modal Frequencies

To conduct a stress analysis on the assembled NPSCuL-v2 FEM, a detailed model is required. Each wall of NPSCuL-v2 must be represented using only shell or solid elements. For complex geometry, according to leading structural engineers Dr. Young Kwon (NPS) and Joseph Maly (CSA Engineering), higher order solid elements are preferred and considered to provide the most accurate results. Taking into account industry standards, Wall-FEM-3, consisting of 10-noded tetrahedral solid elements, was selected for the NPSCuL-v2 stress model.

2. Unibase FEMs

The unibase, shown in Figure 30, has complicated geometry with many curved surfaces. The unibase was modeled using only 10-noded tetrahedral elements to simplify the modeling process. The unibase is made of aluminum 7075-T7351, and the properties used for this material are summarized in Table 7.

Four unibase FEMs were created, having element sizes of 0.4 inches, 0.35 inches, 0.3 inches and 0.25 inches respectively. A unibase FEM having an element size of 0.30 inches is shown in Figure 44.

A stress analysis was conducted on each of the four unibase FEM's to determine an appropriate element size. Each hole on the 15-inch bolt-hole-circle was tied to a node at the center of the bolt-hole-circle. This node at the center was constrained using a fixed constraint, which means that no movement was allowed in any of the six DOFs. Gravity loads with values of 5 Gs in the X and Y axes and 7Gs in the Z axis, all in the local unibase coordinate system, were applied. Elemental Von-Mises stresses for the FEMs were recovered and plotted. The stress results for a 0.30 inch element size are shown in Figure 45.
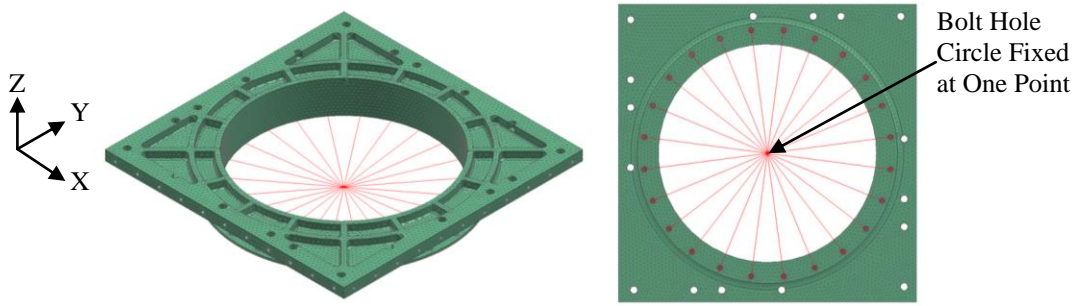
Figure 44.   Unibase-FEM Isometric (Left) and Bottom (Right) Views
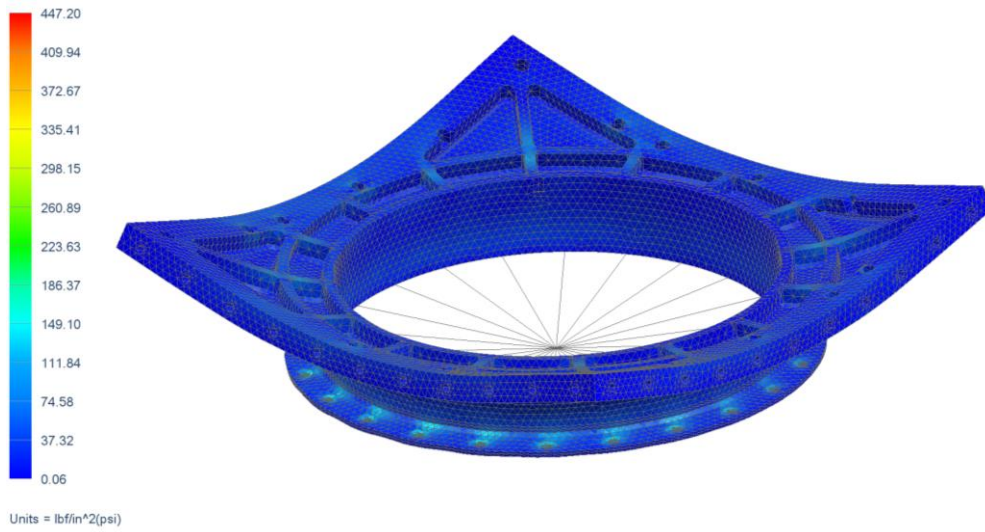
Figure 45.   Unibase FEM Stress Analysis Results

The stress results from all four stress cases are summarized in Table 10. From Table 10, there is no apparent trend visible from the four cases that were run. A possible cause for this may be due to reduction in element quality with reducing element size. To account for the worst-case scenario, the FEM element size that produced the highest stress result was selected as the unibase FEM, i.e., the FEM with 0.3 inch elements. This FEM was used for both the dynamic model NPSCuL FEM and the stress model NPSCuL-v2 FEM.

Model Element Size	Number of Nodes	Maximum Stress (psi)
0.40 inches	174,429	341
0.35 inches	189,910	482
0.30 inches	230,750	513
0.25 inches	276,475	447

Table 10.   Summary of Solid Element Unibase FEM Stress Results

A modal analysis was conducted on the unibase FEM with an element size of 0.3 inches, with free-free boundary conditions. The first two mode shapes that have physical meaning and their modal frequencies are shown in Figure 46.

Mode 1: 253.5 Hz   Mode 2: 360.9 Hz
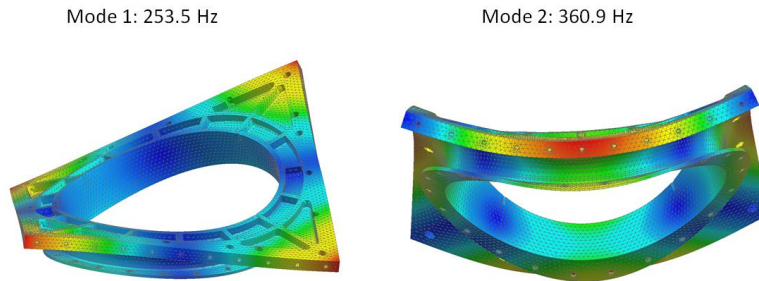
Figure 46.   Unibase FEM Mode Shapes and Frequencies

Using a similar method described in Chapter III, Section D.1, a tap test was conducted on a manufactured full scale unibase model. The test setup for the unibase tap test is shown in Figure 47.
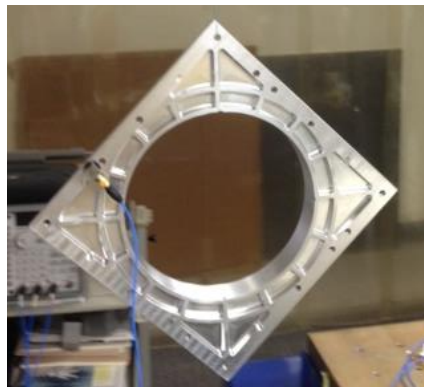
Figure 47.   Unibase Tap Test Setup

Only the primary mode was seen clearly during the unibase tap test. The FEM predicted primary mode frequency was at 253 Hz, whereas the frequency measured from the tap test was at 247 Hz, i.e., within 2.4% of each other. Since the two frequencies are within the generally accepted 10% threshold of each other, the unibase FEM with an element size of 0.3 inches was deemed acceptable for usage in both the dynamic and stress NPSCuL-v2 FEMs.

3. NPSCuL-v2 Dynamic Model

The integrated NPSCuL-v2 dynamic model needed to be simple enough to have a short runtime and to be utilized by ULA for a CLA. Since the Wall-FEM-1, comprised of thin shell elements and beam elements, adequately predicted the first four modes of the isogrid wall, and was simple enough to have a short runtime, it was selected for use in the NPSCuL-v2 dynamic model. While three of the four NPSCuL-v2 walls are identical, one of the walls is unique as the SAD attaches to it. As a result, the FEM for the SAD wall was modified to include mounting rails for the SAD, modeled using thin shell elements. The unibase was modeled using solid tetrahedral elements as described in Chapter III, Section D.2.

The wall and unibase FEMs were assembled into a single FEM. The eight loaded P-PODs and the SAD were modeled using lumped mass elements. These elements were located at the CG coordinates of each P-POD and the SAD within NPSCuL. The masses and CGs of NPSCuL-v2 and its components in NPSCuL coordinates are summarized in Table 11.

The P-POD lumped masses were connected to the NPSCuL-v2 walls using eight RBE2 elements, since each P-POD connects to the NPSCuL-v2 walls using eight #10-32 fasteners. A beam element, having the cross section of a #10-32 fastener and a length of 0.05 inches was inserted between each of the eight RBE2 elements and the corresponding nodes on the NPSCuL-v2 wall. Since the fasteners on NPSCuL-v2 are made of A-286 super alloy, these beam elements were assigned A-286 material properties. The advantage of modeling a fastener using a short beam element is that the stiffness can be adjusted to improve correlation between predicted and measured results.

Item	Mass (lbm)	X_{CG} (in)	Y_{CG} (in)	Z_{CG} (in)
P-POD 1	17.8	15.85	15.89	28.80
P-POD 2	17.8	15.85	2.42	28.80
P-POD 3	17.8	15.89	-15.85	28.80
P-POD 4	17.8	2.42	-15.85	28.80
P-POD 5	17.8	-15.85	-15.89	28.80
P-POD 6	17.8	-15.85	-2.42	28.80
P-POD 7	17.8	-15.89	15.85	28.80
P-POD 8	17.8	-2.42	15.85	28.80
SAD	4.5	0.00	29.74	19.65
NPSCuL-v2 Sturcture	17.81	0.00	0.00	14.65
Integrated NPSCuL-v2	186.15	0.00	0.28	10.07

Table 11.   NPSCuL-v2 Integrated and Component Masses and CGs

The P-POD lumped mass element to NPSCuL-v2 wall connections are shown in Figure 48. A similar approach was utilized for all wall-to-wall connections. The wall-to-wall connections are made using #10-32 fasteners, and beam elements with the cross section of a #10-32 fastener, and length of 0.05 inches were utilized to connect nodes on two adjacent walls. Similarly the SAD-to-wall connections were made using a combination of RBE2 and beam elements with the cross section of a #10-32 fastener.
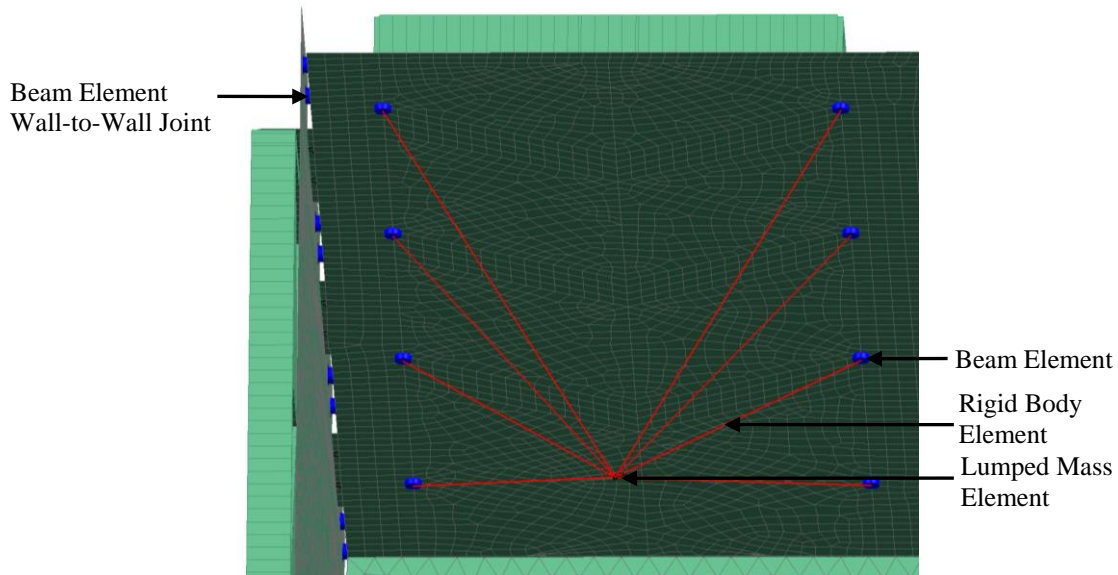
Figure 48.   Wall-to-Wall and P-POD to Wall FEM Connections

The connections between the unibase and NPSCuL walls were made by tying all the nodes in each fastener hole on the unibase to a single node using RBE2 elements. The RBE2 elements were constrained in DOFs 4, 5 and 6, as solid elements do not have rotational DOFs. The single RBE2 source node was then connected to the appropriate node on the NPSCuL-v2 wall using a beam element. Since the fasteners used to make the connection between the NPSCul-v2 walls and baseplate have a ¼ inch diameter, the beam elements were given a ¼ inch cross-section, and material properties corresponding to A-286 super alloy. The length of the beam elements was kept at 0.05 inches. A detailed view of the unibase-to-wall connections is shown in Figure 49.
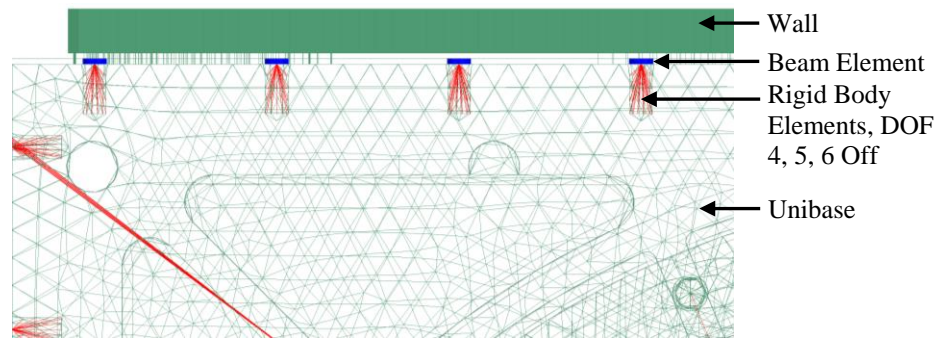
Figure 49.   Unibase-to-Wall FEM Connections

The assembled NPSCuL-v2 dynamic FEM is shown in Figure 50.
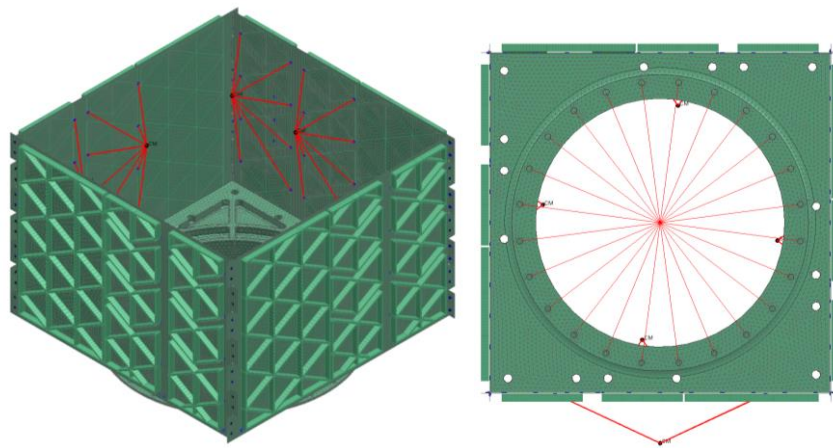
Figure 50.   NPSCuL-v2 Dynamic FEM Isometric (Left) and Bottom View (Right)

71

The NPSCuL-v2 dynamic FEM was fixed in all six DOFs at the center of the 15 inch bolt-hole-circle on the unibase as shown in Figure 50. A modal analysis was conducted on the NPSCuL-v2 dynamic FEM. The first mode shape, along with the primary mode shapes in each axis, and their modal frequencies are shown in Figure 51.

Mode 1: 49.23 Hz, Low Mass Participation

Mode 2: 77.6 Hz, Primary Y-axis Mode

Mode 3: 79.5 Hz, Primary X-axis Mode

Mode 8: 172.7 Hz, Primary Z-axis Mode
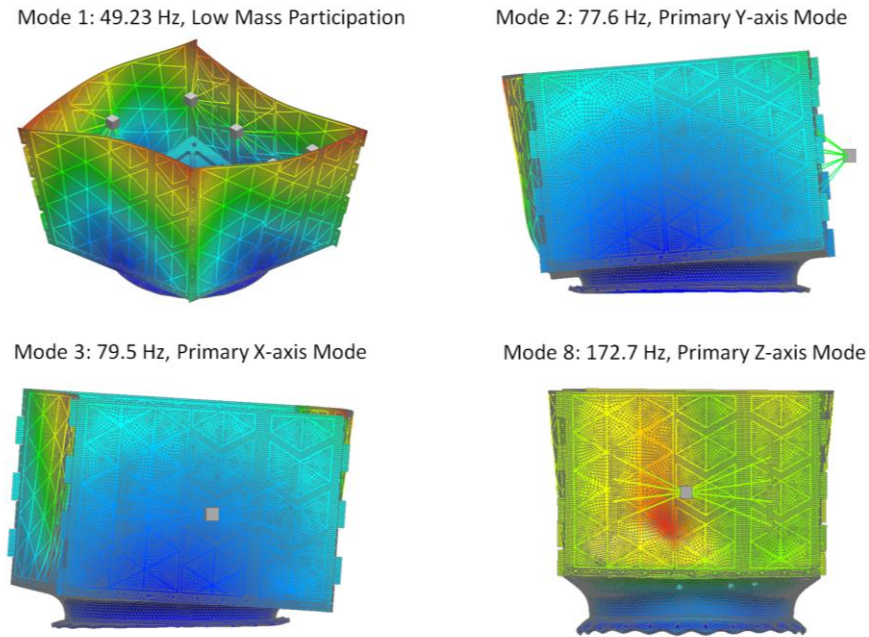
Figure 51.   NPSCuL-v2 Primary Modes, Dynamic FEM

A summary of the first eight modes along with their effective mass fractions is shown in Table 12. A comparison of the fundamental frequencies of NPSCuL-v2, shown in Table 12, to the fundamental frequencies of NPSCuL-v1, shown in Table 1, shows that NPSCuL-v2 is indeed stiffer than NPSCuL-v1. The fundamental frequencies of the re-designed structure are ~24 Hz higher than those of the original structure in the X and Y axes, and ~ 76 Hz higher than the original structure in the Z axis.

Mode	Description	Frequency (Hz)	Effective Mass (X)	Effective Mass (Y)	Effective Mass (Z)
1	First mode with low mass participation	49.23	0.000	0.000	0.000
2	First Y axis rocking mode	77.67	0.023	0.664	0.000
3	First X axis rocking mode	79.39	0.667	0.023	0.000
4	Wall panel bending, Y axis	104.22	0.000	0.000	0.003
5	Wall panel bending, X axis	107.69	0.004	0.000	0.008
6	Higher order rocking mode	141.27	0.003	0.004	0.001
7	Higher order rocking mode	142.93	0.040	0.002	0.000
8	First Z axis pogo mode	172.66	0.000	0.000	0.813

Table 12.   NPSCul-v2 Modes and Effective Mass Summary

To verify the dynamic FEM, sine sweeps were conducted on the assembled NPSCul-v2 structure. The sweeps were conducted at 0.5 G from 20 Hz - 2000 Hz at a sweep rate of 4 oct/min.

Two separate test setups were utilized. The first, referred to as a true fixed-base setup, involved using a solid, 2 inch thick adapter plate between NPSCuL and the shaker. The second, referred to as the FLVT setup was previously described in Chapter II, Section C.4. The rationale behind using two separate setups was that the true fixed-base setup is expected to be stiffer than the FLVT setup, since the FLVT plate is hollowed out in the middle to minimize mass. The fixed-base test setup is shown in Figure 52.
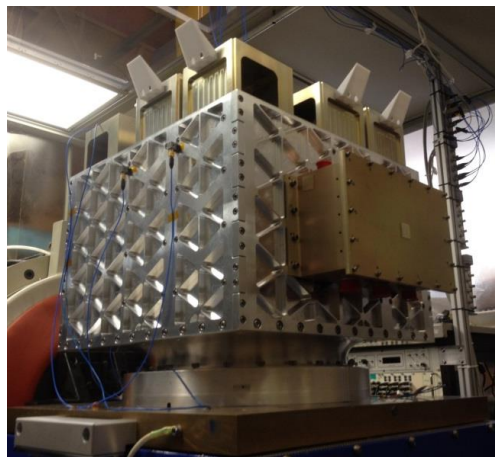

Figure 52.   NPSCuL-v2 Fixed-Base Test Setup

The fixed-base sine sweep was only conducted in the Y-axis to demonstrate that the FLVT setup is less stiff than the true fixed-base setup. The results of the Y-axis sine sweep tests on both setups are shown in Table 13.

Dynamic FEM Predicted Frequencies (Hz)	Measured Frequncies, Fixed Base Setup (Hz)	% Difference Between FEM and Fixed-Base Frequencies	Measured Frequncies, FLVT Setup (Hz)	% Difference Between FEM and FLVT Frequencies
49.2 Low Mass Participation	54.3	9.3	51.7	4.8
77.6 Primary Y-Axis Mode	75.1	3.3	63.0	23.1
104.2	96.2	8.3	81.1	9.8

Table 13.   Comparison of Dynamic FEM Predicted Frequencies with Fixed-Base and FLVT Test Setup Measured Frequencies

From Table 13, it can be seen that at the primary Y-axis mode, the frequency measured from the true fixed-base test setup differs by only 3.3% from the FEM predicted frequency, whereas the frequency measured from the FLVT test setup differs by 23.1% from the FEM predicted frequency. This result shows that variations around 23% can be expected between the FLVT test setup measured frequencies and FEM predicted frequencies, and that the true-fixed base test-setup frequency can still be well within 10% of the FEM predicted frequencies. This result also shows that the Y-axis FEM results are verified. Using this argument, X and Z axis sine sweeps were conducted on the FLVT test setup. The results of the X and Z sine sweeps, compared to the FEM results are shown in Table 14.

Based on the result that frequencies measured using the FLVT test setup can vary by approximately 20% from the FEM predicted frequencies, Table 14 shows that the dynamic FEM frequencies are verified through test.

Mode	Dynamic FEM Predicted Frequency (Hz)	Measured Frequncies, FLVT Setup (Hz)	% Difference Between FEM and FLVT Frequencies
X Axis Primary	79.4	67.4	17.7
Z Axis Primary	172.6	168.9	2.1

Table 14.   Comparison of Dynamic FEM Predicted Primary Frequencies with FLVT Test Setup Measured Frequencies

4.   Stress FEM

The stress FEM was created purely to conduct a stress analysis on the NPSCuL-v2 structure. As stated in Chapter III, Sections D.1 and D.2, the stress model is comprised of walls and the unibase meshed using 10-noded tetrahedral elements. All joints on the structure were modeled using a combination of RBE2 and beam elements. The RBE2 elements were used to connect multiple nodes along the fastener length to a single point, to ensure that no artificial stress concentrations would be seen. Examples of the joints are shown in Figure 53.
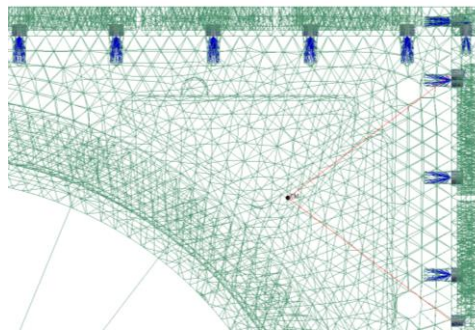
Figure 53.   Examples of Joints on NPSCuL-v2 Stress FEM

P-PODs and the SAD were added in as lumped mass elements. The masses and CGs of the P-PODs and SAD are summarized in Chapter III Section D.3, Table 11. Joints between the lumped mass elements and the NPSCuL walls were modeled using a combination of RBE2 and beam elements, similar to the dynamic FEM. The assembled FEM was fixed at the center of the 15-inch bolt-hole circle, and is shown in Figure 54.
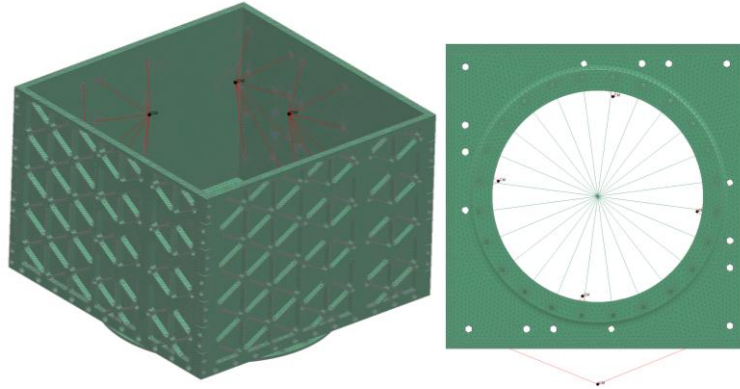
Figure 54.   NPSCuL-v2 Stress FEM Isometric (left) and Bottom Views (right)

Prior to running a stress analysis on the NPSCuL-v2 stress FEM, a modal analysis was conducted to ensure that the stress model mode shapes and frequencies were similar to the test-verified dynamic model mode shapes and frequencies. The results of the dynamic analysis on the NPSCuL-v2 stress FEM are shown in Figure 55.
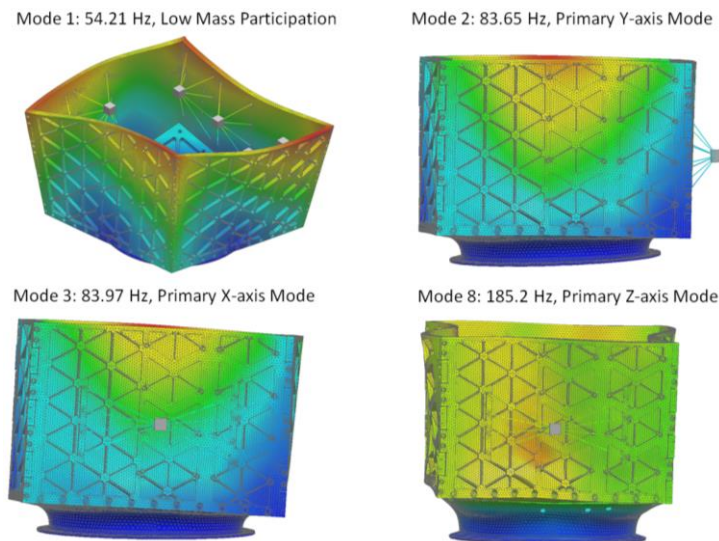
Figure 55.   NPSCuL-v2 Primary Modes, Stress FEM

By comparing the fundamental frequencies derived from the dynamic model, shown in Figure 51, and those derived from the stress model, shown in Figure 55, it is evident that the frequencies derived from the stress model are higher than those derived from the dynamic model, however, the fundamental frequencies of both models are

within 10% of each other. Since both models have the same mass, and since frequency is directly proportional to system stiffness, the stress model is stiffer than the dynamic NPSCuL FEM. It is important to note, however, that stress is independent of system stiffness and is dependent on the boundary and loading conditions applied. Since the mode shapes and fundamental frequencies for both the stress model and test-verified dynamic model are similar, it is evident that the boundary conditions have been correctly applied on the NPSCuL-v2 stress model. Further, each individual component of the NPSCuL-v2 stress FEM has been shown to yield higher stress results than the individual components of the NPSCuL-v2 dynamic FEM, making it more suitable to conduct a stress analysis on the NPSCuL-v2 stress FEM.

For the stress analysis, the stress FEM was constrained at the center of the 15 inch bolt-hole circle, similar to the dynamic FEM. Acceleration load factors, not including factors of safety, of 7gs axially, and 5gs in each of the lateral directions, were applied simultaneously, as previously stated in Chapter I, Section B. Since the requirement flowed down to NPS from ULA does not specify the loading directions, eight load cases were run for all eight possible directional combinations of 5g's in the X and Y axes and 7g's in the Z axis. The values recovered from the stress analyses included maximum von-mises stress and shear and tensile loads at all fastener locations.

The maximum stress values occurred on the unibase flange, along the 15-inch blot-hole circle, as expected. The maximum stress value was 13.9 ksi for the +5g in the X axis, +5g in the Y axis and -7g in the Z axis loading case. The stress plot for the maximum stress loading case is shown in Figure 56.
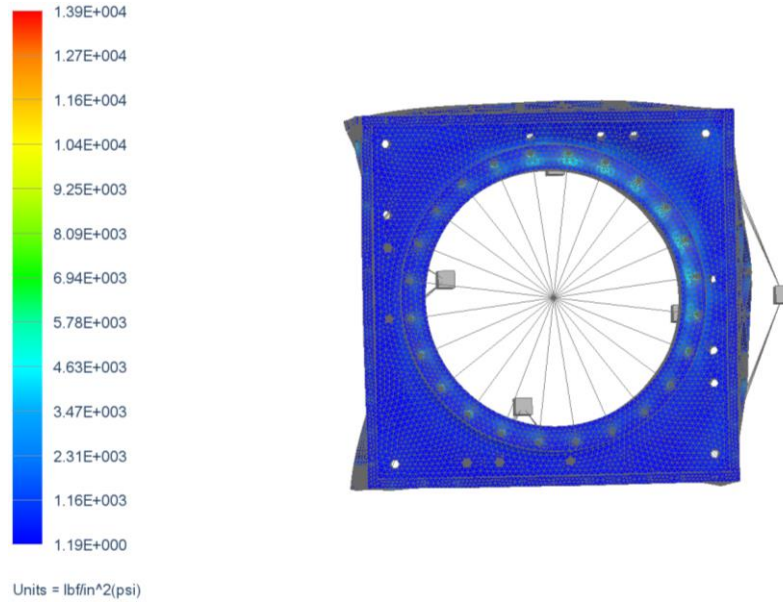
Figure 56.   Von-Mises Stress Plot for +5g, +5g, -7g Loading Case

To evaluate margins of safety on aerospace hardware, Equation 1.16 [14, p. 228] is used:

$$Margin\ of\ Safety\ (M.S.) = \left(\frac{Allowable\ load\ or\ stress}{Design\ load\ or\ stress} \right) - 1 \qquad 1.16$$

where the allowable stress values are material specific and for the purposes of this thesis, are sourced from MIL-HDBK-5H, and the design stress is the stress value calculated from the stress analysis and includes appropriate safety factors. The safety factors for yield and ultimate stress are 1.1 and 1.4 respectively, for an article that is to be tested to verify structural integrity [14, p. 370]. For aluminum 7075-T7351, the allowable yield stress is 57 ksi, and the allowable ultimate stress is 68 ksi. Using these values, the yield and ultimate stress margins of safety for the NPSCuL-v2 structure were calculated. A summary of the ultimate and yield margins of safety for all eight load cases is shown in Table 15.

Maximum Von Mises Stress for Eight Load Cases								
Load Case	(+,+,+)	(+,+,-)	(+,-,+)	(-,+,+)	(+,-,-)	(-,+,-)	(-,-,+)	(-,-,-)
Stress (psi)	1.25E04	1.39E04	1.32E04	1.33E04	1.33E04	1.32E04	1.39E04	1.25E04
Margins of Safety								
Yield	3.15	2.73	2.93	2.90	2.90	2.93	2.73	3.15
Ult.	2.90	2.49	2.68	2.65	2.65	2.68	2.49	2.90

Table 15.   Von-Mises Stress Values and Margins of Safety for Eight Load Cases

Since the margins of safety on both yield and ultimate stresses are greater than zero, the NPSCuL structure meets its criteria for strength analysis.

To ensure that all fasteners on the NPSCuL structure had positive margins of safety for all failure modes including yield, ultimate, shear, tension and gapping, axial and shear loads were recovered at the beam locations on all fasteners in the FEM for all eight load cases. The maximum axial and shear loads for all joints on the NPSCuL-v2 structure are summarized in Table 16.

Joint/Property	P-POD to Wall	Wall to Wall	Wall to Unibase	SAD to Wall
Axial Force (lbf)	265.54	80.07	61.08	23.28
Shear Force QXY (lbf)	108.72	61.32	160.01	40.86
Shear Force QXZ (lbf)	51.41	137.87	109.98	114.44
RSS Shear (lbf)	120.26	150.89	194.16	121.51

Table 16.   Maximum Axial and Shear Forces for all NPSCuL-v2 Joints

A fastener analysis was conducted for each of the joints on NPSCuL-v2 using the shear and axial forces retrieved from the stress analysis. Details of the analysis are shown in Appendix D. To maximize the margin of safety on gapping, the margin of safety on yield was driven down to 10%. The resulting margins and torque values for all joints on the NPSCuL-v2 structure are shown in Table 17.

Joint/Property	P-POD to Wall	Wall to Wall	Wall to Unibase	SAD to Wall
Calculated Torque (in-lbf)	38.5	40.5	98	41
M.S. Yield	10 %	10 %	10 %	10 %
M.S. Ultimate	71 %	71 %	73 %	72 %
M.S. Shear	400 %	300 %	500 %	400 %
M.S. Gapping	110 %	630 %	1680 %	2450 %
M.S. Tension	50 %	51 %	190 %	51 %

Table 17.　　　Torque and Margins of Safety for NPSCuL-v2 Joints

Since there are positive margins of safety across all the NPSCuL-v2 joints, it has been shown through analysis that NPSCuL-v2 is capable of withstanding the loads specified in the AP to LV ICD.

E.　　COMPARISON OF NPSCUL-V1 AND NPSCUL-V2

After completion of the stress and dynamic analyses, it became necessary to compare the results of sine sweeps and random vibration tests on both the NPSCuL-v1 and NPSCuL-v2 structures. Both structures were integrated with eight P-POD mass models and the SAD and were tested on the FLVT setup. The P2M2s were ballasted so that both structures weighed ~188 lbs. The structures then underwent sine sweep tests from 20 Hz – 2000 Hz at 0.5G's and force limited random vibration testing at ABC MPE – 3dB levels, i.e., 5.4 GRMS at the base of NPSCuL, in all three axes. The sine sweep comparisons between the NPSCuL-v1 structure and the NPSCuL-v2 structure are shown in Figure 57—Figure 59.

From Figure 57—Figure 59, it is evident that the primary modes of NPSCuL-v2 occur at higher frequencies than the NPSCuL-v1 structure. From all three plots it can also be seen that the magnitude of amplification seen on the NPSCuL-v2 structure is generally lower than or equal to the magnitude of amplification on the NPSCuL-v1 structure. Both these observations point to the result that payloads mounted to the NPSCuL-v2 structure would likely see lower amplification and lower displacements, due to the higher natural frequencies, than when mounted to the NPSCuL-v1 structure. To verify that hypothesis, the two NPSCuL structures underwent random vibration testing to MPE – 3dB. A

comparison of the P-POD responses seen on the two structures is shown in Figure 60—
Figure 62.
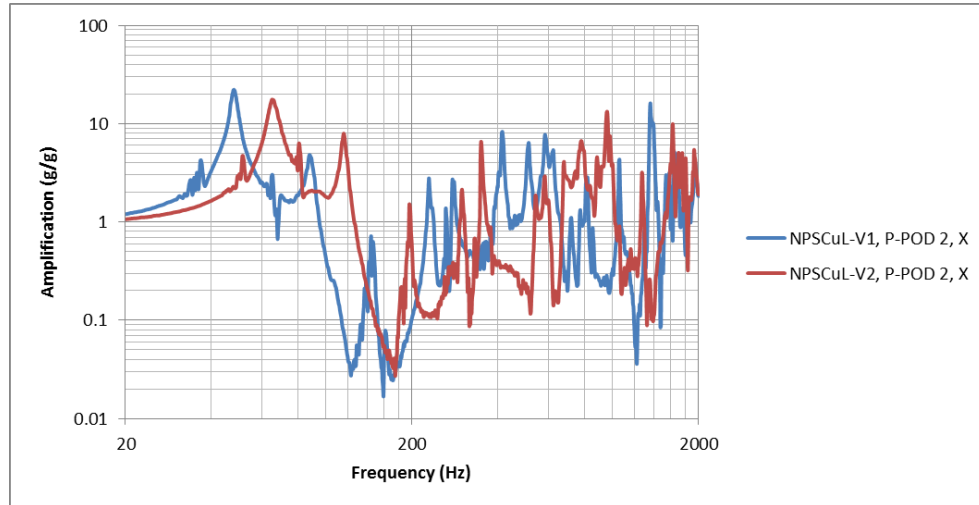
Figure 57.   X Axis Sine Sweep Comparisons between NPSCuL-v1 and NPSCuL-v2
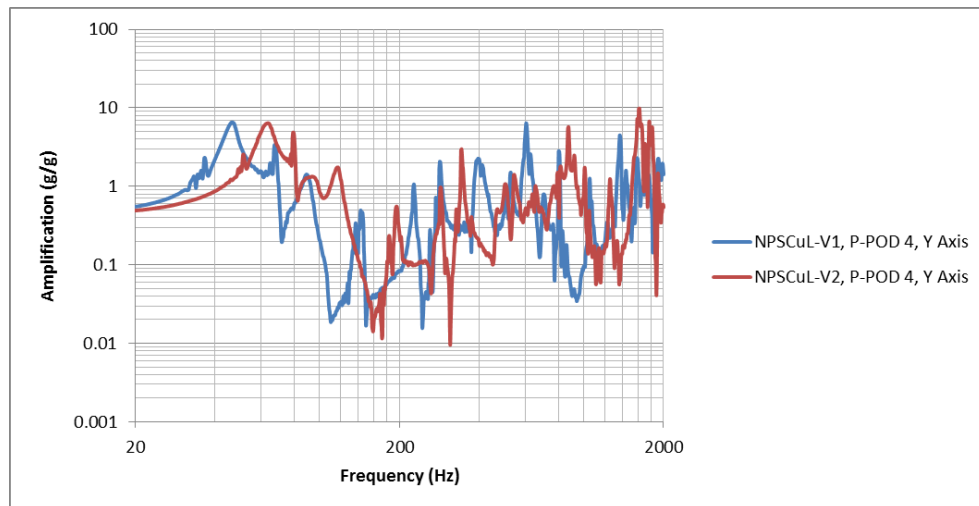
Figure 58.   Y Axis Sine Sweep Comparisons between NPSCuL-v1 and NPSCuL-v2
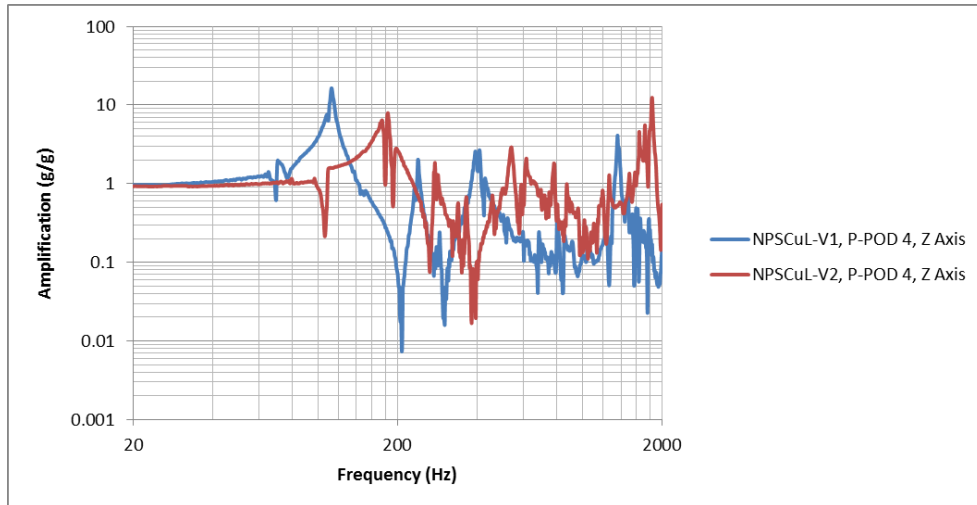
Figure 59.   Z Axis Sine Sweep Comparisons between NPSCuL-v1 and NPSCuL-v2
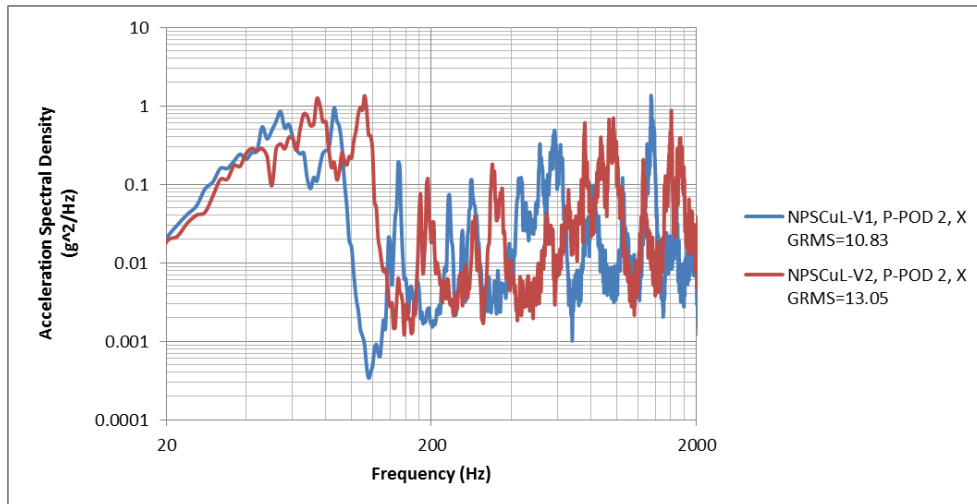
Figure 60.   X Axis Random Vibration Response Comparison of NPSCuL-v1 and
NPSCuL-v2 at MPE – 3dB
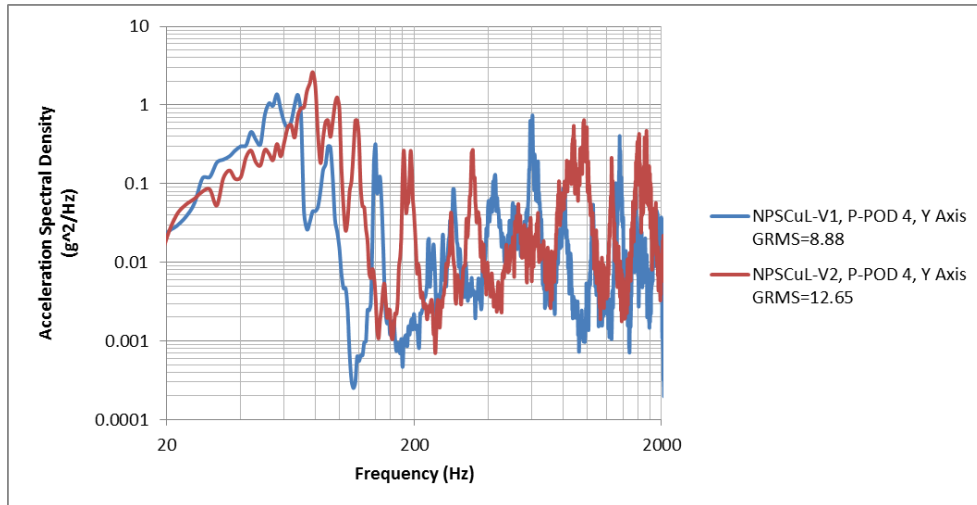
Figure 61.   Y Axis Random Vibration Response Comparison of NPSCuL-v1 and
NPSCuL-v2 at MPE − 3dB

Figure 62.   Z Axis Random Vibration Response Comparison of NPSCuL-v1 and
NPSCuL-v2 at MPE − 3dB

A comparison of the GRMS values at the NPSCuL-to-P-POD interface in all three axes of test is summarized in Table 18.

	X Axis GRMS P-POD 2	Y Axis GRMS P-POD 4	Z Axis GRMS P-POD 4
NPSCuL-v1	10.83	8.88	5.57
NPSCuL-v2	13.05	12.65	7.73

Table 18.   NPSCuL-v1 and NPSCuL-v2 NPSCuL-to-P-POD Interface GRMS Comparison

From Figure 60–Figure 62 and Table 18, it can be seen that, contrary to the initial hypothesis, the P2M2s mounted to the NPSCuL-v2 structure see higher GRMS values than the P2M2s mounted to the NPSCuL-v1 structure. One possible reason for the mismatch between the random vibration results expected by analyzing the sine sweep results and the actual random vibration results is the implementation of force limiting.

It can also be seen, especially in Figure 60 and Figure 61 for frequencies less than 200 Hz, that the peak ASD values occur at higher frequencies on NPSCuL-v2 than on the NPSCuL-v1 structure. The FLVT equations shown in Chapter II, Section C.3 are dependent on the first fundamental frequency of a structure. For any system, the force begins to roll-off at frequencies above the first fundamental frequency of the system. Since NPSCuL-v2 has a higher first fundamental frequency than the NPSCuL-v1 structure in all three axes, force roll-off doesn't take effect until a higher frequency, which results in less relief in random vibration levels for the NPSCuL-v2 levels. The effects of force limiting are most visible in the random vibration control plots for the NPSCuL-v1 and NPSCuL-v2 structures, shown in Figure 63–Figure 65.

Figure 63.   X Axis Random Vibration Control Comparison of NPSCuL-v1 and NPSCuL-v2 at MPE − 3dB

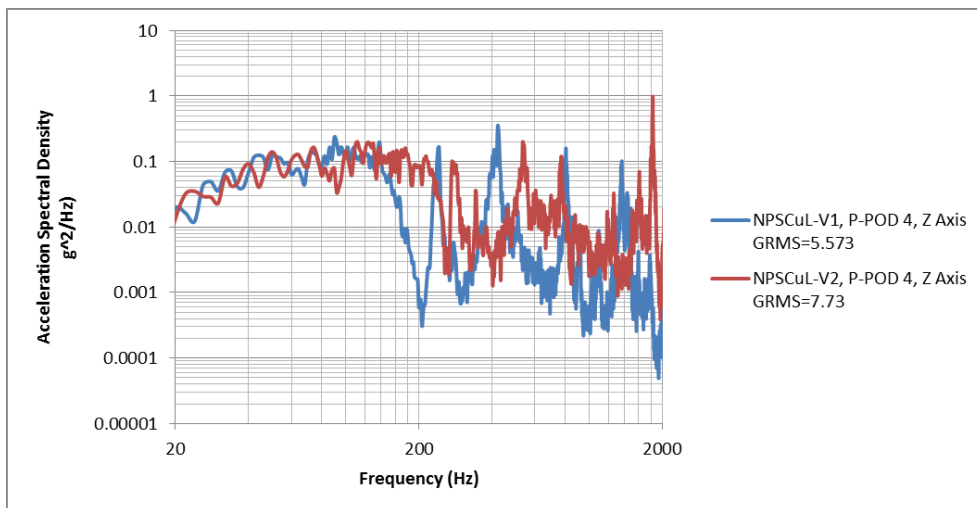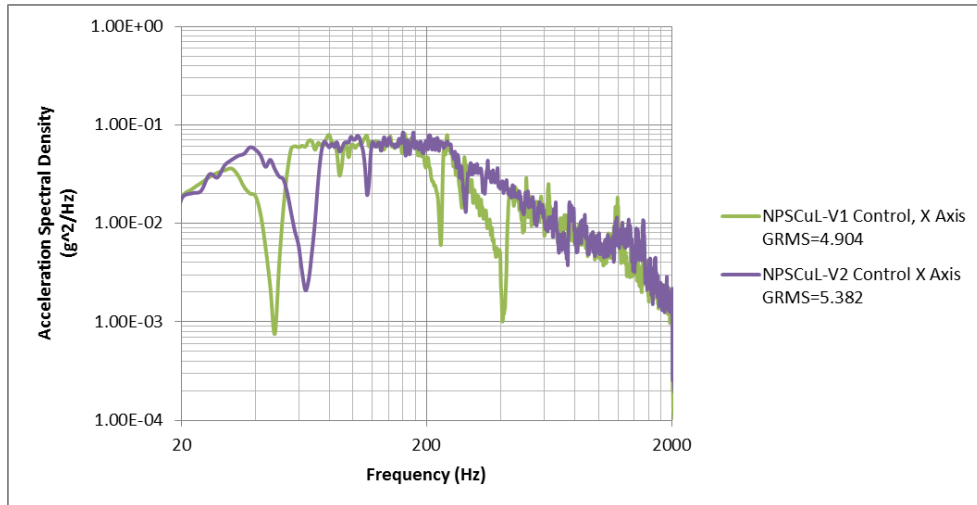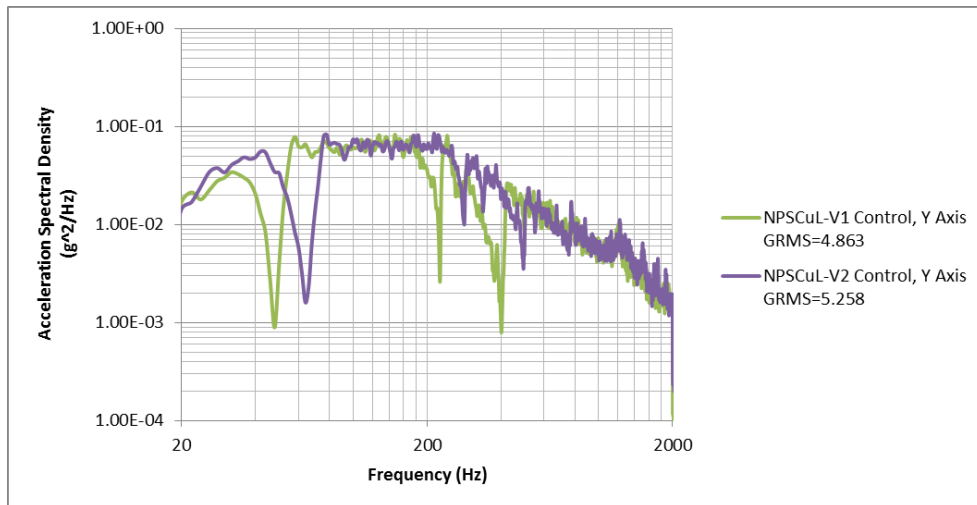Figure 64.   Y Axis Random Vibration Control Comparison of NPSCuL-v1 and NPSCuL-v2 at MPE − 3dB
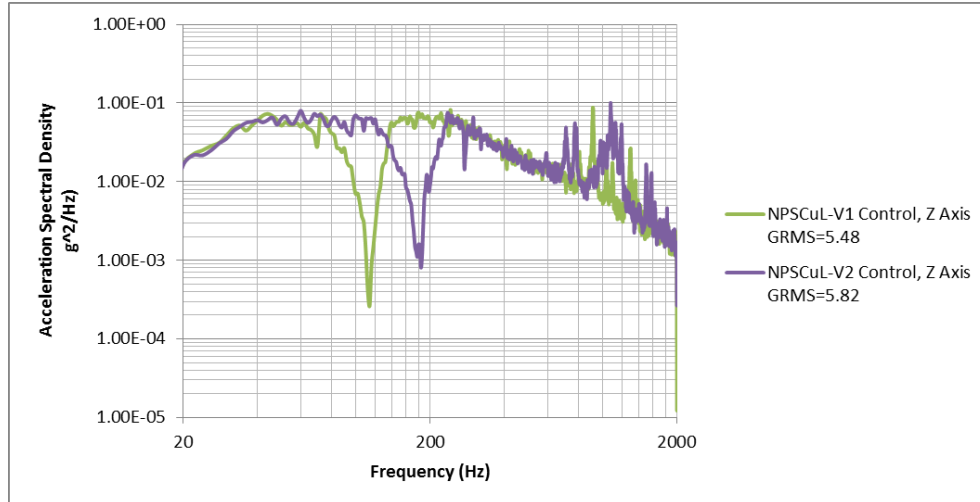
Figure 65.   Z Axis Random Vibration Control Comparison of NPSCuL-v1 and NPSCuL-v2 at MPE − 3dB

From Figure 63–Figure 65, it can be seen that the notches at the fundamental frequencies in the control spectrum for the NPSCuL-v1 structure are deeper than the notches at the fundamental frequencies in the control spectrum for NPSCuL-v2. From the X and Y axis control plots, it is also evident that above the first fundamental frequency, there are more and deeper notches for the NPSCuL-v1 structure, which implies that force limiting provides more relief when testing the NPSCuL-v1 structure. The effect of force limiting at high frequencies is particularly evident from the notch at ~400 Hz on the NPSCuL-v1 structure. The NPSCuL-v1 structure has a mode at ~400 Hz (See Appendix A for force plots). Since the force roll-off begins at a lower frequency on the NPSCuL-v1 structure as opposed to the stiffer NPSCuL-v2 structure, the allowable force at ~ 400 Hz is lower for the NPSCuL-v1 structure. To prevent the force input from exceeding the force limit at ~400 Hz, the acceleration input at that frequency is dropped, resulting in a notch. The depth of the notch is directly proportional to the amplification that would have been seen had there been no FLVT implemented. It is also worth noting that the same FLVT technique, with C = √2 was applied to both NPSCuL-v1 and NPSCuL-v2 structures. The GRMS values for all three control plots show that the input at the base of the NPSCuL-v1 structure is lower than the input at the base of the NPSCuL-v2 structure, further verifying that force limiting is more effective on the NPSCuL-v1 structure. Thus, part of the reason why the random vibration responses for NPSCuL-v2 are greater than

the random vibration responses for the NPSCuL-v1, is that the lower the test article fundamental frequency, the greater the effect of force limiting. This outcome was not understood during the NPSCuL-v2 design process, and shows that a structural redesign process may need a different approach when FLVT is implemented. Further, the relief in NPSCuL vibration levels gained from FLVT is on the order of 10% to 60%, depending on the axis of test. Structural changes for the NPSCuL system, where changing the entire system configuration was not a possibility due to mass and volume constraints, did not provide significant relief to the NPSCuL payload vibration levels. This is because the fundamental system characteristics including mass and CG varied little between the original and re-designed structures. This result may be applicable to other structures besides NPSCuL, and should be evaluated before proceeding with any structural re-design process.

Another possible reason that the responses measured on NPSCuL-v2 are not lower than the responses on the NPSCuL-v1 is the reduction in the total number of joints on the NPSCuL-v2 structure. The NPSCuL-v1 structure has 204 joins, whereas NPSCuL-v2 has 172 joints. Since joints dissipate energy and result in overall damping, the NPSCuL-v2 structure has less damping mechanisms than the NPSCuL-v1 structure.

Another metric for analyzing the random vibration responses for both the NPSCuL-v1 and NPSCuL-v2 structures is to convert the measured ASD into displacement spectral density (DSD) to evaluate the random vibration results from a displacement perspective. Equation 1.17 outlines the conversion from ASD to DSD.

$$DSD = ASD \bullet \left(\frac{g^2}{\left(2\pi f\right)^4} \right) \qquad 1.17$$

In Equation 1.17, the *DSD* has units of in^2/Hz, *ASD* has units of g^2/Hz, *g*, also known as the acceleration due to gravity has units of in^2/sec and the frequency, *f* has units of Hz. Plots of the response DSDs for all three axes for both the NPSCuL-v1 and NPSCuL-v2 structures are shown in Figure 66–Figure 68. The plots also reflect the displacement root-mean-square (DRMS) values to create a metric for comparing the DSD plots.

From Figure 66–Figure 68, it can be seen that just by comparing the DSD plots, there is no clear indication of which structure has lower displacements. At certain frequencies, NPSCuL-v1 has lower DSD values, and at other frequencies, NPSCuL-v2 has lower displacement values. The DRMS values, similar to the concept of GRMS for ASD curves, give an indication of which structure sees lower displacements. A common trend for all three axes is that the NPSCuL-v2 structure has a lower DRMS than the NPSCuL-v1 structure, and is a better structure for NPSCuL payloads from a displacement perspective.
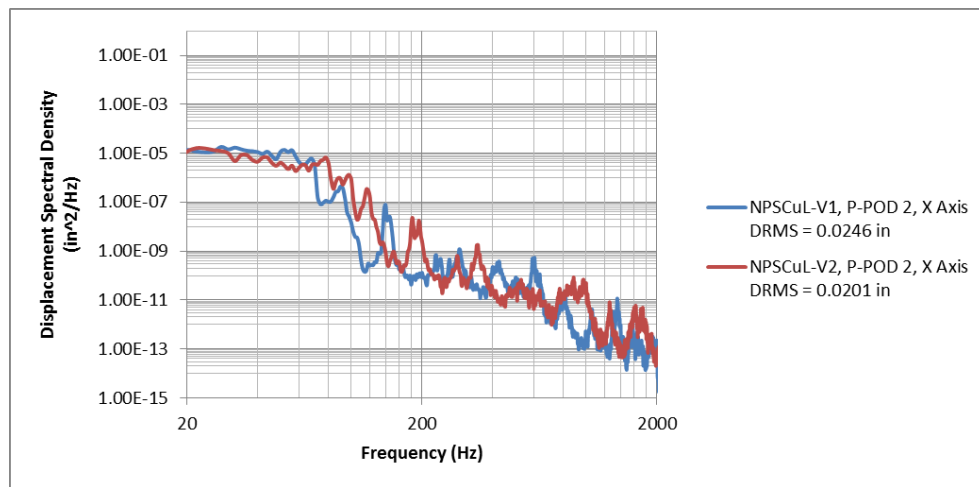

Figure 66.   X Axis Displacement Spectral Density Comparison of NPSCuL-v1 and NPSCuL-v2 at MPE − 3dB
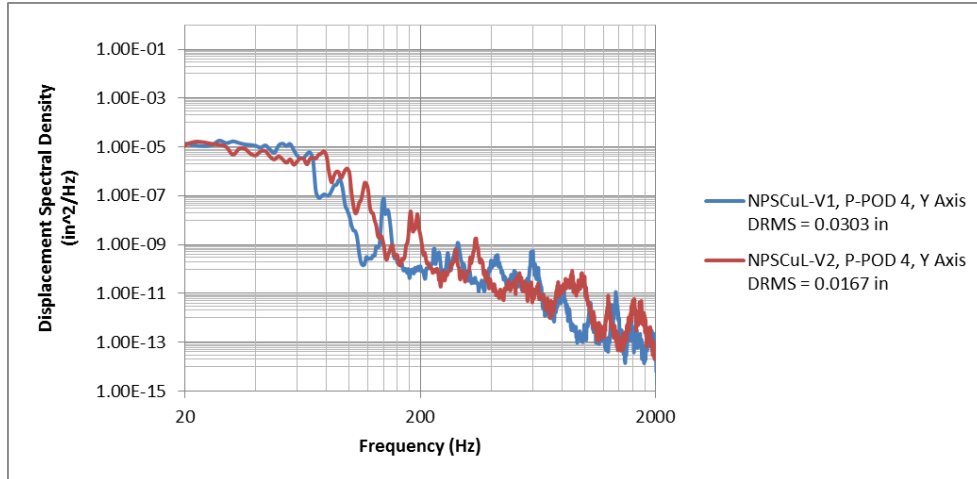
88

Figure 67.   Y Axis Displacement Spectral Density Comparison of NPSCuL-v1 and
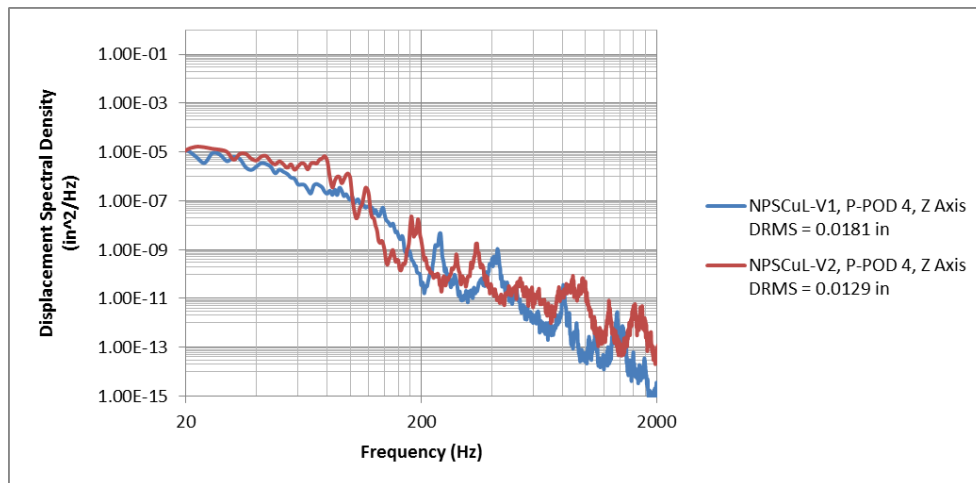NPSCuL-v2 at MPE − 3dB

Figure 68.   Z Axis Displacement Spectral Density Comparison of NPSCuL-v1 and
NPSCuL-v2 at MPE − 3dB

THIS PAGE INTENTIONALLY LEFT BLANK

IV. CONCLUSION

A. SUMMARY

NPSCuL, as manifested on the ABC plate on the Atlas V LV, is uniquely located on the aft-end of the upper stage of the LV. The vibration environment at this location is harsh to begin with, i.e., 7.6 GRMS at acceptance levels, and additionally, NPSCuL amplifies the input vibration environment at the NPSCuL-to-P-POD interface. To improve the vibration environment at the NPSCuL-to-P-POD interface, a two-pronged approach was evaluated, which included reducing over-test during vibration testing by utilizing a method known as Force Limited Vibration Testing (FLVT), and re-deigning the NPSCuL structure to increase the fundamental frequencies in each of the three test axes to reduce displacement during vibration testing.

Most satellite providers fulfill the random vibration testing requirement levied by the LV by utilizing established acceleration-controlled vibration tests. However, sometimes acceleration-controlled vibration tests can result in significant over-test and cause failures that would not occur in flight. The over-test is a result of the inability to replicate the exact flight mounting configuration during ground-based vibration testing. These test-induced failures can prove to be costly as they can cause scheduling issues and high costs to fix a problem that likely wouldn't occur during flight.

Force limiting simulates impedance characteristics of the flight mounting structure, thereby enabling a more realistic vibration test. FLVT was successfully implemented during NPSCuL qualification and acceptance testing for the OUTSat and GEMSat missions. The force limit was derived using the semi-empirical approach, as outlined in Chapter II, Section C.2.

During FLVT, a force limit is applied based on the test-item mass, fundamental frequency in the axis of test and flight mounting configuration. The force channel acts as a "watchdog" channel, which means that the test is acceleration-controlled until the force-limit is reached. At frequencies where the force limit is reached, the test becomes force controlled, and the software controller doesn't allow the limit to be exceeded,

which results in a notch in the acceleration spectrum. The notches occur at the modal frequencies of the test item in the axis of test, with the deepest notch generally occurring at the test-item fundamental frequency. The resulting acceleration spectrum is more realistic and generally more benign than the traditional acceleration-controlled vibration test spectrum. For the NPSCuL case outlined in this thesis, FLVT provided ~10% relief for NPSCuL payloads in the X axis, ~20% relief in the Y axis and ~65% relief in the Z axis, as compared to an un-notched vibration test. Though the relief provided was significant, the resulting levels were still considered harsh by prospective NPSCuL payloads.

To further reduce the vibration test levels for NPSCuL payloads, a re-design of the NPSCuL structure was attempted. The base assumption while making design modifications was based on the fact that as frequency increases, displacement decreases. Lower displacement is desirable as it induces lower stress in structural components. Increasing the natural frequency of NPSCuL was achieved by increasing the structural stiffness without increasing the overall system mass. This was achieved by doubling the NPSCuL wall thickness from ¼ inch to ½ inch, while implementing an isogrid design to ensure that the system mass did not increase. An isogrid panel is a plate or face sheet with triangular integral stiffening ribs, commonly referred to as stringers. Much of the material from a solid plate can be removed, leaving behind a lattice of intersecting ribs and a thin face-sheet, without compromising the structural integrity of the plate. Additionally, the NPSCuL baseplate and adapter ring were fused into a single, thicker part, with a circular sectional cut-outs on the baseplate to reduce mass. This part was called the unibase. The modified structure was known as NPSCuL-v2.

Two finite element models of NPSCuL-v2 were created; one to serve as the dynamic analysis model and the other to serve as the stress analysis model. The dynamic analysis model consisted of thin shell and beam elements, whereas the stress analysis model consisted of 10-noded tetrahedral elements. Generally, the stress model is more detailed than the dynamic model, so as to adequately predict stress distributions and stress concentrations due to expected flight loading conditions. The dynamic model predicted that the fundamental frequencies of NPSCuL-v2 would be higher than the

fundamental frequencies of NPSCuL-v1by ~ 24 Hz in the X and Y axes, and ~76 Hz in the Z axis. Additionally, the stress FEM predicted that NPSCuL-v2 would be able to survive the expected flight loading conditions with adequate margin.

Since the survivability and design objectives of the NPSCuL-v2 structure were proven by analysis, an EDU of the NPSCuL-v2 structure was manufactured. The EDU then underwent sine sweep testing at 0.5 G's from 20-2000 Hz and force limited random vibration testing at ABC MPE – 3 dB. The sine sweep results were used to validate the NPSCuL-v2 dynamic FEM. The dynamic FEM and sine sweep test results agreed to within 10% of each other, which is acceptable, however, better results may be achieved by adjusting the FEM properties.

The FLVT test results of NPSCuL-v2 and NPSCuL-v1 were compared to determine if the NPSCuL-v2 structure was indeed better than the NPSCul-v1 structure from a vibration environment perspective. It was found that since the first fundamental frequencies of NPSCul-v2 in each axis are higher than those of NPSCuL-v1, FLVT is less effective on NPSCuL-v2. As a result the input vibration environment at the base of the structure is higher on NPSCuL-v2 than NPSCuL-v1, or in other words, the notch seen in the input spectrum is shallower for NPSCuL-v2 than for NPSCuL-v1. The higher input at the base results in slightly higher GRMS values at the NPSCuL-to-P-POD interface on NPSCuL-v2, making the vibration environment more severe from a GRMS perspective. Additionally, since the baseplate and adapter ring are fused together to form the unibase on NPSCuL-v2, there are fewer joints to dissipate energy input into the structure. However, since the fundamental frequencies in all three axes are higher on NPSCuL-v2, the displacement seen at these frequencies is expected to be lower than the displacement seen by payloads at the fundamental frequencies of the NPSCuL-v1 structure. However, when the displacement plots are analyzed for the entire frequency range of 20 Hz- 2000 Hz, no apparent trend is visible, with the NPSCuL-v1 structure having lower displacements at certain frequencies and the NPSCuL-v2 structure having lower displacement at other frequencies.

These results show that the NPSCuL-v2 structure, tested in an FLVT configuration does not result in lower vibration environments for NPSCuL payloads.

FLVT itself provides significant relief in terms of the vibration environment and overshadows any relief gained from stiffening the structure. As a result, it is not recommended to transition to NPSCuL-v2 for future flights of NPSCuL.

B.   FUTURE WORK

As discussed in Chapter III, the NPSCuL-v2 FEM agrees with the NPSCuL-v2 EDU test results to within 10%. It may be desirable to have better correlation between the FEM and EDU test results. To achieve this, the joint stiffness on the NPSCuL-v2 FEM can be adjusted by changing the beam properties for all joints, until the FEM and EDU tests results agree more closely.

Additionally, it may be desirable to re-introduce 24 joints into the baseplate-ring connection to help dissipate some of the input energy and hence increase damping. While re-designing the adapter ring for NPSCuL-v2, the height of the adapter ring should be minimized to keep the system CG as low as possible, as systems with lower CGs tend to show lower amplification. The flanges on the adapter ring should be designed for ease of integration so that ratcheting tools may be utilized for fastening the adapter ring to the ABC plate and NPSCuL baseplate.

The lessons learned during the NPSCuL-v2 design and analysis process are expected to be applied to the continuing vibration reduction efforts for NPSCuL payloads. For instance, one important lesson learned from this thesis shows that a redesign process for a structure undergoing FLVT may need to be approached differently than a redesign process where a structure is tested without the implementation of FLVT. It is now clear that rather than stiffening the NPSCuL structure, perhaps increasing damping will result in better environments for NPSCuL payloads, by reducing amplification. Opportunities such as increasing damping and implementing vibration isolation will provide exciting and challenging research projects in the future.

APPENDIX A. GEMSAT QUALIFICATION FORCE SENSOR PLOTS

The force sensor plots for the X and Y axes as measured during the GEMSat qualification testing are shown in Figure 69–Figure 70.
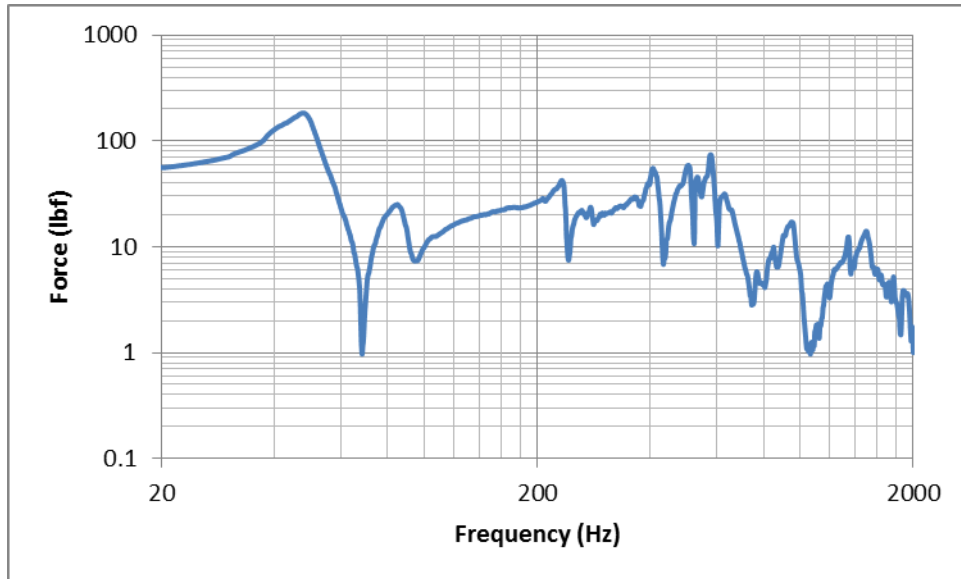
Figure 69.   X-axis Force, NPSCuL EDU Z-Axis Sine Sweep
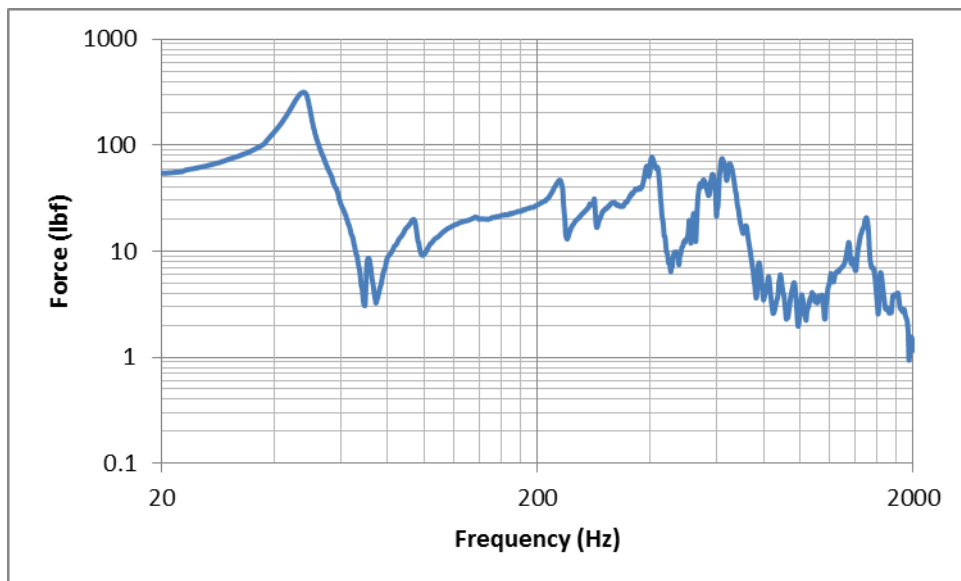
Figure 70.   X-axis Force, NPSCuL EDU Z-Axis Sine Sweep

THIS PAGE INTENTIONALLY LEFT BLANK

APPENDIX B. NOTCHED AND UN-NOTCHED FORCE PLOTS

Comparisons of the X and Y notched and un-notched force spectral density plots are shown in Figure 71–Figure 72.
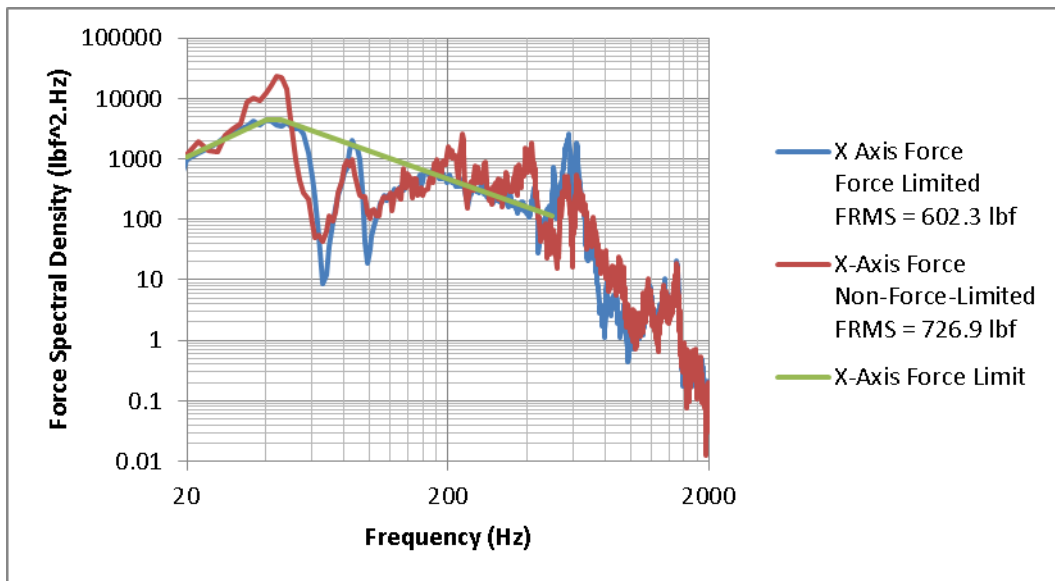
Figure 71.   Force Measurement, X-Axis Test, MPE – 3dB
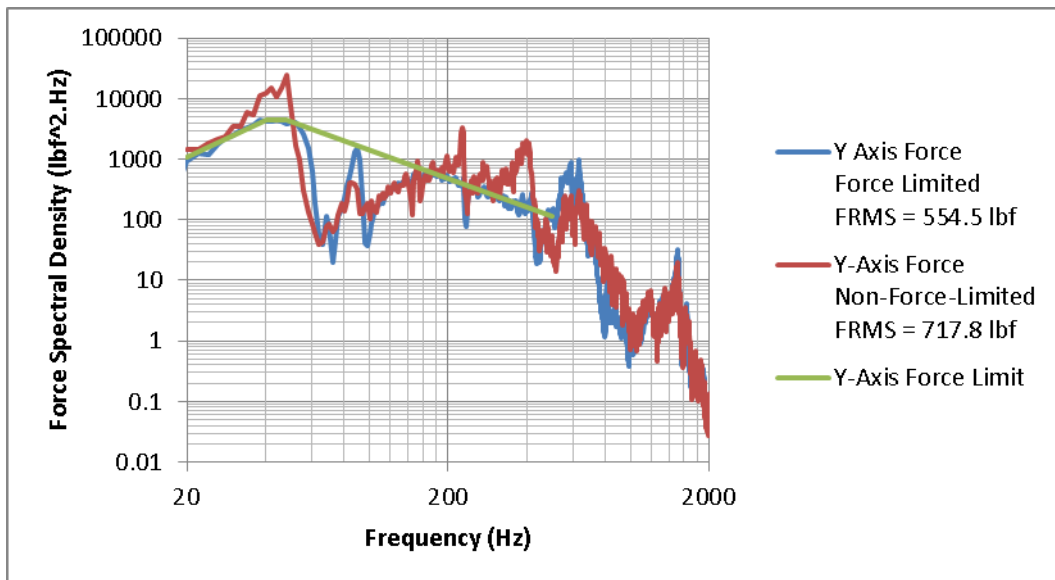
Figure 72.   Force Measurement, Y-Axis Test, MPE – 3dB

THIS PAGE INTENTIONALLY LEFT BLANK

APPENDIX C. GEMSAT CUBESAT VIBRATION LEVELS

GEMSat vibration test levels were derived from the OUTSat acceptance test. The OUTSat acceptance test data at the NPSCuL to P-POD interface, both in-axis and cross-axis, were enveloped and scaled up by 3dB to arrive at proto-qualification levels for all CubeSats, regardless of their position within GEMSat. This was advantageous from a programmatic perspective, since no CubeSat was tied to a specific position within GEMSat. The GEMSat CubeSat proto-qualification test levels are shown in Figure 73–Figure 75.
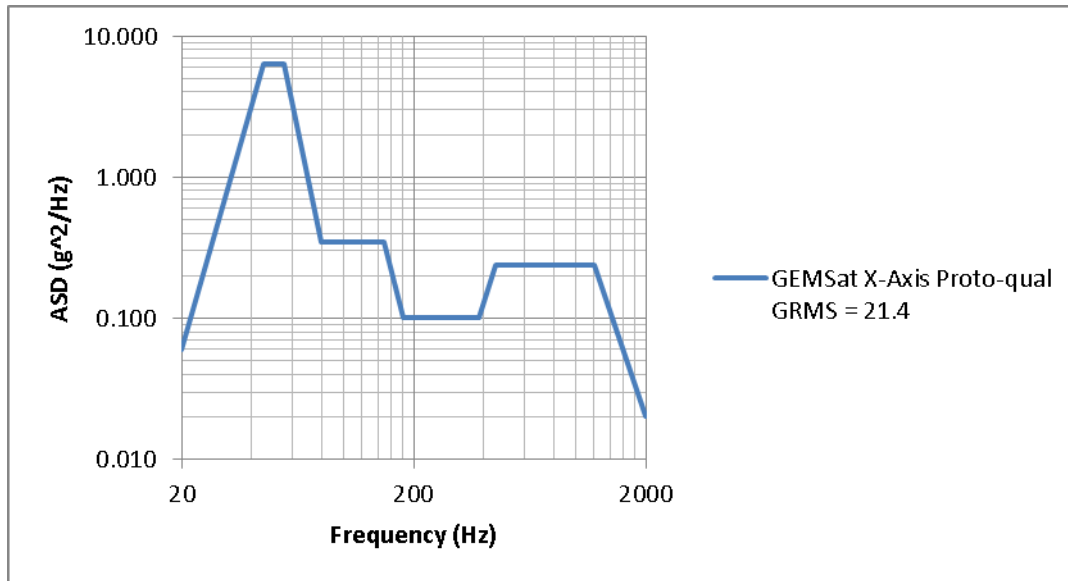
Figure 73.   GEMSat X-Axis CubeSat Proto-qual Envelope
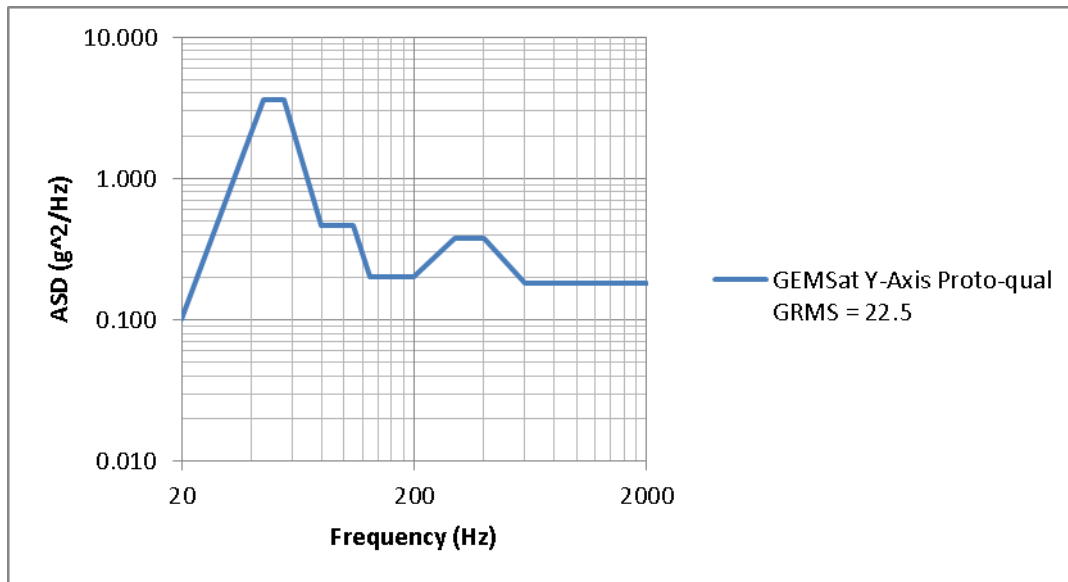
Figure 74.   GEMSat Y-Axis CubeSat Proto-qual Envelope
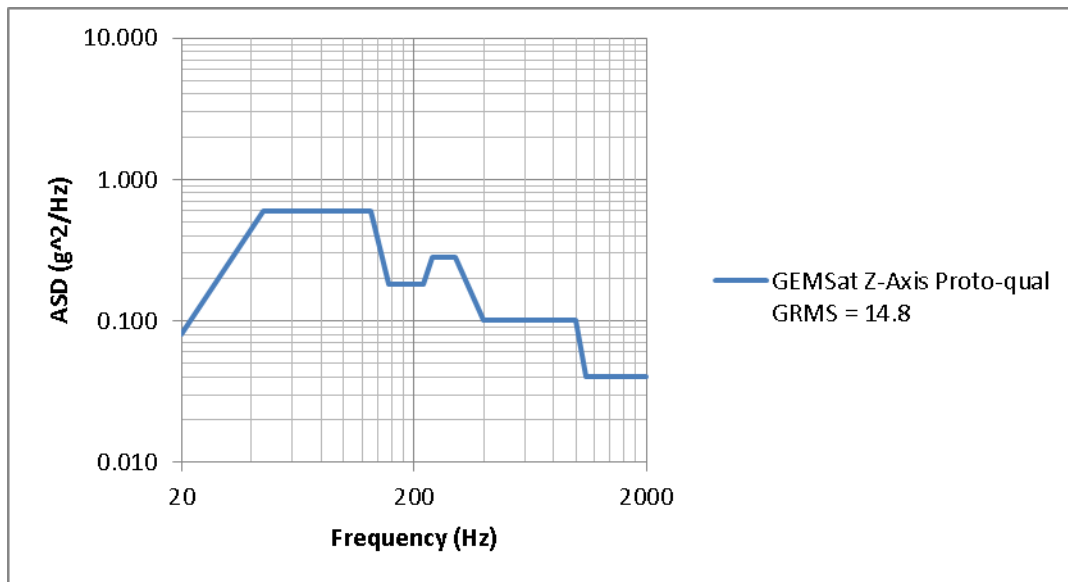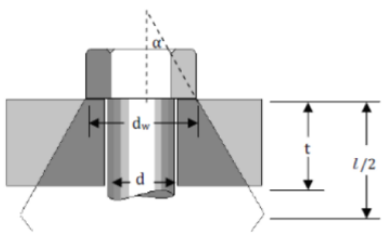
Figure 75.   GEMSat Y-Axis CubeSat Proto-qual Envelope

APPENDIX D. NPSCUL-V2 FASTENER ANALYSIS TOOL

The NPSCuL fastener analysis tool was created in Microsoft Excel to calculate fastener torques from shear and tensile loads on each joint type derived from the NPSCuL stress analysis.

Fastener Analysis Tool

All dimensions in inches, pounds,seconds and degrees farenheit. User entries are highlighted in blue, calculations in gray, and outputs in yellow. Equations for calculated values can be found in the cell notes. **Disclaimer:** Torque and margins calculator is designed for cap screws (no nut) and high vibration environment. If environment is static yield safety margin should be increased, or another method of analysis should be used.

User inputs	Calculations	Outputs

Safety Factors

	Safety Factor	Fitting Factor	Total Applied Safety Factor		
Yield	1.1	1.15	1.265		This is the product of the safety factor and the fitting factor (X*1.5).
Ultimate	1.4	1.15	1.61		
Yield Safety Margin	0.1				

|								bracket joint material	9.66E+07

Material Parameters

				bracket joint material	9.66E+07

ppod joint material: 9.66E+07

	Material	Yield Strength (psi)	Ultimate Strength (psi)	Proof Strength (psi)	Shear Ultimate Strength (psi)	Modulus of Elasticity (psi)	Coefficient of Thermal Expansion, α (in/(in*°F))	
Fastener	SS A286	1.20E+05	1.60E+05	1.02E+05	1.02E+05	2.91E+07	9.39E-06	These values are taken from MIL-HDBK-5-H section 6.2.1.1
Member 1	Al	5.70E+04	6.90E+04	4.85E+04	3.80E+04	1.06E+07	1.31E-05	These values are taken from MIL-HDBK-5-H section 3.7.4.1
Last Member	Al 7075-T7351	5.70E+04	6.90E+04	4.85E+04	3.80E+04	1.06E+07	1.31E-05	

Friction Coefficient	1.4						This factor is taken from Marks' Standard Handbook for Mechanical Engineers Table 3.2.2 page 3-22

Joint Geometry

	Baseplate/ Wall	Wall/ Wall	PPOD/ Wall	Sequencer/ Wall		
d	0.25	0.19	0.19	0.19		
t	0.0625	0.0625	0.0625	0.0625		
t_1	0.1875	0.25	0.25	0.2		
t_2	0.375	0.285	0.19	0.285		
l_d	0.06	0.06	0.06	0.06		
L	0.625	0.625	0.625	0.625		
h	0.25	0.3125	0.3125	0.2625		
L_T	0.375	0.3125	0.3125	0.3625		
l'	0.375	0.4075	0.4075	0.3575		
l_t	0.315	0.3475	0.3475	0.2975		
A_tt	0.26	0.074	0.074	0.074		Effective shear stress area for thread tear-out (Bickford, p. 32, Table 2.2)

Fastener Stiffness

	Baseplate/ Wall	Wall/ Wall	PPOD/ Wall	Sequencer/ Wall		
A_d	0.04908739	0.028353	0.028353	0.02835287		Shank cross sectional area
A_t	0.0364	0.0200	0.0200	0.0200		Threaded portion cross-sectional area
K_B	2.95E+06	1.49E+06	1.49E+06	1.71E+06		Fastener stiffness

$$K_B = \frac{A_B A_T E}{l_t A_B + l_B A_t}$$

Member Stiffness

	Baseplate/ Wall	Wall/ Wall	PPOD/ Wall	Sequencer/ Wall		
d_w	0.468	0.355	0.355	0.355		See diagram below
K_M	5.64E+06	3.46E+06	3.46E+06	3.73E+06		Member stiffness

$$K_M = \frac{\pi E\, d \tan(\alpha)}{2 \ln \frac{(l \tan(\alpha) + d_w - d)(d_w + d)}{(l \tan(\alpha) + d_w + d)(d_w - d)}}$$

It should be noted that d_w should be measured as the width across the flats for a hex head fastener

Load Factor

fraction of external load carried in fastener

	Baseplate/ Wall	Wall/ Wall	PPOD/ Wall	Sequencer/ Wall		
C	0.34317469	0.301204	0.301204	0.31488827		Fraction of tensile load carried by fastener

$$C = \frac{K_B}{K_B + K_M}$$

Nut Factor

K	0.18	Nut factor			

	Nut factor spread	Creep Derate	Tool Error	Total Error	
Gamma_h	35%	0%	4%	39%	High bound on 3σ
Gamma_l	-21%	-5%	-4%	-30%	Low bound on 3σ

87	**Thermal**							
88	T_init	72	Assembly Temperature					
89	T_high	188	Max Service Temperature					
90	T_low	-10	Min Service Temperature					
91	Preload gain							
92	F_T_high		312	183	183	181		Additional preload due to increase in temperature
93	F_T_low		-220.8	-129.3	-129.3	-127.6		Additional preload due to decrease in temperature
94								
95								
96	**Maximum Loads**							
97	L_ten		61.08	80.07	265.54	23.28		Greatest tensile load from FEM
98	L_shear		194.16	150.89	120.26	121.5		Greatest shear load from FEM
99								
100								Greatest tensile load from FEM
101	**Torque Calculations**							Greatest shear load from FEM
102	maximum allowable preload: P_m_a							
103	P_m_a		3349	1824	1753	1845		
104	Torque based on maximum allowable preload							
105	T		98	40.5	38.5	41		
106	P_nom		2178	1184	1126	1199		Average achieved preload
107	P_max		3339	1829	1748	1847		Maximum achieved preload
108	P_min		1304	700	659	712		Minimum achieved preload

$$F_T = \frac{K_B K_M}{K_B + K_M} l' \Delta T(\alpha_J - \alpha_B)$$

$$P_{max,allow} = \frac{S_p A_T}{MOS_{yield}+1} - L_{E,T,max} CX_{yield}$$

$$P_{max} = P_{nominal}(1+\Gamma) + F_{T,High}$$

$$T = \frac{Kd(P_{ma} - F_{T high})}{1 + \Gamma\_high}$$

$$P_{min} = P_{nominal}(1-\Gamma) + F_{T,Low}$$

$$P_{nom} = \frac{T}{Kd}$$

Yield margin of safety
Ultimate margin of safety
Shear margin of safety
Gapping margin of safety
tear-out margin of safety

120	**Margin of Safety Calculations**					
121	MOS_y		0.10	0.10	0.10	0.10
122	MOS_u		0.73	0.71	0.71	0.72
123	MOS_s		5	3.0	4	4
124	MOS_g		16.8	6.3	1.1	24.5
125	MOS_t		1.9	0.51	0.50	0.51

$$MOS_{yield} = \frac{S_p A_T}{L_{E,T,max} CX_{yield} + P_{max}} - 1$$

$$MOS_{gap} = \frac{P_{min}}{X_{ult} L_{E,T,max}} - 1$$

$$MOS_{ult} = \frac{S_{TU} A_T}{L_{E,T,max} CX_{ult} + P_{max}} - 1$$

$$MOS_{gap} = \frac{P_{min}}{X_{ult} L_{E,T,max}} - 1$$

$$MOS_{shear} = \frac{P_{min}\mu}{X_{ult} L_{E,S,max}} - 1$$

$$MOS_{tearout} = \frac{S_{shear} A_{TT}}{F_{E,T,max} CX_{ult} + P_{max}} - 1$$

The NPSCuL fastener analysis tool was developed primarily by Shane Driscoll, a former NPS Research Assistant, with inputs from Scott Peck, Engineering Specialist at The Aerospace Corporation, Dan Sakoda, Research Associate at NPS and Vidur Kaushish, Research Associate at NPS.

THIS PAGE INTENTIONALLY LEFT BLANK

LIST OF REFERENCES

[1]   W. D. Lan, "Poly Picosatellite Orbital Deployer Mk III ICD," California Polytechnic State University, San Luis Obispo, CA, 2007.

[2]   S. Lee, A. Hutputanasin, A. Toorian, W. Lan and R. Munakata, "CubeSat design specification (revision 12)," California Polytechnic State University, San Luis Obispo, CA, 2009.

[3]   Pumpkin, Inc. (2007, January 1). 3D CAD design. [Online]. Available: http://www.cubesatkit.com/content/design.html

[4]   J. H. Newman, D. Sakoda, and R. Panholzer, "CubeSat Launchers, ESPA-rings, and education at the Naval Postgraduate School." *SSC07-III-10, 21st Annual AIAA/USU Conference on Small Satellites*, Logan, UT, August 2007.

[5]   C. M, Hicks, "NPS CubeSat Launcher program management," M.S. thesis, SSAG., Naval Postgraduate School, Monterey, CA, 2009.

[6]   F. Roßberg, "Structural design of a NPS CubeSat Launcher," M.S. thesis, SSAG, Naval Postgraduate School, Monterey, CA, 2008.

[7]   A. C. DeJesus, "Integration and Environmental Qualification Testing of spacecraft structures in support of the Naval Postgraduate School CubeSat Launcher Program," M.S. thesis, SSAG, Naval Postgraduate School, Monterey, CA, 2009.

[8]   M. R. Crook, "NPS CubeSat Launcher design, process and requirements," M.S. thesis, SSAG, Naval Postgraduate School, Monterey, CA, 2009.

[9]   United Launch Alliance, "Aft Bulkhead Carrier Secondary Payload User's Guide," Document No. ULA-ATLAS-UG-08-001, United Launch Alliance, Denver, CO, July 2013.

[10]   United Launch Alliance, "AtlasV/Aft Bulkhead Carrier to OUTSat ICD," Document No. ULA-ATLAS-ICD-11-002, United Launch Alliance, Denver, CO, June 2011.

[11]   United Launch Alliance, "Range imagery pictures," [Compact Disc], United Launch Alliance, Vandenberg Air Force Base, CA, May 2012.

[12]   The Aerospace Corporation, "Test requirements for launch, upper stage, and space vehicles," Document No. TR-2004(8583)-1 REV. A or MIL-STD-1540E, The Aerospace Corporation, El Segundo, CA, September 2006.

[13]   R. Coelho, "AI&T – OUTSat integration and test strategy," OUTSat Gate 1, Denver, CO, August 2011.

[14]   T. P. Sarafin and W. J. Larson, *Spacecraft Structures and Mechanisms – From Concept to Launch*, El Segundo, CA: Microcosm Inc. and Kluwer Academic Publishers, 2003.

[15]   D. Sakoda, S. D. Driscoll, V. Kaushish, R. Panholzer and J. H. Newman, "NPS CubeSat Launcher (NPSCuL) structural design and verification," presented at CNES Small Satellite Systems and Services Symposium, Madeira, Spain, 2010.

[16]   B. Controls, (May 1, 2013). Random vibration—An overview.[Online]. Available: http://www.emtengineering.com/wp-content/uploads/2013/04/RANDVIB.pdf

[17]   R. Simmons (August ,1997). Creating a random vibration component test specification. [Online]. Available: http://femci.gsfc.nasa.gov/random/randomtestspec.html

[18]   T. D. Scharton, *Force Limited Vibration Testing, NASA Technical Handbook*, Document No. NASA-HDBK-7004B, Jet Propulsion Laboratory, Pasadena, CA, January 31, 2003.

[19]   V. R. Dharanipathi, "Investigation of the semi-empirical method for force limited vibration testing," M.S. thesis, MIE, Concordia University, Canada, 2003.

[20]   T. D. Scharton. (1997, May). *Force Limited Vibration Testing Monograph*, Document No. RP-1403, Jet Propulsion Laboratory, Pasadena, CA.

[21]   T. D. Scharton, "Force limits measured on a space shuttle flight." *European Conference on Spacecraft Structure*, Noordwijk, Netherlands, 2001.

[22]   M. H. Richardson (January, 2000). Modal mass, stiffness and damping, vibrant Tech. Paper No. 31. [Online]. http://www.vibetech.com/assets/papers/paper31.pdf

[23]   PCB Piezotronics (June 23, 2008). Model 260A03 Specifications. [Online] http://www.pcb.com/Products.aspx?m=260A03

[24]   NASA FEMCI. (February 1, 2001). Isogrid Plate Modeling.[Online]. Available: http://femci.gsfc.nasa.gov/Isogrid

[25]   *Isogrid Design Handbook*, McDonnell Douglas Astronautics Company, Huntington Beach, CA, February 1973.

[27]   *Metallic Materials and Elements for Aerospace Vehicle Structures*, Document No. MIL-HDBK-5H, Department of Defense, December 1998.

106

INITIAL DISTRIBUTION LIST

1. Defense Technical Information Center
   Ft. Belvoir, Virginia

2. Dudley Knox Library
   Naval Postgraduate School
   Monterey, California